A Multiphasic Continuum Mechanical Model for Design Investigations of an Effusion-Cooled Rocket Thrust Chamber

Von der Fakultät Bau- und Umweltingenieurwissenschaften
der Universität Stuttgart zur Erlangung der Würde
eines Doktor-Ingenieurs (Dr.-Ing.)
genehmigte Abhandlung

vorgelegt von

Dipl.-Ing. Saeed Reza Ghadiani

aus
Teheran

Hauptberichter: Prof. Dr.-Ing. Wolfgang Ehlers
Mitberichterin: Prof. Dr.-Ing. Stefanie Reese

Tag der mündlichen Prüfung: 19. Mai 2005

Institut für Mechanik (Bauwesen) der Universität Stuttgart
Lehrstuhl II (Kontinuumsmechanik)
Prof. Dr.-Ing. W. Ehlers
2005

Report No. II-13
Institut für Mechanik (Bauwesen)
Lehrstuhl II (Kontinuumsmechanik)
Universität Stuttgart, Germany, 2005

Editor:
Prof. Dr.-Ing. W. Ehlers

© Saeed Reza Ghadiani
Institute of Structures and Design
Space System Integration
German Aerospace Center
Pfaffenwaldring 38-40
70569 Stuttgart
Germany

Produced by Verlag Glückauf GmbH, Essen, Germany
Printed by DIP – Digital Print, Witten, Germany, 2005

ISBN 3–937399–13–5
(D 93 – Dissertation, Universität Stuttgart)

Verliere dich nie in einer Sache, so interessant sie auch sein mag!
Das wahre Leben findet stets woanders statt.

Don’t lose yourself in a matter, however interesting it may be!
Real life always takes place somewhere else.

Acknowledgments

The work presented in this thesis was carried out within the framework of my research activities at the German Aerospace Center (DLR) in Stuttgart. The close and highly productive cooperation between the Institute of Structures and Design at the DLR and the Institute of Applied Mechanics (Civil Engineering) at the University of Stuttgart has resulted in an important contribution to the design investigations of actively cooled space constructions. The realization of this work would not have been possible without the support of my fellow workers and friends at both institutes to whom I am very grateful.

First of all, I want to thank my supervisor Professor Wolfgang Ehlers for his scientific support and his never-ending patience for the proof-reading of this thesis. Not only did I have an arbitrary access to the valuable store of knowledge at his chair but also he gave me many useful and essential advice in numerous discussions. His research in the field of continuum mechanics represents a substantial contribution for the physical treatment of multiphase problems.

My special thanks go also to Professor Stefanie Reese for her interest in my work and acting as the external examiner of this thesis.

Next, I would like to express my gratitude to Dr. Hermann Hald, head of the department of Space System Integration, from the DLR for his boundless confidence and support in my research activities as well as for the numerous scientific and philosophic discussions. Furthermore, I would like to thank my room mate and dear friend Roger Schäfer for the good time, constructive discussions and the friendly atmosphere in our office at the DLR. Special thanks go also to my fellow workers and dear friends Martin Ammann, Tobias Graf and Oliver Klar at the University of Stuttgart who supported me at any time with programming, computation of boundary-value problems and the better understanding of continuum mechanical foundations. I am also very grateful to Nicole Lützenburger from the DLR for her very friendly linguistic support in writing this thesis.

Finally, I would like to thank my fellow workers from the Institute of Space Propulsions at the DLR Lampoldshausen, particularly Dirk Greuel, for the long-standing fruitful cooperation.

Stuttgart, July 2005 Saeed Ghadiani

Deutsche Zusammenfassung

In der vorliegenden Arbeit wird ein kontinuumsmechanisches Modell auf der Grundlage der Theorie Poröser Medien (TPM) formuliert, die einen geeigneten Zugang zur makroskopischen Beschreibung gekoppelter Festkörper-Fluid-Probleme bietet, vgl. z. B. de Boer [13] und Ehlers [27]. Das in dieser Dissertation formulierte Modell soll als Werkzeug dienen, die im porösen Mantel einer effusiv gekühlten Raketenbrennkammer auftretenden physikalischen Vorgänge zu verstehen und somit die Auslegung einer solchen Konstruktion in Realgröße zu ermöglichen. Dabei ergibt sich die Problemformulierung aus der Funktionsweise der Effusionskühlung, bei der eine thermisch belastete poröse Wand von einem Kühlmittel durchströmt wird. Abgesehen von der Wärmemenge, die das Kühlmittel beim Durchströmen des porösen Materials dem umgebenden Festkörperskelett entzieht, kommt der eigentliche Kühleffekt dadurch zustande, daß sich an der thermisch belasteten Austrittstelle ein *Kühlfilm* bildet, der die Wärmebelastung der porösen Struktur reduziert (Abbildung 1.5).

Die Realisierung einer auf diese Weise gekühlten Raketenbrennkammer in Keramikbauweise, bestehend aus einem inneren, porösen C/C-Mantel (kohlefaserverstärkter Kohlenstoff) und einem äußeren, nicht-porösen CFK-Mantel (kohlefaserverstärkter Kunststoff), ist der Inhalt eines Forschungsprojekts an den Instituten Raumfahrtantriebe (RA) und Bauweisen- und Konstruktionsforschung (BK) des Deutschen Zentrums für Luft- und Raumfahrt (DLR), vgl. Hald und Haidn [45].

Um das vorliegende Problem im Rahmen der TPM zu formulieren, werden in Kapitel 1 die Grundlagen dieser Theorie vorgestellt. Darin werden die kinematischen Beziehungen der als superponierte Kontinua zu behandelnden Konstituierenden eines Mehrphasenmaterials[1] diskutiert. Darüber hinaus zeigt die Struktur der Bilanzrelationen mit den darin enthaltenen Koppeltermen, wie in der TPM die Interaktion der jeweiligen Bilanzgrößen zwischen den einzelnen Phasen Berücksichtigung findet. Aus dem fundamentalen Aufbau dieser Theorie läßt sich schließlich der poröse C/C-Mantel, ausgehend von einem thermoelastischen Festkörperskelett sowie einem kompressiblen Porengas und unter Berücksichtigung unterschiedlicher Temperaturfelder für die jeweiligen Phasen, durch ein nicht isothermes Zweiphasenmodell beschreiben. Dieses ermöglicht die gleichzeitige Berücksichtigung von mechanischen und thermischen Lasten sowie die Definition eines Fluidmassenstroms als eine weitere Randbedingung.

In Kapitel 3 werden die notwendigen Annahmen für die einzelnen Phasen, wie beispielsweise das *ideale Gasgesetz* für das Porenkühlgas, im Rahmen der Konstitutiven Theorie diskutiert. Anschließend werden alle notwendigen Beziehungen für die Formulierung des Problems durch die Auswertung der maßgebenden Entropieungleichung bereitgestellt. Unter anderem werden für die in der Dissipationsungleichung enthaltenen Funktionen adäquate Ansätze formuliert, die sich aus deren Linearisierung ergeben. Es stellt sich dabei die zentrale Frage, ob in der Nähe des thermodynamischen Gleichgewichts linearisiert

[1] Unter dem Begriff „Mehrphasenmaterial“ ist ein poröser Körper bestehend aus einem Festkörperskelett (Festkörperphase) und dem im Porenraum enthaltenen Fluid (Fluidphase) zu verstehen. Dabei kann die Fluidphase aus mehreren Flüssigkeiten und/oder Gasen bestehen.

werden darf. Auch wenn beim vorliegenden Modell die Annahme von kleinen Temperaturgradienten und einer langsamen Gasströmung berechtigt ist, darf die Auswertung der Entropieungleichung nur dann in der Nähe des thermodynamischen Gleichgewichts durchgeführt werden, wenn zusätzlich von kleinen Temperaturunterschieden zwischen den beiden Phasen ausgegangen werden kann. Mit anderen Worten, auch wenn jede Phase für sich im thermodynamischen Gleichgewicht oder in dessen Nähe sein kann, so kann sich die gesamte Mischung aufgrund unterschiedlicher Temperaturen der einzelnen Phasen dennoch weit entfernt vom Gleichgewicht befinden. An dieser Stelle kommt der Existenz des *Kühlfilms*, der wie eine Grenzschicht zwischen dem porösen Körper und der heißen Umgebung verstanden werden kann, eine zentrale Bedeutung zu. Es wird davon ausgegangen, daß die eigentliche Kühlung zwischen dieser Grenzschicht und der heißen Umgebung stattfindet. Somit werden die hohen Temperaturen innerhalb des *Kühlfilms* abgebaut (Abbildung 1.12), so daß das poröse Festkörperskelett mit annähernd gleichen Temperaturen wie das Kühlfluid belastet wird. Es kann daher innerhalb des zweiphasigen Modells von kleinen Temperaturunterschieden zwischen den beiden Phasen ausgegangen werden, so daß die Entropieauswertung in der Nähe des thermodynamischen Gleichgewichts durchgeführt werden darf.

Die Bestimmung der in der Dissipationsungleichung enthaltenen Funktionen in der Nähe des thermodynamischen Gleichgewichts bedeutet, daß man die Transportvorgänge, wie beispielsweise den Wärmetransport in einer Phase oder den Wärmeaustausch zwischen den Phasen, isoliert voneinander betrachtet. So wird beispielsweise bei der Ermittlung der Wärmestromvektoren der einzelnen Konstituierenden davon ausgegangen, daß der Wärmetransport nur von dem jeweiligen Temperaturgradienten gesteuert wird. Die gleichzeitige Beeinflussung des Temperaturgradienten durch andere Größen, wie z. B. die Temperaturdifferenz zwischen den beiden Phasen, wird ausgeschlossen. Dies führt zu einfachen Proportionalitätsbeziehungen für die jeweiligen Größen. So ergibt sich beispielsweise für den Wärmestromvektor die *Fourier*sche Wärmeleitungsgleichung, die eine einfache Proportionalität zwischen dem jeweiligen Wärmestromvektor und dem dazugehörigen Temperaturgradienten beschreibt. Es ist zu beachten, daß bei Betrachtung von Transportvorgängen, die gleichzeitig ablaufen und sich somit gegenseitig beeinflussen, diese einfachen Proportionalitätsbeziehungen nicht mehr gegeben sind. Überkreuzen sich zwei Transportvorgänge, so tauchen sogenannte Kreuzbeiwerte auf. Solche *cross phenomena* werden im Rahmen der Nichtgleichgewichtsthermodynamik behandelt, vgl. z. B. Fitts [40].

Nachdem alle erforderlichen Beziehungen sinnvoll definiert worden sind, kann das maßgebende Gleichungssystem formuliert werden. Um die Primärvariablen des Modells, einerseits die Verschiebungen und die Temperatur des Festkörperskeletts, andererseits den Druck, die Geschwindigkeit und die Temperatur des Gases, zu bestimmen, sind zunächst fünf Gleichungen notwendig. Diese ergeben sich aus der Impulsbilanz der gesamten Mischung, der Impulsbilanz sowie der Massenbilanz des Gases und letztlich aus den beiden Energiebilanzen der jeweiligen Konstituierenden. Es sei an dieser Stelle darauf hingewiesen, daß die Gasgeschwindigkeit durch die Sickergeschwindigkeit, die im Rahmen der TPM als Relativgeschwindigkeit zwischen der Fluidphase und der Festkörperphase definiert ist, substituiert wird. Die Annahme einer schleichenden Sickerströmung, wonach Beschleunigungsterme vernachläßigt werden dürfen, ermöglicht die folgende Vereinfachung. Sie bewirkt, daß aus der Impulsbilanz des Gases eine Bestimmungsgleichung für die Sickergeschwindigkeit formuliert werden kann (Gleichung 3.100), so daß diese den Status einer unabhängigen Variablen verliert und nicht mehr als Primärvariable behandelt wird. Die Anzahl der Gleichungen reduziert sich somit für die sogenannte quasistatische Formulierung des Problems auf vier. Ferner sei erwähnt, daß die auf diese Weise gefundene Gleichung für die Sickergeschwindigkeit in ihrem Kern dem empirischen *Darcy*-Gesetz entspricht.

Die für die Numerik erforderliche *schwache Form* des zu lösenden Gleichungssystems wird im Rahmen der *Finite-Elemente-Methode* mit Hilfe des *Standard-Galerkin-Verfahrens* formuliert. Dabei werden die jeweiligen Gleichungen mit zugehörigen *Testfunktionen* multipliziert, vgl. z. B. Schwarz [67] und Zienkiewicz und Taylor [83]. Als FE-Programm wird das Forschungstool PANDAS [34] verwendet. Mit Hilfe dieses FE-Pakets können nun diverse gekoppelte Randwertprobleme behandelt werden.

In Kapitel 5 wird in Anlehnung an die zu untersuchende keramische Brennkammer anhand von einfachen Modellen der Einfluß der Temperatur auf das Strömungsverhalten des Kühlgases durch das poröse Medium untersucht. Des weiteren wird im Rahmen einer Sensitivitätsanalyse eine Variation der Parameter vorgenommen, die bei der Fertigung des C/C-Materials gezielt gesteuert werden können. Es wird darauf hingewiesen, daß die endgültige Auslegung der geplanten Struktur nicht das Ziel dieser Arbeit ist, da eine solche Konstruktion erst nach zahlreichen Optimierungsberechnungen und aufwendigen Experimenten zur Bestimmung von Materialkennwerten realisiert werden kann. Dennoch lassen sich aus den hier demonstrierten qualitativen Berechnungen bereits Tendenzen bezüglich Geometrieführung und Vordimensionierung von Wandstärken ableiten.

Eines der grundlegendsten Probleme bei der Simulation realistischer Vorgänge in der zu untersuchenden Konstruktion ist die korrekte Erfassung der thermischen Randbedingungen. Die für die poröse Struktur resultierende Wärmebelastung läßt sich nur aus einer aufwendigen Strömungssimulation der Heißgasströmung im Brennraum ermitteln. Hierzu sind jedoch Informationen über die Oberflächentemperaturen des C/C-Materials sowie den aus der Wand austretenden Kühlmittelmassenstrom erforderlich. Eine sinnvolle Berechnung der Wärmebelastung ist somit erst aus der Kopplung des hier entwickelten Modells mit einem Strömungslöser zu erwarten. Es wird derzeit im Rahmen weiterer Forschungsarbeiten am DLR untersucht, ob eine solche Kopplung sinnvoll und realisierbar ist.

Ein weiteres Problem, dem ebenfalls besondere Aufmerksamkeit zu widmen ist, stellt die Beschreibung des Wärmeübergangs dar. In der klassischen Thermodynamik ist die Wärmemenge, die zwei sich berührende Körper untereinander austauschen, proportional zu der Temperaturdifferenz auf deren Kontaktfläche und zu der Größe dieser Fläche. Als Proportionalitätsfaktor dient der flächenspezifische Wärmeübergangskoeffizient. Da ein strömendes Fluid beim Berühren einer Wand auch Reibungswärme erzeugt, ist der klassische Wärmeübergangskoeffizient keine rein kalorische Größe, sondern beinhaltet auch die Einflüsse der Reibung und somit der Geschwindigkeit sowie der Viskosität. Darüber hinaus ist die geometrische Form des angeströmten Festkörpers ebenfalls zu berücksichtigen, da diese die Reibung beeinflußt. Dabei ist die Frage, ob ein Fluid eine runde Kugeloberfläche umströmt oder eine scharfe Kante anströmt, von großer Bedeutung für den gültigen Ansatz zur Berechnung des flächenspezifischen Wärmeübergangskoeffizienten. Daher wird dieser Koeffizient als Funktion von Temperatur, Geschwindigkeit und Viskosität ermittelt und ist in der Literatur für unterschiedliche Geometrien angegeben, vgl. z. B. Grigull [43]. Bei einem porösen Material stellt sich allerdings die Frage, wie die Kontaktfläche zwischen Festkörper und Fluid zu bestimmen ist. Denn in Wirklichkeit ist diese Fläche durch die Summe der inneren Porenoberflächen charakterisiert, die im allgemeinen nicht bekannt ist. Damit der klassische Ansatz für den Wärmeübergang verwendet werden kann, wird in der Literatur die innere Struktur eines porösen Körpers mit einer Kugelpackung in dichtester Lagerung approximiert, vgl. z. B. Whitaker [82]. Im Rahmen der vorliegenden Arbeit wird jedoch nicht von den klassischen Ansätzen Gebrauch gemacht. Bedingt durch die verwendete Theorie und die Art, wie darin die Interaktionsterme definiert sind, ist der Wärmeübergangskoeffizient in dem zu untersuchenden Modell eine rein kalorische Größe. Die Reibungswärme wird mit Hilfe der mechanischen Leistung berechnet, die sich aus dem Produkt zwischen der Interaktionskraft und der Sickergeschwindigkeit ergibt (Gleichung 3.5). Darüber hinaus ist hier der Wärmeübergangskoeffizient eine volumetrische Größe, die nicht auf die Information über die mikroskopische Struktur der Poren angewiesen ist. Da alle anderen Materialparameter unabhängig vom Wärmeübergang bestimmt werden können, kann der Wärmeübergangskoeffizient mittels *Parameteridentifikation* experimentell ermittelt werden. Ein adäquater Versuchsaufbau wird derzeit am DLR konzipiert.

Abschließend sei erwähnt, daß für eine Validierung des entwickelten Modells anhand von realen Testdaten zuerst alle erforderlichen Parameter experimentell ermittelt werden müssen.

Inhaltsverzeichnis

Chapter 1: Introduction

1.1 Motivation and statement of the problem

1.1.1 Conventional rocket thrust chambers

The existing space transportation systems are, more and more, confronted with the ever growing demand for high efficiency such as higher payload and reliable performance without an increase in their dry-weight. In order to meet these requirements, as an expedient measure, the capability of the existing space propulsion systems has to be increased. This implicates, inevitably, a rise in pressure and temperature in the subsystems of the engine, in particular, within the thrust chamber.

Figure 1.1: Space shuttle [http://spaceflight.nasa.gov/gallery].

In the existing oxygen/hydrogen rocket thrust chambers (cf., e. g., Figure 1.2), combustion temperatures up to 3500 K (cf., e. g., Lezuo [53]) as well as the relatively low heat resistance of the applied materials are the reasons, why these constructions have generally to be cooled. Many different methods exist to cool thrust chambers, cf., e. g., NASA Design Criteria [61, 62]. However, the existing methods have been already optimized in such a way that a further increase in their efficiency cannot be reached, unless major changes are conducted in the total design of the propulsion systems. Figure 1.3 shows the design of the conventional regeneratively cooled combustion chamber VULCAIN. The principle functioning of the regenerative cooling, which is schematically illustrated in Figure 1.4 (a), should serve to comprehend the aforementioned problems.

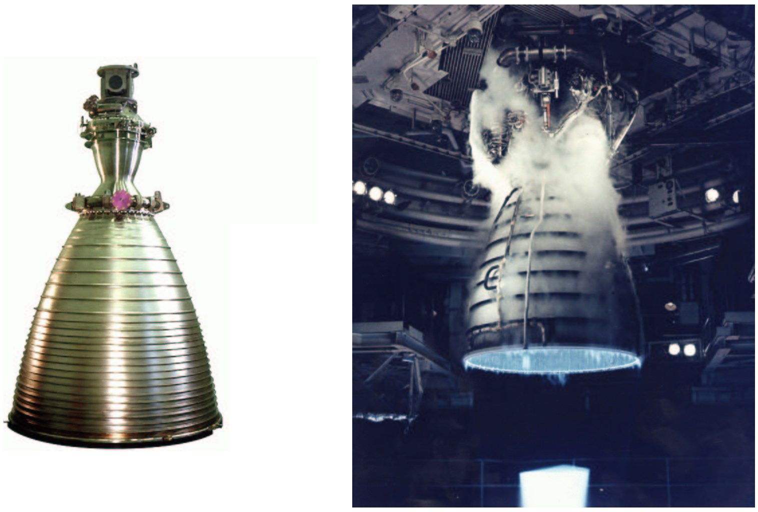

VULCAIN thrust chamber Space Shuttle Main Engine SSME

Figure 1.2: Regeneratively cooled thrust chamber consisting of the combustion chamber and the expansion nozzle.

In a regeneratively cooled combustion chamber, the heat load acting on the inner contour of the metallic liner arrives at the cooling channels via heat conduction and is then absorbed by the cryogenic propellant. As depicted in Figure 1.4 (a), the cryogenic propellant flows through the channels in the opposite direction to the hot gas stream of the combustion space. In this way, the metallic liner is cooled and, on the other hand, the propellant is heated up before being injected into the combustion space.

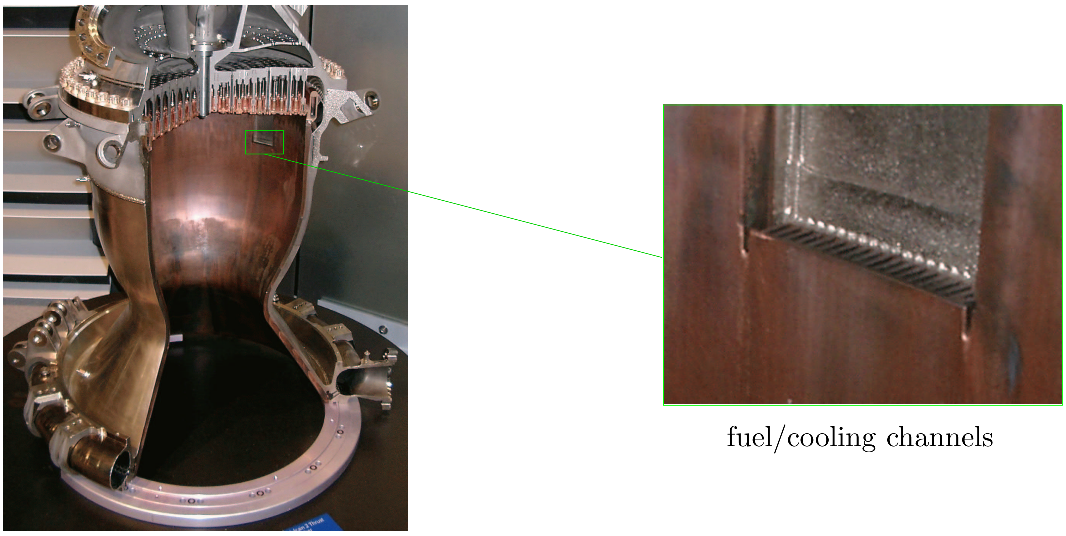

Figure 1.3: Regeneratively cooled VULCAIN combustion chamber powering the cryogenic core stage of ARIANE 5.

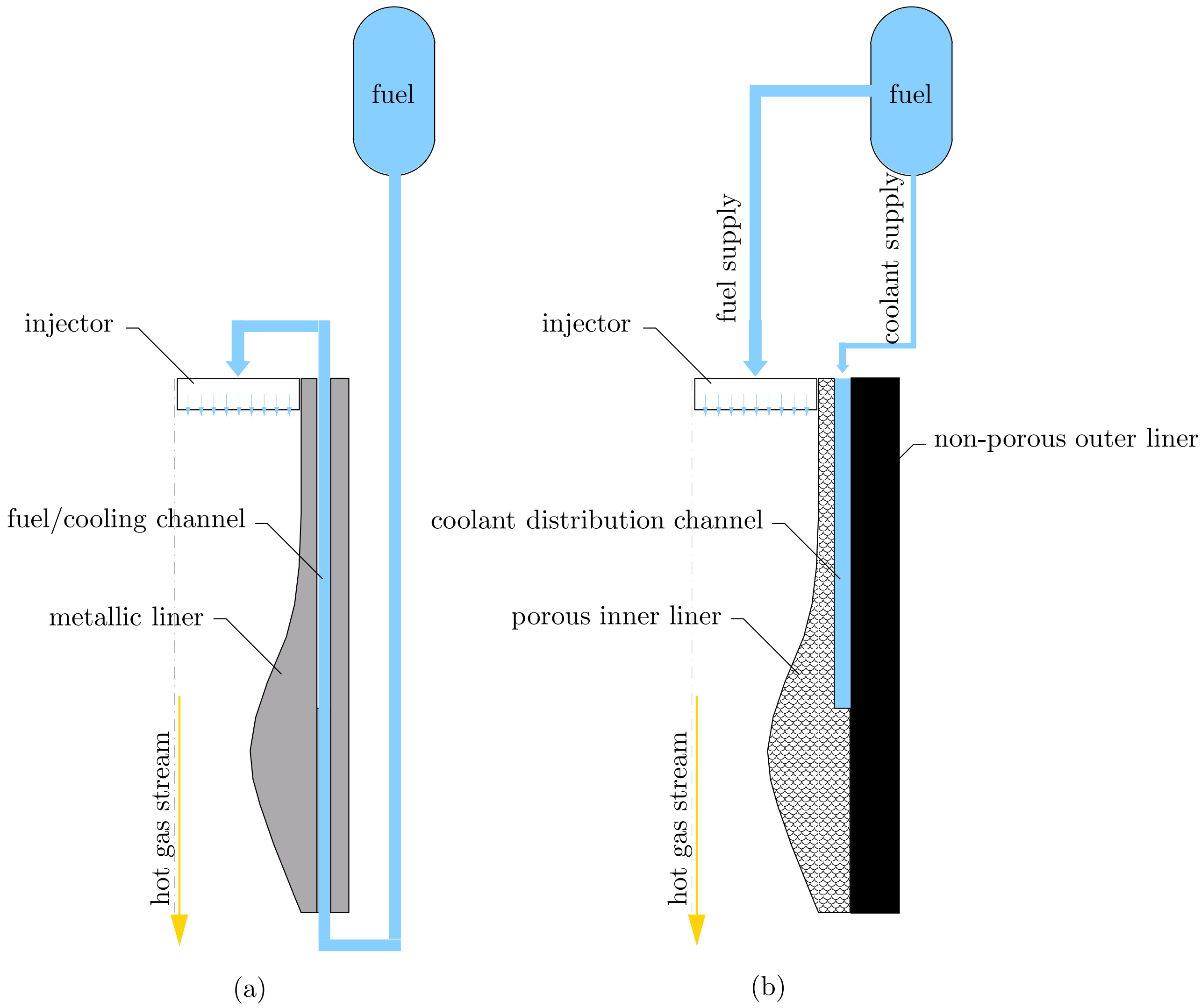

Figure 1.4: Schematical illustration of (a) a regeneratively cooled combustion chamber; (b) an *effusion*-cooled combustion chamber.

The pressure required in order to establish the propellant flow through the channels is generated by turbo pumps. This pressure must be increased, the higher the thermal loads rise in the combustion space. The maintenance of this cooling principle hence involves pressure losses in the whole propulsion system. In other words, the pressure to be generated in the overall system must be higher than the operational pressure realized in the combustion chamber.

Taking the aforementioned remarks into consideration, one can imagine that the operation of a regeneratively cooled combustion chamber at a higher performance demands a huge effort from the turbo pumps. However, without an increase in the dimension and, as a consequence, the weight of these components, the requirement for a better performance cannot be fulfilled. Therefore, major changes are necessary in conventional systems in order to improve their capability without an increase in the dry-weight of their subsystems.

The application of a more efficient cooling technique as well as new materials with a higher heat resistance might be one of the expedient changes in the existing systems, cf. Hald and Haidn [45]. Experimental results from the German Aerospace Center (DLR) and others have shown that *effusion cooling* might be one of the most promising candidates for a highly efficient cooling method. In general parlance, it cools a hot permeable wall by passing a coolant mass flow through this wall. Furthermore, the flow takes place at very low velocities in such a manner that the out-flowing coolant creates a so-called *cooling film* along the hot surface, cf. Figure 1.5. Applying this method, the cooling effect is predominantly achieved by the thin *film*, which covers and protects the exposed wall surface from excessive heat transfer. In addition, the residual heat flow, which penetrates into the solid material via heat conduction, is absorbed by the contrary flowing coolant.

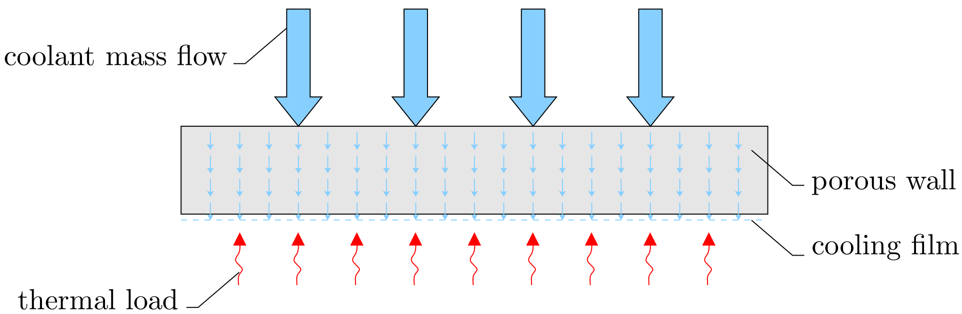

Figure 1.5: The basic principle of the *effusion cooling*.

As schematically depicted in Figure 1.4 (b), in contrast to the regeneratively cooled chamber, the propellant is directly led to the injector of the *effusion cooled* combustion chamber. Only a minor rate of the cryogenic fuel is branched off for the cooling. The lesser the pressure is needed in order to press the coolant through the porous wall of the chamber, the lesser are the pressure losses in the propulsion system. Simultaneously, the lesser coolant is required, the more propellant remains for the thrust generation. This holds, since the coolant flowing through the porous wall into the chamber does not participate in the combustion.

In first experimental chambers using this cooling method, metallic porous materials were applied, cf., e. g., Lezuo [53], May and Burkhardt [58] and Mueggenburg et al. [59]. These attempts failed, however, by the heavy weight of the chambers as well as the low heat tolerance of metallic materials (approx. 400 K). The latter leads to the so-called *hot spots*, where the porous metal melts locally due to temperature peaks. As a consequence of this effect, the porosity dwindles away and the cooling collapses around the *hot spot* region. This, in turn, causes a further increase in temperature and leads at last to the total failure of the construction.

In the framework of research activities made on this area at the DLR in recent years, a new concept has been developed, patented and investigated, in which a ceramic combustion chamber for oxygen/hydrogen rocket engines is cooled entirely by *effusion cooling*, cf. Hald and Haidn [45]. To this end, the cooling method is applied in conjunction with porous carbon fiber reinforced ceramics C/C, which possesses an extremely high temperature limit (more than 2000 K). Additionally to this advantage, which relieves the cooling circuit, C/C materials have also a negligible thermal expansion, cf., e. g., Hald [44]. This property entails that the risk of the *hot spot* effect does not exist for this kind of materials. More details of the intended design for the ceramic combustion chamber are discussed in the following subsection.

1.1.2 A new rocket thrust chamber

As schematically depicted in Figure 1.6, where the main principle of the intended concept is illustrated, the coolant distribution channels have to be arranged in the porous liner in specific distances and, furthermore, have to be closed at their ends. As a result, the permanent mass flow rate of the coolant into the distribution channels causes an increase of the pressure within the channels so that, consequently, the coolant is pressed through the porous liner towards the internal space of the chamber, cf. Figure 1.7. This takes place, since the load-bearing outer liner is a non-porous material.

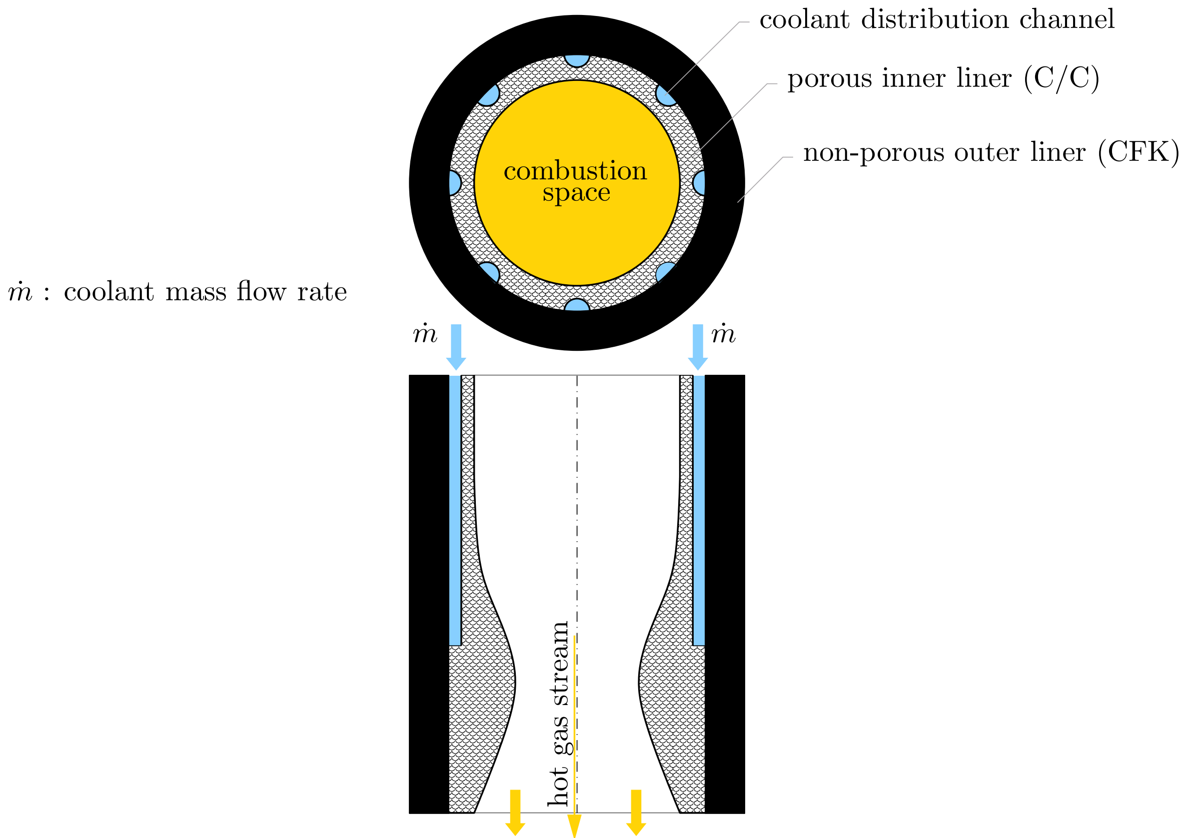

Figure 1.6: A new concept for an *effusion cooled* ceramic rocket combustion chamber [*German Aerospace Center*].

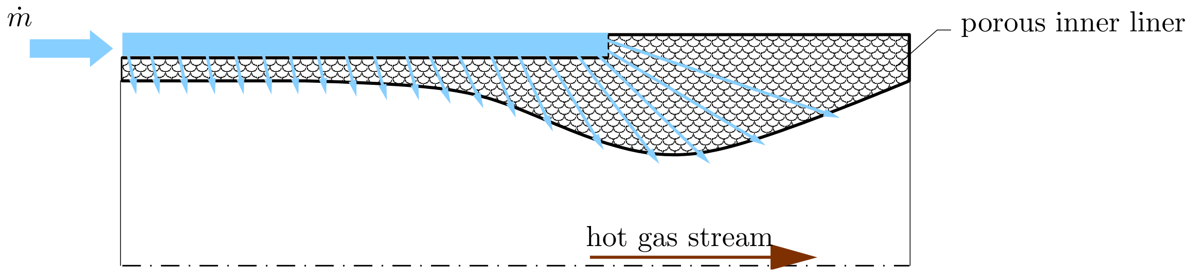

Figure 1.7: Coolant transport through the porous liner.

The porous C/C material possesses the density $\rho = 1.3$ g/cm^3, whereas the density of the non-porous outer liner CFK (carbon fiber reinforced plastic) amounts to $\rho = 1.6$ g/cm^3. Compared to copper ($\rho = 8.96$ g/cm^3) and nickel ($\rho = 8.9$ g/cm^3) applied in conventional thrust chambers, the extremely low densities of C/C and CFK are a further significant advantage of the new ceramic combustion chamber. However, in order to technically realize the intended *effusion*-cooled combustion chamber, several questions must be discussed before.

The main goal of the cooling procedure in the construction under consideration is not only to reduce the thermal loads on the inner contour of the C/C liner. It must also be ensured that high temperatures do not reach the outer liner, which has a low heat capacity. The determination of the required number of coolant distribution channels as well as their optimal run along the longitudinal axis of the C/C liner is therefore one of the most important aspects to be investigated. However, due to some operational difficulties, the design investigation of the porous liner is nontrivial. The major difficulties will be discussed in the following.

Operational difficulties. The pressure gradient over the liner thickness, which represents the driving force for the coolant flow through the porous wall, varies along the chamber contour. This occurs, since the pressure distribution is not uniform in the chamber, whereas the pressure in the coolant distribution channels is assumed to be uniformly along a channel, cf. Figure 1.9. Therein, the pressure magnitude is indicated by the length of arrows. It can be seen that the highest pressure on the interior walls exists inside the chamber and decreases steadily in the nozzle, until it reaches the nozzle exit pressure. On the other hand, large differences exist in the heat load along the chamber contour, cf. Figure 1.8. Thus, different local mass flow rates of the coolant are necessary in order to cool down several temperature ranges.

The determination of the mass flow rates locally required on the inner contour is based on the hot gas boundary layer investigations, cf., e. g., Greuel et al. [42], Lezuo [53] or Serbest [69]. Primary theoretical investigations on this kind of problems were already made at the end of 1940s, cf. Rannie [64]. Since that time, numerous theoretical and empirical approaches have dealt with heat transfer phenomena occurring between the *cooling film* and its hot environment, cf., e. g., Chen [20], Fröhlke et al. [41], Kays and Crawford [51], Larch [52], Liu and Chen [54], May and Burkhardt [58], Mueggenburg et al. [59], Rubesin and Pappas [65], Serbest et al. [70], Walton [80] and Wheeler and

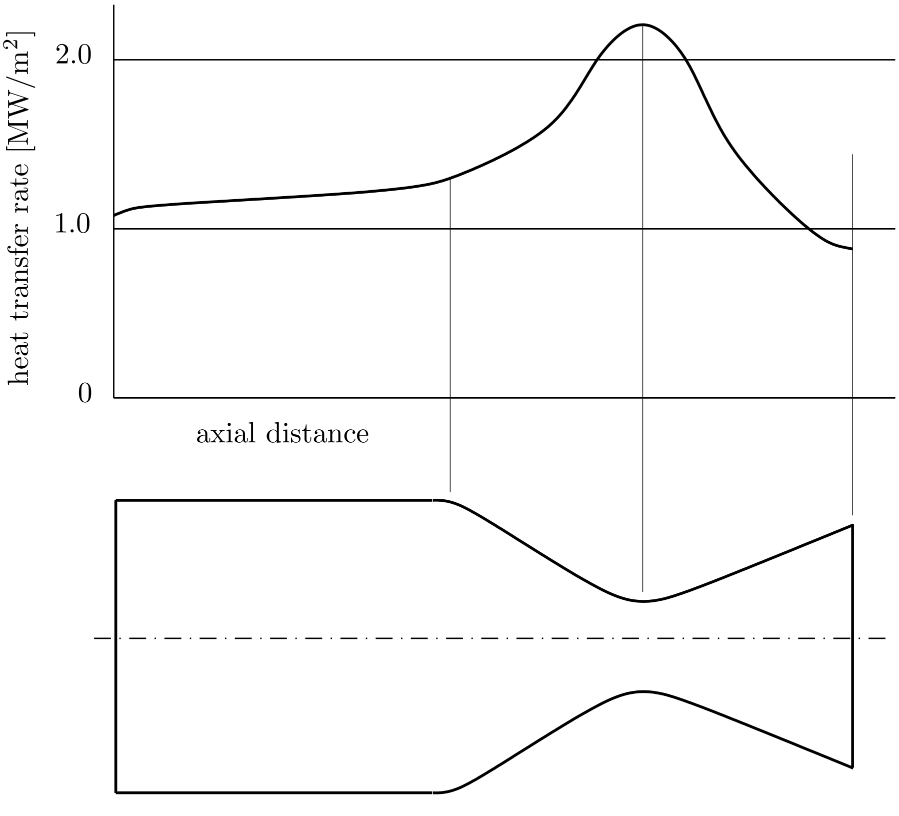

Figure 1.8: Typical axial heat transfer rate distribution for liquid propellant thrust chambers and solid propellant rocket motors, cf. Sutton and Biblarz [72].

Duwez [81]. Considering the approaches above, the required coolant dosages along the inner contour can be determined, e. g., by means of numerical tools such as the Two Dimensional Kinetics (TDK) [63]. However, these investigations are not the subject of the present work. It is also not the intention of this work to discuss the integration of an *effusion*-cooled chamber in a full-scale rocket engine or to investigate its operational influences on the system architecture of a conventional transportation system. These investigations are the subject of other on-going researches at the DLR, cf., e. g., Herbertz [50].

The major task in the present work is to find out, how the construction under consideration must be designed in order to supply each point of the chamber interior walls with the necessary cooling and, furthermore, to ensure the operational stability of the porous liner. This requires a precise knowledge about the behavior of the fluid flow inside of the porous material under thermal influences. In addition, a deformable solid material should be considered.

The model to be created must allow for the investigation of the physical effects in stationary processes as well as during transient conditions. One of the critical transient processes is, e. g., the ignition sequence, where the pressure as well as the temperature in the combustion chamber rapidly increase within milliseconds, cf. Figure 1.10.

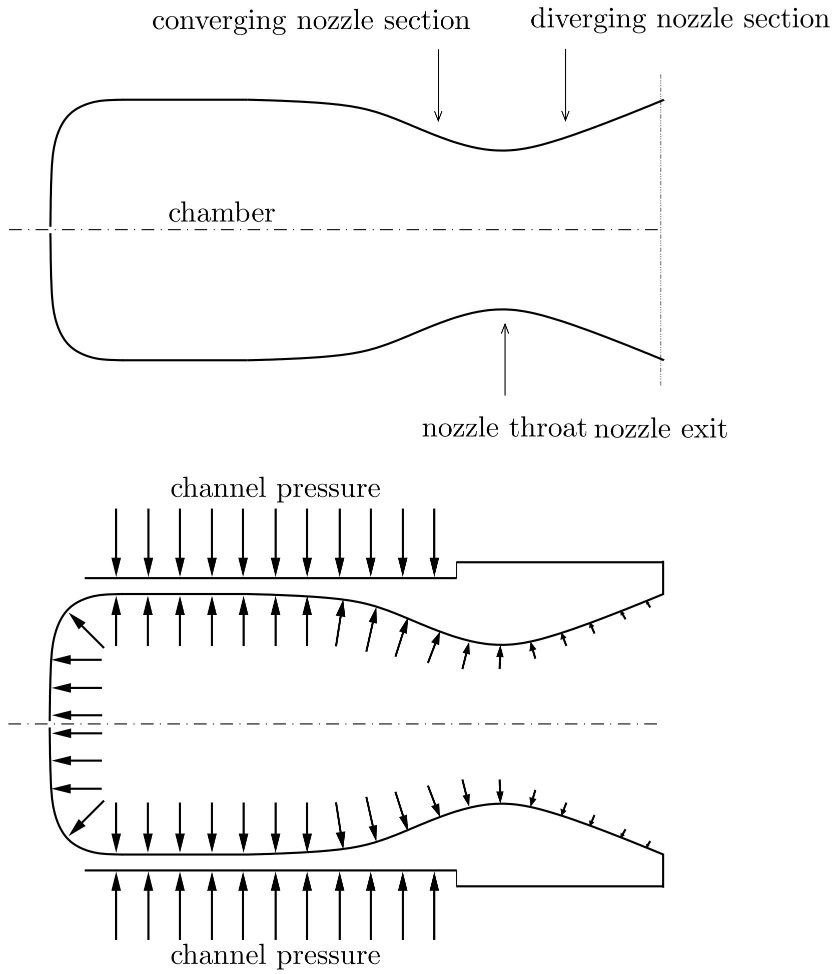

Figure 1.9: Pressure balance on chamber and nozzle interior walls.

Furthermore, it must be pointed out that large temperature differences might exist within the fluid-saturated porous material between the coolant and the solid skeleton, if the cooling takes place inside of the porous material. This would hold, if one abandons the presence of the cooling film between the porous construction and the hot environment, cf. Figure 1.11. However, using the *effusion cooling*, it is assumed (cf. Subsection 1.1.1) that the effective cooling takes place outside of the porous wall, cf. Figure 1.12. Following this assumption, one can proceed from small temperature differences between the solid skeleton and the pore-fluid. Note that this effect plays a decisive role for the entropy evaluation and will be taken up later on.

Following the aforementioned remarks on the operation conditions of the construction under study, it is now obvious that the consideration of the porous liner as a fluid-saturated solid material, admitting the coolant through its pores under non-isothermal conditions, leads to a multiphasic model. This model must provide the possibility for the definition of mechanical loads, thermal loads and also a fluid mass flow across the boundary. Proceeding from such a model, the pressure, the velocity and the temperature of the pore-fluid have to be computed as field functions, on the one hand. On the other hand, the displacement and also the temperature of the solid skeleton must be determined as supplementary field variables. However, coupled solid-fluid problems of this category cannot be uniquely classified within the well-known disciplines of *solid mechanics* or *fluid mechanics* but they have to be treated as multiphase problems.

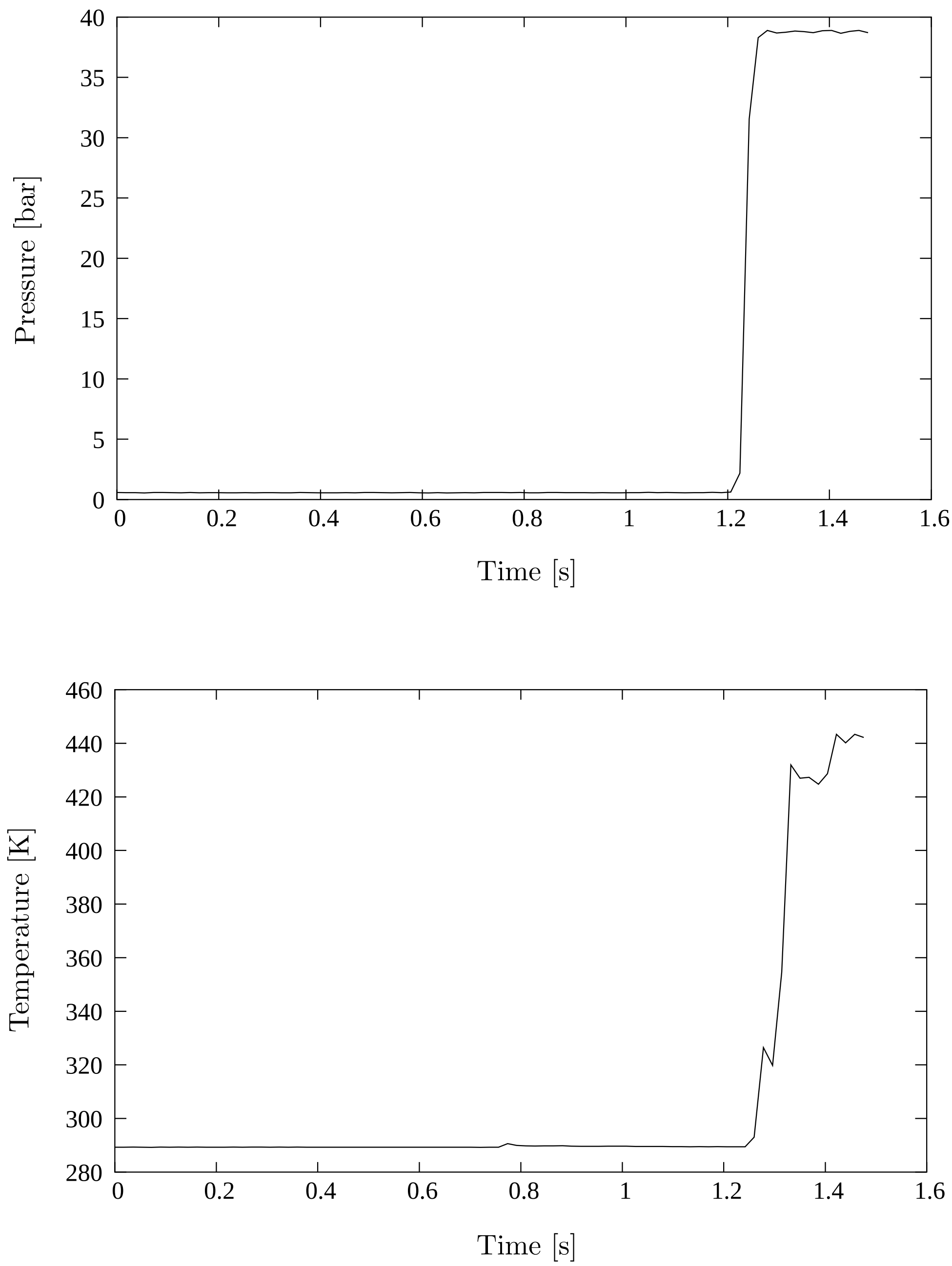

Figure 1.10: Temporal development of the chamber-pressure and temperature during the ignition of a testing chamber with the operating pressure of 38 bar and the temperature of $\approx 470\,\mathrm{K}$ [*Experiments at DLR*].

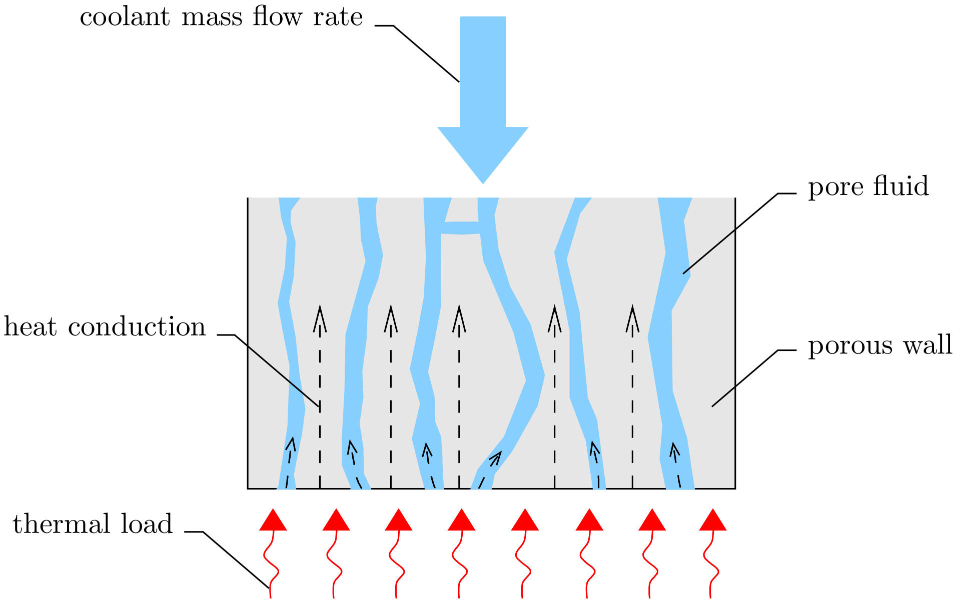

Figure 1.11: Large temperature differences between the solid and the pore-fluid (in the absence of the cooling film) due to their different heat conduction behavior.

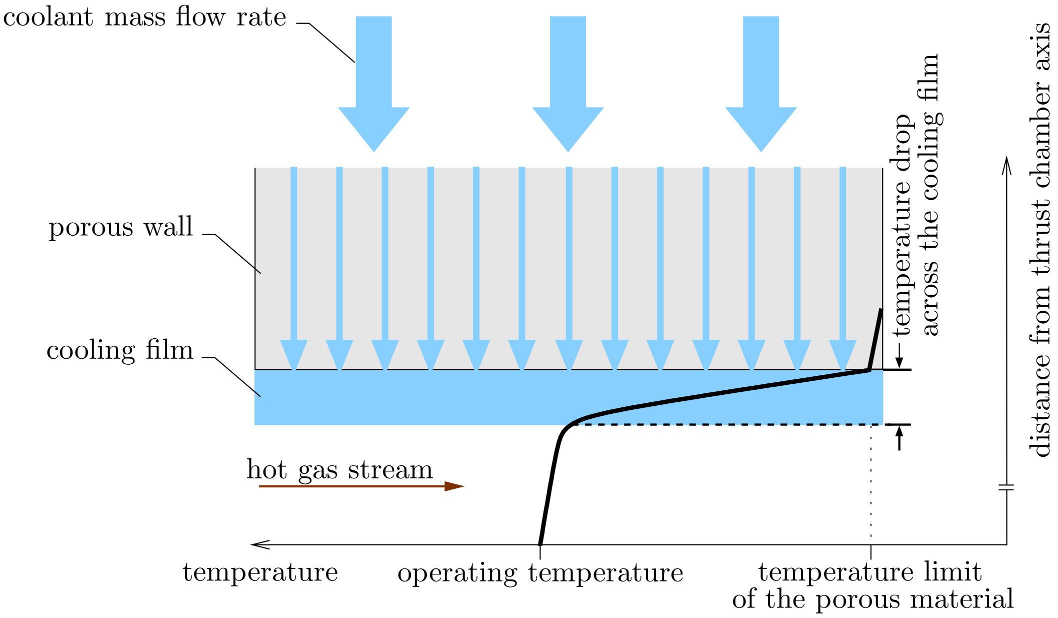

Figure 1.12: Steep temperature drop across the cooling film.

1.1.3 Multiphase problems

The origin of multiphase problems, where fully or partially saturated porous materials had to be investigated, stems from geomechanical sciences, cf., e. g., Biot [5, 6], Fillunger [39], Heinrich and Desoyer [48] or Terzaghi [73]. To this end, theoretical approaches were necessary in order to describe the ground-water flow as well as the behavior of the surrounding porous soil material. The gained knowledges on this area have then been used in other branches of engineering such as the petroleum industry as well as chemical engineering, cf., e. g., Bowen [17–19].

Nowadays, progresses in material science enable the application of natural or industrial porous materials in new technology sectors. In consideration of the increasingly new application fields of these materials, the necessity of a consistent theory to describe fully or partially saturated deformable porous media became obvious. However, as was remarked before, problems of this kind cannot be uniquely classified within the well-known disciplines of either *solid mechanics* or *fluid mechanics*. Instead, it has to be taken into consideration that they require a unified treatment of volumetrically coupled solid-fluid aggregates and fall hence into the categories of either mixtures or porous media, cf., e. g., Bowen [17–19], Truesdell and Toupin [77], de Boer [11, 13], de Boer and Ehlers [14–16] and Ehlers [26–31].

The main difficulty to theoretically treat so-called multiphasic materials consisting of a solid skeleton and an arbitrary number of pore-fluids is the description of the different motions of the participating constituents. Thus, the efficiency of the theoretical approaches describing problems of this kind depends on the way, how the mechanical as well as the thermodynamic interactions between the constituents are taken into account. At first sight, one may expect that such coupled solid-fluid problems can be discussed on the basis of a continuum mechanical method by use of two different strategies, the micro-mechanical and the macro-mechanical approach. However, the internal pore structure of porous materials, in general, is of an arbitrary and irregular shape. Therefore, the sufficient definition of coupling mechanisms at the internal interfaces between the constituents is almost impossible. This is why the micro-mechanical strategy proves to be unsuitable.

Proceeding from macroscopic procedures, the individual aggregates of the multiphasic body are statistically smeared out through the considered domain in the sense of superimposed and interacting continua. Following this, the axioms of the classical *Theory of Mixtures* can be utilized, wherein heterogeneously composed continua consisting of an arbitrary number of miscible and interacting constituents are assumed. However, in a real saturated solid skeleton one cannot proceed from the principle assumption of this theory, since the solid and the fluid are in reality immiscible. In consideration of this fact, the *Concept of Volume Fractions* is introduced as a measure for the local portions of the individual constituents of the overall medium. This provides in combination with the *Theory of Mixtures* an excellent tool, the *Theory of Porous Media* (TPM), for the macroscopic description of general immiscible multiphasic aggregates. Therein, all incorporated fields are understood as local averages of the corresponding quantities of an underlying microstructure.

1.2 Outline of the thesis

The present thesis is divided into six chapters. After the problem under study has been extensively depicted in Section 1.1, where *inter alia* the necessity of the coupled treatment of the physical effects was established, **Chapter 2** covers the fundamentals of the continuum mechanical description of coupled solid-fluid problems, the *Theory of Porous Media*. Therein, additionally to the concept of volume fractions and the basic kinematical relations, the mechanical as well as the thermodynamic balance relations for multiphasic materials are discussed.

In **Chapter 3**, a biphasic non-isothermal model consisting of a thermoelastic solid skeleton and a compressible fluid is created. Therein, the fluid constituent is assumed to be an *ideal gas*. The required thermodynamic potentials as well as the restrictions for the formulation of constitutive equations are gained on the basis of the fundamental principles of the constitutive theory through the evaluation of the entropy inequality. However, before the entropy evaluation can be carried out, the determining inequality must be given. To this end, a specific constraint is formulated specially for the model under consideration, cf. Subsection **3.1.1**. Furthermore, for the evaluation of the dissipation inequality, the included response functions are linearized by *Taylor series* around the equilibrium state. This assumption is justified, since small gradients and small temperature differences are presumed in the model under consideration.

At the end of this chapter, the determining set of the field equations is presented for quasi-static processes. The consideration of quasi-static processes enables the formulation of a new conditional equation for the seepage velocity, which can be understood as an extended *Darcy* law for non-isothermal processes, cf. Subsection **3.4.1**. Note that this equation is formulated on the basis of the assumptions made in this work.

Chapter 4 discusses briefly the material parameters of the model, where it is generally recommended to perform experiments in such a way that coupled effects can be avoided when the individual coefficients are determined. Concerning the heat conduction coefficient of the fluid constituent, it is pointed out that inaccuracies must be taken into consideration, which are induced due to the heat exchange between the fluid and the solid. As a consequence of this fact, it is finally recommended to proceed from the realistic (microscopic) heat conduction of the gas. Furthermore, the heat exchange coefficient is the only parameter, which remains to be determined and should hence be identified by means of standard *parameter identification* procedures.

Chapter 5 presents the numerical computation of some representative physical effects occurring in the construction under study. Although the developed model allows for the investigation of numerous physical effects, nevertheless, the numerical examples in this work are restricted predominantly to those dealing with the compressible gas flow under thermal influences. The last example investigates heat exchange phenomena.

In **Chapter 6**, the basic assumptions and conditions as well as the most important results of the investigations in this thesis are briefly summarized.

Chapter 2: Theory of Porous Media

In this chapter, the foundations of the continuum mechanical description of multiphasic materials are briefly discussed. Therein, based on the *Theory of Porous Media* (TPM), the basic principles of the kinematics as well as the balance relations, as far required for the present work, are explained. An extensive treatment of the fundamentals of the TPM can be found in de Boer [11, 13], de Boer and Ehlers [16] and Ehlers [31].

The TPM arises from the *Theory of Mixtures* (cf., e. g., Bowen [17–19]) combined with the *Concept of Volume Fractions* and provides thus a convenient approach for the description of immiscible multiphasic aggregates. The principle framework of the TPM is based on a macro-mechanical view, i. e., no geometrical informations about the location and the structure of the pores are considered. It is rather assumed that the pores are statistically distributed over the control space, which is represented by the porous solid. As a consequence of this assumption, the real constituents, the porous solid included, are treated as smeared volumes over the control space, cf. Figure 2.1.

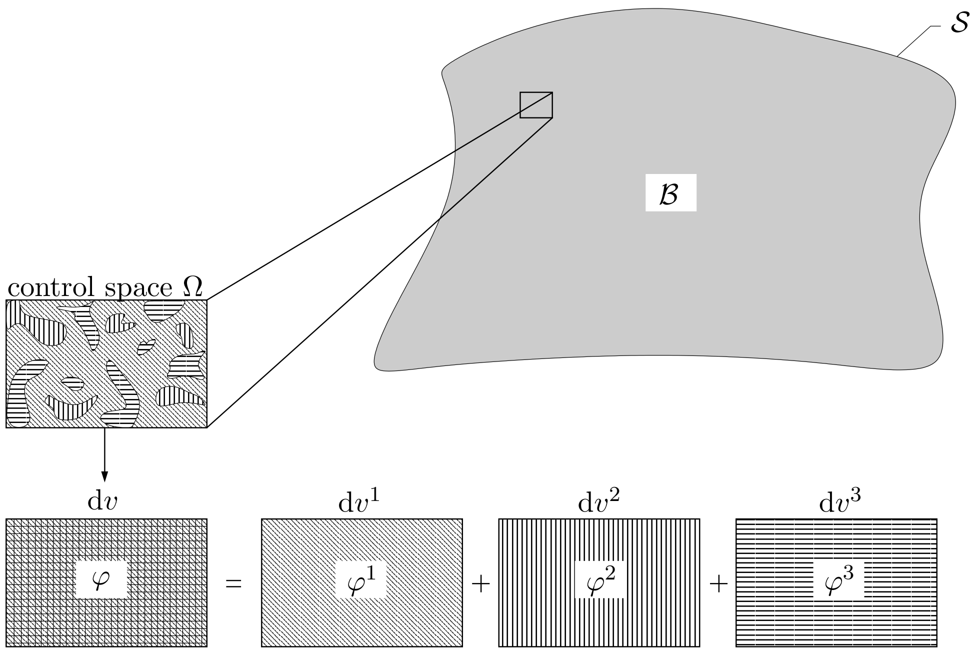

Figure 2.1: Smeared volume element $\mathrm{d}v$ of a porous material consisting of three constituents.

The respective portions of the participating constituents, which, emanating from the preceding assumptions, are considered as superimposed continua, can then be defined with the aid of the *Concept of Volume Fractions*.

2.1 The concept of volume fractions

Proceeding from the statistical distribution of all k individual materials composing the multiphasic body $\mathcal{B}$, the overall model φ arises from the superimposition of the interacting continua φ^α (cf. Figure 2.1) via

$$\varphi = \sum_{\alpha=1}^{k} \varphi^\alpha \, . \tag{2.1}$$

Furthermore, the overall volume V of $\mathcal{B}$ is given by the sum of the partial volumes V^α, which, in turn, can be obtained by integrating the respective volume elements $\mathrm{d}v^\alpha$ over $\mathcal{B}$, i. e.,

$$V = \int_{\mathcal{B}} \mathrm{d}v = \sum_{\alpha=1}^{k} V^\alpha = \sum_{\alpha=1}^{k} \int_{\mathcal{B}} \mathrm{d}v^\alpha \, . \tag{2.2}$$

Since the local mass $\mathrm{d}m^\alpha$ of a constituent can now be related to two different volume elements $\mathrm{d}v^\alpha$ and $\mathrm{d}v$, respectively, two densities, $\rho^{\alpha R}$ and ρ^α, can be defined for each constituent. Relating the local mass $\mathrm{d}m^\alpha$ to the volume element $\mathrm{d}v^\alpha$, one obtains the material (realistic or effective) density of a constituent given by

$$\rho^{\alpha R} = \frac{\mathrm{d}m^\alpha}{\mathrm{d}v^\alpha} \, , \tag{2.3}$$

whereas the partial (global or bulk) density ρ^α relates the same mass to the volume element $\mathrm{d}v$ via

$$\rho^\alpha = \frac{\mathrm{d}m^\alpha}{\mathrm{d}v} \, . \tag{2.4}$$

Introducing the *Concept of Volume Fractions*, the ratio of a partial volume element $\mathrm{d}v^\alpha$ to $\mathrm{d}v$ is defined by

$$n^\alpha = \frac{\mathrm{d}v^\alpha}{\mathrm{d}v} \, . \tag{2.5}$$

From superposition of relations (2.3), (2.4) and (2.5), it can be easily concluded that the different densities of φ^α are related to each other by

$$\rho^\alpha = n^\alpha \rho^{\alpha R} \tag{2.6}$$

with ($\rho^{\alpha R} = \text{const.}$) for the case of the mechanical incompressibility. However, note that $\rho^{\alpha R}$ is a variable parameter, if thermal expansions have to be considered. Moreover, relation (2.5) leads immediately to the so-called saturation condition

$$\sum_{\alpha=1}^{k} n^\alpha = 1 \, , \tag{2.7}$$

which asserts that, in the framework of the TPM, only saturated mixtures are considered.

2.2 Kinematical relations

The fundamentals of the kinematics in continuum mechanics can be found in the common literature, cf., e. g., Altenbach and Altenbach [1], Becker and Bürger [4], Haupt [47] or Truesdell [77]. Concerning multiphasic materials, the corresponding kinematical relations are elaborately discussed, e. g., by de Boer [13] or Ehlers [28, 31]. For the problem to be studied in the present work, the most important relations have been taken from Ehlers [28, 32]. These relations are summarized in this section.

2.2.1 Motion

Presuming superimposed continua, each spatial point of the current configuration, identified by the position vector $\mathbf{x}$, is simultaneously occupied by particles P^α of all k constituents φ^α ($\alpha = S$: solid skeleton, $\alpha = \beta$: $k-1$ pore-fluids). Based on the principles of mixture theories, each constituent is assigned an independent state of motion via

$$\mathbf{x} = \boldsymbol{\chi}_\alpha(\mathbf{X}_\alpha,\, \mathbf{t})\,. \tag{2.8}$$

Thus, the material points of the individual constituents proceed from different reference positions at time $t = t_0$, cf. Figure 2.2.

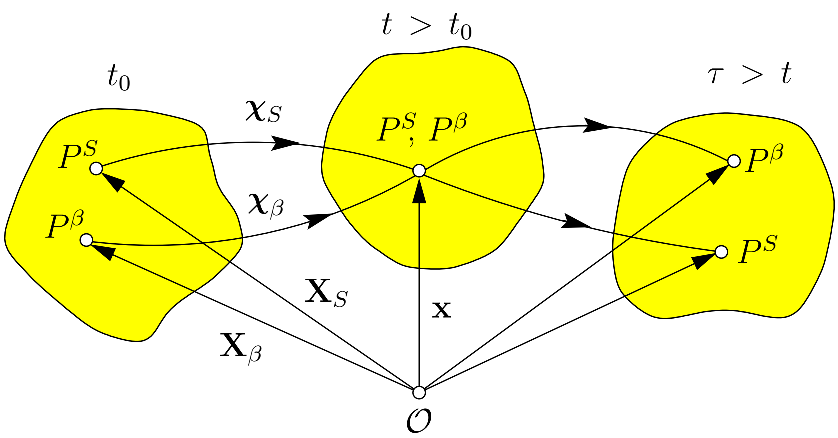

Figure 2.2: Motion of a multiphasic continuum.

According to (2.8), each spatial point can only be occupied by one single material point of each constituent. Furthermore, since the function $\boldsymbol{\chi}_\alpha$ is postulated to be unique and uniquely invertible at any time t, each material point P^α can also be identified by its reference position at time $t = t_0$, viz.:

$$\mathbf{X}_\alpha = \boldsymbol{\chi}_\alpha^{-1}(\mathbf{x},\, t)\,. \tag{2.9}$$

The mathematically necessary and sufficient condition for the existence of the inverse motion $\boldsymbol{\chi}_\alpha^{-1}$ is given by non-negative *Jacobi*an determinants J_α of the constituents:

$$J_\alpha = \det \frac{\partial \boldsymbol{\chi}_\alpha}{\partial \mathbf{X}_\alpha} \neq 0 \,. \tag{2.10}$$

2.2.2 Velocity and acceleration fields

Considering separate functions of motion for each constituent, separate velocity as well as acceleration fields exist for the individual phases, which, in the *Lagrange*an description, are given as follows:

$$\begin{aligned} \overset{\prime}{\mathbf{x}}_\alpha = \overset{\prime}{\mathbf{x}}_\alpha\,(\mathbf{X}_\alpha,\, t) &= \frac{\partial \boldsymbol{\chi}_\alpha(\mathbf{X}_\alpha,\, t)}{\partial t}\,, \\ \overset{\prime\prime}{\mathbf{x}}_\alpha = \overset{\prime\prime}{\mathbf{x}}_\alpha\,(\mathbf{X}_\alpha,\, t) &= \frac{\partial^2 \boldsymbol{\chi}_\alpha(\mathbf{X}_\alpha,\, t)}{\partial t^2}\,. \end{aligned} \tag{2.11}$$

These fields can also be formulated in the *Euler*ian description by use of the inverse motion functions (2.9). Thus,

$$\begin{aligned} \overset{\prime}{\mathbf{x}}_\alpha &= \overset{\prime}{\mathbf{x}}_\alpha\,(\mathbf{x},\, t), \\ \overset{\prime\prime}{\mathbf{x}}_\alpha &= \overset{\prime\prime}{\mathbf{x}}_\alpha\,(\mathbf{x},\, t)\,. \end{aligned} \tag{2.12}$$

In the framework of the TPM, the solid phase φ^S is described, in general, by a *Lagrange*an formulation using the displacement vector $\mathbf{u}_S$, which is introduced as

$$\mathbf{u}_S = \mathbf{x} - \mathbf{X}_S\,. \tag{2.13}$$

Unlike this, the $(k-1)$ pore-fluids φ^β are related to the deforming solid skeleton in a modified *Euler*ian view. This is achieved by introducing the seepage velocities via

$$\mathbf{w}_\beta = \overset{\prime}{\mathbf{x}}_\beta - \overset{\prime}{\mathbf{x}}_S\,, \tag{2.14}$$

which describe the fluid motion with respect to the deforming solid skeleton.

After separate velocity fields have been stated for each constituent, the so-called mixture velocity, also referred to as *barycentric velocity*, can be defined as an average of density-weighted velocities of the individual phases, viz.:

$$\dot{\mathbf{x}} = \frac{1}{\rho} \sum_{\alpha=1}^{k} \rho^\alpha\, \overset{\prime}{\mathbf{x}}_\alpha\ . \tag{2.15}$$

Therein, ρ represents the so-called mixture density and is given as

$$\rho = \sum_{\alpha=1}^{k} \rho^\alpha\,. \tag{2.16}$$

A further kinematical measure is the *diffusion velocity* stated as the relative velocity of the phase φ^α with respect to the mixture φ via

$$\mathbf{d}_\alpha = \overset{\prime}{\mathbf{x}}_\alpha - \dot{\mathbf{x}}\ . \tag{2.17}$$

Combining (2.15), (2.16) and (2.17), one immediately obtains

$$\sum_{\alpha=1}^{k} \rho^\alpha \, \mathbf{d}_\alpha \;=\; \mathbf{0}\,, \tag{2.18}$$

which proves that the diffusion mass flows of the constituents are summing up to zero. Furthermore, it should be noted that the two velocities $\overset{\prime}{\mathbf{x}}_\alpha$ and $\dot{\mathbf{x}}$, respectively, follow different time derivatives. Suppose that Γ is an arbitrary, steady, and sufficiently often steadily differentiable scalar function of $(\mathbf{x},\, t)$, then, the material time derivative of Γ reads

$$(\Gamma)'_\alpha := \frac{\mathrm{d}_\alpha}{\mathrm{d}t}\,\Gamma \;=\; \frac{\partial \Gamma}{\partial t} + \operatorname{grad}\Gamma \cdot \overset{\prime}{\mathbf{x}}_\alpha \;\;. \tag{2.19}$$

As seen in (2.19), $(\Gamma)'_\alpha$ follows the motion of φ^α. Unlike this, the so-called mixture derivative of Γ is related to the motion of the overall medium φ, i. e.,

$$\dot{\Gamma} := \frac{\mathrm{d}}{\mathrm{d}t}\,\Gamma \;=\; \frac{\partial \Gamma}{\partial t} + \operatorname{grad}\Gamma \cdot \dot{\mathbf{x}} \;\;. \tag{2.20}$$

The operator "grad$\,(\,\cdot\,)$" in the time derivatives above denotes the partial derivative of $(\,\cdot\,)$ with respect to the local position $\mathbf{x}$. With the aid of the time derivative (2.19) and the seepage velocity (2.14), any material time derivative of the fluid constituent φ^β can now be expressed with respect to the solid constituent φ^S via

$$(\Gamma^\beta)'_\beta = (\Gamma^\beta)'_S + \operatorname{grad}\Gamma^\beta \cdot \mathbf{w}_\beta \,. \tag{2.21}$$

In addition, the combination of (2.18), (2.19) and (2.20) enables the formulation of material time derivatives for φ^α with respect to the mixture:

$$(\Gamma^\alpha)'_\alpha = (\Gamma^\alpha)^{\boldsymbol{\cdot}} + \operatorname{grad}\Gamma \cdot \mathbf{d}_\alpha \,. \tag{2.22}$$

2.2.3 Deformation gradient

Proceeding from (2.8), the material deformation gradient $\mathbf{F}_\alpha$ is introduced for each constituent via

$$\mathbf{F}_\alpha = \frac{\mathrm{d}\boldsymbol{\chi}_\alpha(\mathbf{X}_\alpha)}{\mathrm{d}\mathbf{X}_\alpha} = \frac{\mathrm{d}\mathbf{x}}{\mathrm{d}\mathbf{X}_\alpha} = \operatorname{Grad}_\alpha \mathbf{x} \,. \tag{2.23}$$

Therein, the operator "Grad$_\alpha\,(\,\cdot\,)$" denotes the partial derivative of $(\,\cdot\,)$ with respect to the reference position $\mathbf{X}_\alpha$ of φ_α. Furthermore, $\mathbf{F}_\alpha$ can be considered as a mapping in order to carry a line element $\mathrm{d}\mathbf{X}_\alpha$ of the reference configuration into a line element $\mathrm{d}\mathbf{x}$ of the current configuration. According to this, the reverse transformation of the line element from the actual configuration to the referential configuration can be achieved by using the inverse of the deformation gradient, which is defined as

$$\mathbf{F}_\alpha^{-1} = \frac{\mathrm{d}\boldsymbol{\chi}_\alpha^{-1}(\mathbf{X}_\alpha)}{\mathrm{d}\mathbf{x}} = \frac{\mathrm{d}\mathbf{X}_\alpha}{\mathrm{d}\mathbf{x}} = \operatorname{grad}\mathbf{X}_\alpha \,. \tag{2.24}$$

Recall that $\mathbf{X}_\alpha$ and $\mathbf{x}$ represent the position vectors of the material point P^α at the time $t = t_0$ and t, respectively. Furthermore, the vectors $\mathrm{d}\mathbf{X}_\alpha$ and $\mathrm{d}\mathbf{x}$ can be interpreted to identify the position of an arbitrary point in the referential neighborhood of P at the different times.

2.2.4 Deformation and strain measures

In order to describe local deformations, use is made of the right and left *Cauchy-Green* deformation tensors

$$\mathbf{C}_\alpha = \mathbf{F}_\alpha^T \mathbf{F}_\alpha\,, \quad \mathbf{B}_\alpha = \mathbf{F}_\alpha \mathbf{F}_\alpha^T\,. \tag{2.25}$$

Furthermore, the *Green-Lagrange*an strain $\mathbf{E}_\alpha$ and the *Karni-Reiner* strain $\mathbf{K}_\alpha$ are introduced as corresponding strain measures via

$$\begin{aligned} \mathbf{E}_\alpha &= \tfrac{1}{2}(\mathbf{C}_\alpha - \mathbf{I})\,, \\ \mathbf{K}_\alpha &= \tfrac{1}{2}\,(\mathbf{B}_\alpha - \mathbf{I})\,. \end{aligned} \tag{2.26}$$

2.2.5 Strain and deformation rates

The previously introduced measures for strain and deformation are only applicable in solid mechanics. Describing fluid particles in motion, the emphasis is put on the determination of the **velocities** of the material points in the control space. Considering the velocity as the dependent variable, it seems reasonable to determine the time rate of deformations. Proceeding from the definition of the *Lagrange*an velocity field $(2.11)_1$, the material velocity gradient is identified as

$$(\mathbf{F}_\alpha)'_\alpha = \mathrm{Grad}_\alpha\, \overset{\prime}{\mathbf{x}}_\alpha\ . \tag{2.27}$$

Since fluids are described in the *Euler*ian view, the introduction of the spatial velocity gradient $\mathbf{L}_\alpha$ is of higher interest, when deformation rates have to be calculated. Proceeding from $(2.12)_1$, the spatial velocity gradient is defined via

$$\mathbf{L}_\alpha = \mathrm{grad}_\alpha\, \overset{\prime}{\mathbf{x}}_\alpha = (\mathbf{F}_\alpha)'_\alpha \mathbf{F}_\alpha^{-1}\,, \tag{2.28}$$

where

$$\mathbf{L}_\alpha \cdot \mathbf{I} = \mathrm{div}\, \overset{\prime}{\mathbf{x}}_\alpha \tag{2.29}$$

holds; $\mathrm{div}\,(\cdot)$ is the divergence operator corresponding to $\mathrm{grad}\,(\cdot)$. The material velocity gradient $\mathbf{L}_\alpha$ can be additively decomposed into the symmetric rate of deformation

$$\mathbf{D}_\alpha = \tfrac{1}{2}(\mathbf{L}_\alpha + \mathbf{L}_\alpha^T) \tag{2.30}$$

and the skew-symmetric rate of rotation

$$\mathbf{W}_\alpha = \tfrac{1}{2}(\mathbf{L}_\alpha - \mathbf{L}_\alpha^T)\,. \tag{2.31}$$

Thus,

$$\mathbf{L}_\alpha = \mathbf{D}_\alpha + \mathbf{W}_\alpha = \tfrac{1}{2}(\mathbf{L}_\alpha + \mathbf{L}_\alpha^T) + \tfrac{1}{2}(\mathbf{L}_\alpha - \mathbf{L}_\alpha^T)\,. \tag{2.32}$$

Furthermore, for the *Green-Lagrange*an strain rate $(\mathbf{E}_\alpha)'_\alpha$, the following relation holds

$$(\mathbf{E}_\alpha)'_\alpha = \tfrac{1}{2}(\mathbf{C}_\alpha)'_\alpha\,. \tag{2.33}$$

2.3 Stress

Following *Cauchy*'s fundamental theorem, the partial stress tensor $\mathbf{T}^\alpha$ is defined as

$$\mathbf{t}^\alpha(\mathbf{x}, t, \mathbf{n}) = \mathbf{T}^\alpha\,\mathbf{n} \tag{2.34}$$

with $\mathbf{t}^\alpha$ being the partial stress vector acting on a cut surface and $\mathbf{n}$ as the outward oriented unit surface normal. In addition, the *Kirchhoff* stress is introduced as

$$\boldsymbol{\tau}^\alpha = \det\mathbf{F}_\alpha\mathbf{T}^\alpha\,. \tag{2.35}$$

2.4 Balance relations

The balance relations for multiphasic materials are extensively discussed in the works by de Boer [11, 13], de Boer and Ehlers [16], Bowen [17–19], Diebels and Ehlers [24] and Ehlers [27, 28, 31, 32]. In the following section, first the general structure of balance relations will be explained. Furthermore, the partial balance relations are given according to the axiomatic definition (cf., e. g., Ehlers [28]) of the individual mechanical and thermodynamic physical quantities to be balanced.

2.4.1 General framework

Taking the interaction mechanisms between the individual constituents of a multiphasic material into consideration, the balance relations for a mixture body can be formulated in analogy to those for single-phasic materials in the classical continuum mechanics. The foundation for the constitution of balance relations in multiphasic bodies is comprised in *Truesdell*'s "metaphysical principles" of mixture theories, cf. [76, p. 221] :

1. *All properties of the mixture must be mathematical consequences of properties of the constituents.*

2. *So as to describe the motion of a constituent, we may in imagination isolate it from the rest of the mixture, provided we allow properly for the actions of the other constituents upon it.*

3. *The motion of the mixture is governed by the same equations as is a single body.*

Proceeding from the second principle, the general structure of balance relations for a constituent φ^α (cf., e. g., Ehlers [28]) is of the form

$$
\begin{aligned}
\frac{\mathrm{d}_\alpha}{\mathrm{d}t}\int_{\mathcal{B}} \Psi^\alpha \,\mathrm{d}v &= \int_{\mathcal{S}} (\boldsymbol{\phi}^\alpha \cdot \mathbf{n})\,\mathrm{d}a + \int_{\mathcal{B}} \sigma^\alpha \,\mathrm{d}v + \int_{\mathcal{B}} \hat{\Psi}^\alpha \,\mathrm{d}v\,,\\
\frac{\mathrm{d}_\alpha}{\mathrm{d}t}\int_{\mathcal{B}} \mathbf{\Psi}^\alpha \,\mathrm{d}v &= \int_{\mathcal{S}} (\mathbf{\Phi}^\alpha \, \mathbf{n})\,\mathrm{d}a + \int_{\mathcal{B}} \boldsymbol{\sigma}^\alpha \,\mathrm{d}v + \int_{\mathcal{B}} \hat{\mathbf{\Psi}}^\alpha \,\mathrm{d}v\,.
\end{aligned}
\tag{2.36}
$$

Therein, Ψ^α or $\mathbf{\Psi}^\alpha$, respectively, are the volume-specific scalar- or vector-valued physical quantities to be balanced in φ^α. Furthermore, $(\boldsymbol{\phi}^\alpha \cdot \mathbf{n})$ or $(\mathbf{\Phi}^\alpha\, \mathbf{n})$, respectively, are the efflux terms of the physical quantities at the surface $\mathcal{S}$ of $\mathcal{B}$ (the external vicinity of φ^α), whereas supply terms, generated from the external distance of φ^α, are represented by σ^α or $\boldsymbol{\sigma}^\alpha$, respectively. In addition, the production term $\hat{\Psi}^\alpha$ incorporates possible interactions between φ^α and its surrounding. Analogously, $\hat{\mathbf{\Psi}}^\alpha$ represents these couplings for vector-valued physical quantities.

Using the *Gauss*ian integral theorem (cf., e. g., de Boer [12]), the surface integrals of the right-hand side in (2.36) can be transformed into volume integrals. Furthermore, all integrands are assumed to be steady and steadily differentiable so that the differentiation of the left-hand side of (2.36) yields the corresponding local forms of the general balance relations for a constituent φ^α:

$$
\begin{aligned}
(\Psi^\alpha)'_\alpha + \Psi^\alpha \operatorname{div} \overset{\prime}{\mathbf{x}}_\alpha &= \operatorname{div} \boldsymbol{\phi}^\alpha + \sigma^\alpha + \hat{\Psi}^\alpha\,,\\
(\mathbf{\Psi}^\alpha)'_\alpha + \mathbf{\Psi}^\alpha \operatorname{div} \overset{\prime}{\mathbf{x}}_\alpha &= \operatorname{div} \mathbf{\Phi}^\alpha + \boldsymbol{\sigma}^\alpha + \hat{\mathbf{\Psi}}^\alpha\,.
\end{aligned}
\tag{2.37}
$$

Concerning the specific balance equations of the constituents, the well-known axioms for the individual physical quantities to be balanced, namely, the mass density, linear momentum, moment of momentum (m. o. m.), the total energy and the entropy, lead to the representation given in Table 2.1, cf. Ehlers [28].

	Ψ^α, $\mathbf{\Psi}^\alpha$	$\boldsymbol{\phi}^\alpha$, $\boldsymbol{\phi}^\alpha$	σ^α, $\boldsymbol{\sigma}^\alpha$	$\hat{\Psi}^\alpha$, $\hat{\mathbf{\Psi}}^\alpha$
mass	ρ^α	$\mathbf{0}$	0	$\hat{\rho}^\alpha$
momentum	$\rho^\alpha \overset{\prime}{\mathbf{x}}_\alpha$	$\mathbf{T}^\alpha$	$\rho^\alpha \mathbf{b}^\alpha$	$\hat{\mathbf{s}}^\alpha$
m. o. m.	$\mathbf{x} \times (\rho^\alpha \overset{\prime}{\mathbf{x}}_\alpha)$	$\mathbf{x} \times \mathbf{T}^\alpha$	$\mathbf{x} \times (\rho^\alpha \mathbf{b}^\alpha)$	$\hat{\mathbf{h}}^\alpha$
energy	$\rho^\alpha \varepsilon^\alpha + \frac{1}{2}\, \overset{\prime}{\mathbf{x}}_\alpha \cdot (\rho^\alpha \overset{\prime}{\mathbf{x}}_\alpha)$	$(\mathbf{T}^\alpha)^T \overset{\prime}{\mathbf{x}}_\alpha - \mathbf{q}^\alpha$	$\overset{\prime}{\mathbf{x}}_\alpha \cdot (\rho^\alpha\, \mathbf{b}^\alpha) + \rho^\alpha r^\alpha$	$\hat{e}^\alpha$
entropy	$\rho^\alpha\, \eta^\alpha$	$\boldsymbol{\phi}^\alpha_\eta$	σ^α_η	$\hat{\eta}^\alpha$

Table 2.1: Balance relations for a constituent φ^α of the overall medium φ.

Therein, $\rho^\alpha\,\mathbf{b}^\alpha$ represents the volume forces (such as the gravitational force) in φ^α. Furthermore, $\mathbf{q}^\alpha$ is the heat influx vector and r^α is the external heat supply. The internal energy of φ^α is given by ε^α.

When balance relations are derived (cf., e. g., Ehlers [27, 28, 32]), it can be seen that lower balances are used in order to obtain higher balances. As a result of this procedure, the respective total productions contain, additionally to the corresponding direct production terms, supplementary expressions arising from lower productions. The composition of the respective total production terms of the constituents reads

$$
\begin{aligned}
\hat{\mathbf{s}}^\alpha &= \hat{\mathbf{p}}^\alpha + \hat{\rho}^\alpha\,\overset{\prime}{\mathbf{x}}_\alpha\,,\\
\hat{\mathbf{h}}^\alpha &= \hat{\mathbf{m}}^\alpha + \mathbf{x}\times(\hat{\mathbf{p}}^\alpha + \hat{\rho}^\alpha\,\overset{\prime}{\mathbf{x}}_\alpha)\,,\\
\hat{e}^\alpha &= \hat{\varepsilon}^\alpha + \hat{\mathbf{p}}^\alpha\cdot\overset{\prime}{\mathbf{x}}_\alpha + \hat{\rho}^\alpha(\,\varepsilon^\alpha + \tfrac{1}{2}\,\overset{\prime}{\mathbf{x}}_\alpha\cdot\overset{\prime}{\mathbf{x}}_\alpha)\,,\\
\hat{\eta}^\alpha &= \hat{\zeta}^\alpha + \hat{\rho}^\alpha\,\eta^\alpha\,.
\end{aligned}
\tag{2.38}
$$

Therein, $\hat{\mathbf{p}}^\alpha$, $\hat{\mathbf{m}}^\alpha$, $\hat{\varepsilon}^\alpha$ and $\hat{\zeta}^\alpha$, respectively, represent the direct production terms of the corresponding physical quantities. The balance relations for φ^α (cf. Ehlers [28]) are given as

$$
\begin{array}{lrcl}
\bullet\ \text{mass:} & (\rho^\alpha)'_\alpha + \rho^\alpha\,\mathrm{div}\,\overset{\prime}{\mathbf{x}}_\alpha & = & \hat{\rho}^\alpha,\\
\bullet\ \text{momentum:} & \rho^\alpha\,\overset{\prime\prime}{\mathbf{x}}_\alpha & = & \mathrm{div}\,\mathbf{T}^\alpha + \rho^\alpha\,\mathbf{b}^\alpha + \hat{\mathbf{p}}^\alpha\,,\\
\bullet\ \text{m. o. m.:} & \mathbf{0} & = & \mathbf{I}\times\mathbf{T}^\alpha + \hat{\mathbf{m}}^\alpha,\\
\bullet\ \text{energy:} & \rho^\alpha(\varepsilon^\alpha)'_\alpha & = & \mathbf{T}^\alpha\cdot\mathbf{L}_\alpha - \mathrm{div}\,\mathbf{q}^\alpha + \rho^\alpha\,r^\alpha + \hat{\varepsilon}^\alpha,\\
\bullet\ \text{entropy:} & \rho^\alpha\,(\eta^\alpha)'_\alpha & = & \mathrm{div}\,(-\dfrac{1}{\theta^\alpha}\,\mathbf{q}^\alpha) + \dfrac{1}{\theta^\alpha}\rho^\alpha\,r^\alpha + \hat{\zeta}^\alpha\,.
\end{array}
\tag{2.39}
$$

Following the "metaphysical principles" of *Truesdell*, the sum of the individual balance equations over all k constituents must result in the balance relations of the mixture. This leads to the specific constraints of the production terms, viz.:

$$
\sum_{\alpha=1}^{k}\hat{\rho}^\alpha = 0\,,\quad \sum_{\alpha=1}^{k}\hat{\mathbf{s}}^\alpha = \mathbf{0}\,,\quad \sum_{\alpha=1}^{k}\hat{\mathbf{h}}^\alpha = \mathbf{0}\,,\quad \sum_{\alpha=1}^{k}\hat{e}^\alpha = 0\,,\quad \hat{\eta} = \sum_{\alpha=1}^{k}\hat{\eta}^\alpha \geq 0\,. \tag{2.40}
$$

2.4.2 The absence of mass productions

The special case of the absence of mass productions should be discussed separately, since this case leads to some special simplifications. In the absence of $\hat{\rho}^\alpha$, the total productions in (2.38) reduce to

$$\hat{\rho}^\alpha \equiv 0 \quad \rightarrow \quad \left\{ \begin{array}{rcl} \hat{\mathbf{s}}^\alpha & = & \hat{\mathbf{p}}^\alpha \,, \\ \hat{\mathbf{h}}^\alpha & = & \hat{\mathbf{m}}^\alpha + \mathbf{x} \times \hat{\mathbf{p}}^\alpha \,, \\ \hat{e}^\alpha & = & \hat{\varepsilon}^\alpha + \hat{\mathbf{p}}^\alpha \cdot \overset{\prime}{\mathbf{x}}_\alpha \,, \\ \hat{\eta}^\alpha & = & \hat{\zeta}^\alpha \,. \end{array} \right. \tag{2.41}$$

Furthermore, as a result of (2.41), one obtains from (2.40) for the sum relations of the total momentum production and the total entropy production

$$\hat{\rho}^\alpha \equiv 0 \quad \rightarrow \quad \left\{ \begin{array}{rcl} \mathbf{0} & = & \sum\limits_{\alpha=1}^{k} \hat{\mathbf{p}}^\alpha \,, \\ \mathbf{0} & = & \sum\limits_{\alpha=1}^{k} \hat{\mathbf{m}}^\alpha \,, \\ 0 & = & \sum\limits_{\alpha=1}^{k} (\hat{\varepsilon}^\alpha + \hat{\mathbf{p}}^\alpha \cdot \overset{\prime}{\mathbf{x}}_\alpha) \,, \\ \hat{\eta} & = & \sum\limits_{\alpha=1}^{k} \hat{\zeta}^\alpha \geq 0 \,. \end{array} \right. \tag{2.42}$$

As a further consequence, the mass balance equation of φ^α $(2.39)_1$ is now identical to the mass balance equation of a single-phasic material. Thus, the partial density $\rho^\alpha_{0\alpha}$ of φ^α at time $t = t_0$ can be integrated via

$$\rho^\alpha_{0\alpha} = \rho^\alpha \det \mathbf{F}_\alpha \,. \tag{2.43}$$

2.4.3 The entropy principle in the TPM

A detailed discussion of the historical development of the entropy principle for multiphasic materials can be found in de Boer [13] or Ehlers [31]. Therein, it can also be seen that the specific internal energy ε^α, analogously to the classical thermodynamics of one-component materials, can be substituted by the free *Helmholtz* energy function ψ^α via

$$\psi^\alpha := \varepsilon^\alpha - \theta^\alpha \eta^\alpha \,. \tag{2.44}$$

By use of $(2.42)_4$ and (2.44), summing up the entropy balances $(2.39)_5$ yields the mostly used form of the entropy principle for multiphasic materials (cf., e. g., Ehlers [28])

$$\begin{aligned} \sum_{\alpha=1}^{k} \frac{1}{\theta^\alpha} \Big[& \mathbf{T}^\alpha \cdot \mathbf{L}_\alpha - \rho^\alpha \left[(\psi^\alpha)'_\alpha + (\theta^\alpha)'_\alpha \eta^\alpha \right] - \hat{\mathbf{p}}^\alpha \cdot \overset{\prime}{\mathbf{x}}_\alpha - \\ & - \hat{\rho}^\alpha \left(\psi^\alpha + \tfrac{1}{2} \overset{\prime}{\mathbf{x}}_\alpha \cdot \overset{\prime}{\mathbf{x}}_\alpha \right) - \frac{1}{\theta^\alpha} \mathbf{q}^\alpha \cdot \operatorname{grad} \theta^\alpha + \hat{e}^\alpha \Big] \geq 0 \,. \end{aligned} \tag{2.45}$$

2.4.4 The modified energy balance equation

The free *Helmholtz* energy (2.44) can also be substituted to the energy balance relation $(2.39)_4$. Thus, the energy balance equation of φ^α can alternatively be written as

$$-\rho^\alpha[\,(\psi^\alpha)'_\alpha + (\theta^\alpha)'_\alpha \eta^\alpha + \theta^\alpha (\eta^\alpha)'_\alpha\,] + \mathbf{T}^\alpha \cdot \mathbf{L}_\alpha - \operatorname{div} \mathbf{q}^\alpha + \rho^\alpha r^\alpha + \hat{\varepsilon}^\alpha = 0\,. \tag{2.46}$$

Chapter 3: The non-isothermal biphasic model

As is seen from the foundations of the TPM in the preceding chapter, a variety of possibilities exist for the definition of coupled solid-fluid models by use of this theory, cf., e. g., Blome [7], Bluhm [9, 10], Diebels [23], Droste [25], Ehlers and Markert [35, 36], Eipper [37], Ellsiepen [38], Mahnkopf [57], Müllerschön [60] or Volk [79].

In particular, since each constituent, taking the interactions into consideration, is treated isolated from its surrounding and, thus, on the basis of its own thermodynamic and mechanical behavior, different material laws can be considered for the individual constituents. For instance, the solid skeleton ($\alpha = S$) can possess elastic, viscoelastic, elasto-plastic or elasto-viscoplastic material properties and may undergo small or finite deformations. In addition, the fluid phase as a single-fluid, single-liquid ($\alpha = L$) or single-gas ($\alpha = G$), or as a multiple fluid consisting of an arbitrary number of several liquids and gases, can behave compressible or incompressible and is generally governed by viscous material behavior.

For the theoretical investigation of the fluid-saturated porous liner under consideration (cf. Chapter 1), one has to create a biphasic model consisting of a materially incompressible solid skeleton φ^S with thermo-elastic material properties and a single viscous pore-fluid φ^G, which behaves materially compressible. It is pointed out that the incompressibility of the solid skeleton only belongs to the mechanical and not to the thermal behavior, i. e.

$$\rho^{SR} := \rho^{SR}\left(\theta^S\right). \tag{3.1}$$

Unlike the solid skeleton, the fluid constituent in terms of both, mechanical and thermal loads, behaves compressible, i. e.,

$$\rho^{GR} := \rho^{GR}\left(\theta^G, p^{GR}\right), \tag{3.2}$$

where p^{GR} is the effective (real) gas pressure.

The biphasic model under consideration must enable the computation of the pressure, the velocity and the temperature of the pore-gas (the coolant) as well as the deformation and the temperature of the solid skeleton (porous C/C liner). In order to determine these five degree od freedoms, a system of five equations is required. However, if quasi-static processes are considered, this system of equation can be reduced to four. This will be shown in Section 3.4. The set of the equations for the dynamic formulation of the problem is given in Appendix B.

All necessary relations, the thermodynamic potentials as well as the constitutive equations, which are required in order to create the corresponding system of equations, will be obtained from the evaluation of the entropy inequality in Sections 3.2 and 3.3. The determining entropy inequality for the model under consideration as well as the determining constitutive variables governing the thermodynamic processes are discussed in Section 3.1. It is pointed out that, for the sake of clarity, the detailed derivation of most of the relations discussed in this chapter is separately given in Appendix B.

It should be pointed out that the evaluation of the entropy inequality for a general non-isothermal biphasic model is given in Bluhm [8], wherein, however, some constitutive equations are not sufficiently physically motivated.

Preliminaries. For the model under consideration, it is assumed that no phase transitions occur during the physical processes. Consequently, the absence of mass productions

$$\hat{\rho}^S = \hat{\rho}^G = 0 \tag{3.3}$$

yields the first simplifications (cf. Subsection 2.4.2) via

$$\begin{aligned} \hat{\mathbf{p}}^S &= -\hat{\mathbf{p}}^G \,, \\ \hat{e}^S &= \hat{\varepsilon}^S + \hat{\mathbf{p}}^S \cdot \overset{\prime}{\mathbf{x}}_S \,, \\ \hat{e}^G &= \hat{\varepsilon}^G + \hat{\mathbf{p}}^G \cdot \overset{\prime}{\mathbf{x}}_G \;. \end{aligned} \tag{3.4}$$

Considering $(2.40)_4$ together with $(3.4)_{2,3}$, one obtains

$$\begin{aligned} \hat{\varepsilon}^S &= -\hat{\varepsilon}^G - \hat{\mathbf{p}}^G \cdot \overset{\prime}{\mathbf{x}}_G + \hat{\mathbf{p}}^G \cdot \overset{\prime}{\mathbf{x}}_S \\ &= -\hat{\varepsilon}^G - \hat{\mathbf{p}}^G \cdot \mathbf{w}_G \,, \end{aligned} \tag{3.5}$$

where the notion of the seepage velocity from (2.14) has been used.

3.1 Constitutive theory

The unknown variables of the model under consideration will be determined from the calculation of the governing system of equations, which, in turn, can be created by the corresponding balance relations. For the quantities included in the balance relations, appropriate constitutive equations must be formulated in such a way that the entropy principle is satisfied, cf., e. g., Ehlers [28, 31]. The thermodynamic restrictions for the formulation of constitutive equations will be obtained from the evaluation of the entropy inequality in Section 3.2.

Before the evaluation of the entropy inequality can be carried out, the determining entropy inequality as well as the set of the governing constitutive variables are discussed in Subsections 3.1.1 and 3.1.3. In Subsection 3.1.2, the deformation of the mechanically and materially incompressible solid constituent will be multiplicatively decomposed, which yields some important informations for the discussion of the governing constitutive variables.

3.1.1 The determining entropy inequality

The entropy inequality for the model under consideration can be obtained from (2.45), which, considering (3.3), yields for ($\alpha = S, G$)

$$\begin{aligned} &\frac{1}{\theta^S}\Big[\mathbf{T}^S\cdot\mathbf{L}_S - \rho^S\,(\psi^S)'_S - \rho^S(\theta^S)'_S\,\eta^S - \hat{\mathbf{p}}^S\cdot\overset{\prime}{\mathbf{x}}_S\ - \\ &-\frac{1}{\theta^S}\,\mathbf{q}^S\ \cdot\mathrm{grad}\,\theta^S + \hat{e}^S\Big] + \frac{1}{\theta^G}\Big[\mathbf{T}^G\cdot\mathbf{L}_G - \rho^G\,(\psi^G)'_G + \\ &+\hat{e}^G - \rho^G(\theta^G)'_G\,\eta^G - \hat{\mathbf{p}}^G\cdot\overset{\prime}{\mathbf{x}}_G\ - \frac{1}{\theta^G}\,\mathbf{q}^G\cdot\mathrm{grad}\,\theta^G\Big] \geq 0\,. \end{aligned} \tag{3.6}$$

Reformulation of the inequality. The multiplication of (3.6) by either θ^S or θ^G would allow for simplifications. Here, θ^S is chosen to be multiplied with the inequality above, by which the prefactor $1/\theta^S$ is eliminated. Thus, the inequality becomes

$$\begin{aligned} &\mathbf{T}^S\cdot\mathbf{L}_S + \frac{\theta^S}{\theta^G}\,\mathbf{T}^G\cdot\mathbf{L}_G - \ \rho^S\,(\psi^S)'_S - \rho^S(\theta^S)'_S\,\eta^S + \hat{e}^S - \hat{\mathbf{p}}^S\cdot\overset{\prime}{\mathbf{x}}_S\ - \\ &-\frac{\theta^S}{\theta^G}\,\rho^G\,(\psi^G)'_G - \frac{\theta^S}{\theta^G}\,\rho^G(\theta^G)'_G\,\eta^G + \frac{\theta^S}{\theta^G}\,\hat{e}^G - \frac{\theta^S}{\theta^G}\,\hat{\mathbf{p}}^G\cdot\overset{\prime}{\mathbf{x}}_G\ - \\ &-\frac{1}{\theta^S}\,\mathbf{q}^S\ \cdot\mathrm{grad}\,\theta^S\ - \frac{\theta^S}{(\theta^G)^2}\,\mathbf{q}^G\cdot\mathrm{grad}\,\theta^G \geq 0\,. \end{aligned} \tag{3.7}$$

Some terms in (3.7) can be reformulated by use of the seepage velocity (2.14) and the specific constraints $(2.40)_2$, $(2.40)_4$ and $(2.42)_1$ as well as by consideration of the total productions $(2.41)_1$ and $(2.41)_3$. First, the total energy productions can be summarized as follows

$$\hat{e}^S + \frac{\theta^S}{\theta^G}\hat{e}^G = \hat{e}^G\left(\frac{\theta^S}{\theta^G} - 1\right) = \hat{\varepsilon}^G\left(\frac{\theta^S}{\theta^G} - 1\right) + \hat{\mathbf{p}}^G\cdot\overset{\prime}{\mathbf{x}}_G\left(\frac{\theta^S}{\theta^G} - 1\right). \tag{3.8}$$

Furthermore, one obtains for the so-called interaction powers

$$-\,\hat{\mathbf{p}}^S\cdot\overset{\prime}{\mathbf{x}}_S - \frac{\theta^S}{\theta^G}\,\hat{\mathbf{p}}^G\cdot\overset{\prime}{\mathbf{x}}_G = -\,\hat{\mathbf{p}}^G\cdot\mathbf{w}_G - \hat{\mathbf{p}}^G\cdot\overset{\prime}{\mathbf{x}}_G\left(\frac{\theta^S}{\theta^G} - 1\right). \tag{3.9}$$

The incorporation of (3.8) and (3.9) in (3.7) yields for the entropy inequality the following form

$$\begin{aligned} &\mathbf{T}^S\cdot\mathbf{L}_S + \frac{\theta^S}{\theta^G}\,\mathbf{T}^G\cdot\mathbf{L}_G - \rho^S\,(\psi^S)'_S - \rho^S(\theta^S)'_S\,\eta^S - \frac{\theta^S}{\theta^G}\,\rho^G\,(\psi^G)'_G - \\ &-\rho^G(\,\theta^G\,)'_G\,\eta^G + \hat{\varepsilon}^G\left(\frac{\theta^S}{\theta^G} - 1\right) - \ \hat{\mathbf{p}}^G\cdot\mathbf{w}_G - \frac{1}{\theta^S}\,\mathbf{q}^S\ \cdot\mathrm{grad}\,\theta^S - \\ &-\frac{\theta^S}{(\theta^G)^2}\,\mathbf{q}^G\cdot\mathrm{grad}\,\theta^G \geq 0\,. \end{aligned} \tag{3.10}$$

Saturation condition as a constraint. It can be seen in articles on the theoretical treatment of isothermal multiphase problems with materially incompressible constituents (cf., e. g., Ehlers [28]) that a modified saturation condition, called the *incompressibility constraint*, is introduced in the corresponding entropy inequality. This is conducted in order to obtain the so-called *extra* terms $(\cdot)_E$ for the stresses as well as the interaction forces. For non-isothermal processes, analogously, it is necessary to formulate an appropriate constraint. The starting point for the definition of such a constraint for non-isothermal processes is likewise the saturation condition, viz.:

$$n^S + n^G = 1 \quad \text{or} \quad (n^S)'_S + (n^G)'_S = 0\,, \tag{3.11}$$

respectively. Taking advantage of (2.21), the saturation condition $(3.11)_2$ can also be expressed as

$$(n^S)'_S + (n^G)'_G - \operatorname{grad} n^G \cdot \mathbf{w}_G = 0\,. \tag{3.12}$$

On the other hand, considering (2.6), $(2.39)_1$ and (3.3), the mass balance equations of φ^S and φ^G, respectively, can be written as

$$(n^S)'_S = -\frac{n^S}{\rho^{SR}}(\rho^{SR})'_S - n^S \operatorname{div} \overset{\prime}{\mathbf{x}}_S \tag{3.13}$$

and

$$(n^G)'_G = -\frac{n^G}{\rho^{GR}}(\rho^{GR})'_G - n^G \operatorname{div} \overset{\prime}{\mathbf{x}}_G\ . \tag{3.14}$$

Now, the time derivatives of the volume fractions in (3.12) can be substituted by (3.13) and (3.14). Relation (3.12) can thus be identified as

$$n^S \operatorname{div} \overset{\prime}{\mathbf{x}}_S + n^G \operatorname{div} \overset{\prime}{\mathbf{x}}_G + \operatorname{grad} n^G \cdot \mathbf{w}_G + n^S \frac{1}{\rho^{SR}} \frac{\partial \rho^{SR}}{\partial \theta^S}(\theta^S)'_S + \frac{n^G}{\rho^{GR}}(\rho^{GR})'_G = 0\,, \tag{3.15}$$

where

$$(\rho^{SR})'_S = \frac{\partial \rho^{SR}}{\partial \theta^S}\,(\theta^S)'_S \tag{3.16}$$

has been considered. By introducing a *Lagrange*an multiplier Λ, one obtains the new modified saturation condition

$$\begin{aligned}\Lambda \Big[& n^S\, \mathbf{L}_S \cdot \mathbf{I} + n^G\, \mathbf{L}_G \cdot \mathbf{I} + \operatorname{grad} n^G \cdot \mathbf{w}_G\, + \\ & + n^S \frac{1}{\rho^{SR}} \frac{\partial \rho^{SR}}{\partial \theta^S}\,(\theta^S)'_S + n^G \frac{1}{\rho^{GR}}\,(\rho^{GR})'_G \Big] = 0\,.\end{aligned} \tag{3.17}$$

Therein, use was additionally made of (2.29). It will be shown in the following that (3.17) is the required constraint for the definition of the *extra* terms in the entropy inequality.

Modification of the inequality by *extra* terms. Since the modified saturation condition (3.17) equals zero, it can be added to the reformulated inequality (3.10). This leads to the new modified inequality

$$\begin{aligned}&\mathbf{T}_E^S\cdot\mathbf{L}_S+\frac{\theta^S}{\theta^G}\,\mathbf{T}_E^G\cdot\mathbf{L}_G-n^S\rho^{SR}\,(\psi^S)'_S-n^S\rho^{SR}(\theta^S)'_S\,\eta_E^S+\Lambda\frac{n^G}{\rho^{GR}}\,(\rho^{GR})'_G-\\&-\frac{\theta^S}{\theta^G}\,n^G\rho^{GR}\,(\psi^G)'_G-\frac{\theta^S}{\theta^G}\,n^G\rho^{GR}(\theta^G)'_G\,\eta^G+\hat{\varepsilon}^G\left(\frac{\theta^S}{\theta^G}-1\right)-\hat{\mathbf{p}}_E^G\cdot\mathbf{w}_G-\\&-\frac{1}{\theta^S}\,\mathbf{q}^S\cdot\operatorname{grad}\theta^S-\frac{\theta^S}{(\theta^G)^2}\,\mathbf{q}^G\cdot\operatorname{grad}\theta^G\geq 0\,,\end{aligned}\tag{3.18}$$

wherein, $\mathbf{T}^S$, $\mathbf{T}^G$, $\hat{\mathbf{p}}^G$ and η^S are substituted by

$$\begin{aligned}\mathbf{T}^S&=-\Lambda\,n^S\,\mathbf{I}+\mathbf{T}_E^S\,,\\\mathbf{T}^G&=-\Lambda\,\frac{\theta^G}{\theta^S}\,n^G\,\mathbf{I}+\mathbf{T}_E^G\,,\\\eta^S&=\Lambda\,\frac{1}{(\rho^{SR})^2}\,\frac{\partial\rho^{SR}}{\partial\,\theta^S}+\eta_E^S\,,\\\hat{\mathbf{p}}^G&=\Lambda\operatorname{grad}n^G+\hat{\mathbf{p}}_E^G\,.\end{aligned}\tag{3.19}$$

Note that (3.18) represents the determining entropy inequality for the description of the model under consideration. The corresponding equations, which have still to be formulated for the *extra* stresses $\mathbf{T}_E^S$ and $\mathbf{T}_E^G$, the *extra* entropy η_E^S of the solid, the *extra* momentum production $\hat{\mathbf{p}}_E^G$ of the gas, the direct energy production $\hat{\varepsilon}^G$ as well as for the respective heat influx vectors $\mathbf{q}^S$ and $\mathbf{q}^G$, must now satisfy this inequality.

3.1.2 Decomposition of the deformation

The entire state of strain of the solid constituent can be decomposed multiplicatively into a mechanical and a thermal part, i. e.,

$$\mathbf{F}_S=\mathbf{F}_{S_m}\mathbf{F}_{S_\theta}\,.\tag{3.20}$$

The incorporation of (3.20) in (2.43) yields for the partial density of the solid

$$\rho^S=\rho_{0S}^S\,(\det\mathbf{F}_{S_\theta})^{-1}(\det\mathbf{F}_{S_m})^{-1}\,.\tag{3.21}$$

Therein, ρ_{0S}^S is the partial solid density in the solid reference configuration. Furthermore, since $\mathbf{F}_{S_\theta}$ represents a measure for thermal deformations, ρ_θ^S is introduced as an additional parameter via

$$\rho_\theta^S=\rho_{0S}^S\,(\det\mathbf{F}_{S_\theta})^{-1}\,.\tag{3.22}$$

This parameter can be understood as the partial solid density in the *purely thermally loaded* configuration B_θ, cf. Figure 3.1. Considering (2.6), the densities of the respective configurations in Figure 3.1 can be expressed by

$$\begin{aligned}\rho^S&=n^S\,\rho^{SR}\,,\\\rho_\theta^S&=n_\theta^S\,\rho_\theta^{SR}\,,\\\rho_{0S}^S&=n_{0S}^S\,\rho_{0S}^{SR}\,.\end{aligned}\tag{3.23}$$

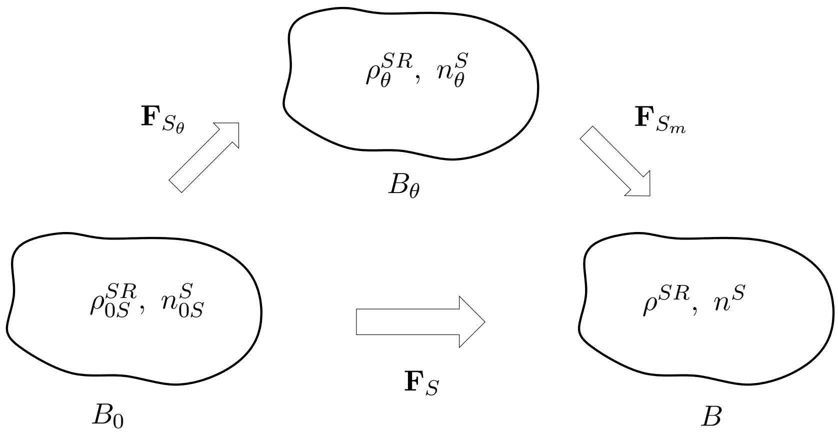

Figure 3.1: Decomposition of the solid deformation gradient.

Therein, ρ^{SR}, ρ^{SR}_θ and ρ^{SR}_{0S} are the effective densities in B, B_θ and B_0, respectively, whereas n^S, n^S_θ and n^S_{0S} represent the corresponding volume fractions.
Incorporating (3.22), $(3.23)_1$ and $(3.23)_2$ in (3.21), one obtains

$$n^S\,\rho^{SR} = n^S_\theta\,\rho^{SR}_\theta\,(\det\mathbf{F}_{S_m})^{-1}\,. \tag{3.24}$$

On the other hand, taking into consideration that relation (3.1) holds for the solid density, it is obvious that ρ^{SR}_θ and ρ^{SR} must be identically. In more precise words, this statement means that the mechanical part of the solid deformation gradient $\mathbf{F}_{S_m}$ (cf. Figure 3.1) does not cause any changes in the solid density. Thus, one has for mechanically and materially incompressible solids

$$\rho^{SR} = \rho^{SR}_\theta\,. \tag{3.25}$$

As a result of (3.25), the equation (3.24) reduces to

$$n^S = n^S_\theta\,(\det\mathbf{F}_{S_m})^{-1}\,. \tag{3.26}$$

Furthermore, under the assumption that thermal loading results in purely homogeneous expansions, it can be shown by means of a simple illustration (cf. Figure 3.2) that during transformations from B_0 into B_θ bulk volume changes only occur due to effective solid density variations and not due to solid volume fraction changes. Thus,

$$n^S_\theta = n^S_{0S}\,. \tag{3.27}$$

Following this, relation (3.26) can also be stated as

$$n^S = n^S_{0S}\,(\det\mathbf{F}_{S_m})^{-1}\,. \tag{3.28}$$

As a further result, the combination of (3.21), $(3.23)_1$, $(3.23)_3$ and (3.28) yields

$$\rho^{SR} = \rho^{SR}_{0S}\,(\det\mathbf{F}_{S_\theta})^{-1}\,. \tag{3.29}$$

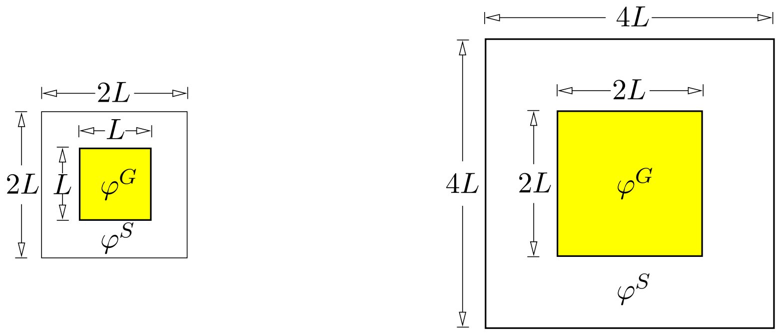

(B_0) (B_θ)

$$n_{0S}^S = \frac{8L^3 - 2L^3}{8L^3} = 0.75 \qquad n_\theta^S = \frac{64L^3 - 16L^3}{64L^3} = 0.75$$

Figure 3.2: Isotropic expansion of a solid volume element containing a pore-gas.

For isotropic thermal expansions, $\det \mathbf{F}_{S_\theta}$ can be expressed by an appropriate constitutive relation, which is *a priori* introduced at this point via

$$\det \mathbf{F}_{S_\theta} = e^{3\,\alpha^S\,\Delta\theta^S}\,. \tag{3.30}$$

Therein, α^S stands for the thermal expansion coefficient of the solid skeleton, and $\Delta\theta^S$ is defined by

$$\Delta\theta^S = \theta^S - \theta_{0S}^S \tag{3.31}$$

with θ_{0S}^S being the initial solid temperature in the reference configuration. Finally, the combination of (3.29) and (3.30) yields the material density of the thermoelastic solid constituent as

$$\rho^{SR} = \rho_{0S}^{SR}\,e^{-3\,\alpha^S\,\Delta\theta^S}\,. \tag{3.32}$$

3.1.3 The determining constitutive variables

The fundamental principles of constitutive modeling are discussed in a large number of articles, cf., e. g., Coleman and Noll [21] or Truesdell [75, 76]. Following the remarks in Ehlers [28, 31], the set $\mathcal{R}$ of response functions to be determined for the non-isothermal biphasic model under consideration is defined as

$$\mathcal{R} := \{\psi^S,\ \psi^G,\ \mathbf{T}_E^S,\ \mathbf{T}_E^G,\ \hat{\mathbf{p}}_E^G,\ \hat{\varepsilon}^G,\ \mathbf{q}^S,\ \mathbf{q}^G\}\,. \tag{3.33}$$

Moreover, the fundamental set of constitutive variables for general porous media consisting of a single elastic porous skeleton φ^S and an arbitrary number of viscous pore-fluids φ^β is given in Ehlers [28] as follows

$$\begin{aligned}\mathcal{V} := \ &\{\theta^\alpha,\ \operatorname{grad}\theta^\alpha,\ n^\beta,\ \operatorname{grad} n^\beta,\ \rho^{\alpha R},\ \operatorname{grad}\rho^{\alpha R},\ \mathbf{F}_\alpha,\ \operatorname{Grad}\mathbf{F}_\alpha,\\ &\ \overset{\prime}{\mathbf{x}}_\beta,\ \operatorname{Grad}_\beta \overset{\prime}{\mathbf{x}}_\beta,\ \mathbf{X}_\alpha\}\,.\end{aligned} \tag{3.34}$$

Concerning the variables in (3.34), some of those are responsible for the thermal state, namely, θ^α and $\operatorname{grad}\theta^\alpha$, and the others, apart from the position vector $\mathbf{X}_\alpha$, which considers possible inhomogeneities, describe the deformation behavior of the constituents.

Unlike single-phasic materials, in which the entire state of the deformation is defined solely by $\mathbf{F}_\alpha$, the partial densities in multiphasic models cannot be determined through the integration of the mass balances, since additional mass productions occur in the mass balance of general multiphasic materials, cf. $(2.39)_1$. As a result of this fact, the partial density ρ^α, given as the product of n^α and $\rho^{\alpha R}$ (2.6), is an independent variable. Hence, n^α and either the partial density or the material density must be considered in the set of the constitutive variables.

Furthermore, the volume fractions are coupled with each other through the saturation condition (3.11), which means that one of them can be determined from the other. Following this, only the fluid volume fractions as well as their gradients, namely, n^β and $\operatorname{grad} n^\beta$, are considered in (3.34) as independent variables.

Note that the general variables included in $\mathcal{V}$ can be reduced depending on the problem to be investigated. For the biphasic model under consideration with homogeneous constituents, $\mathcal{V}$ reduces to

$$\begin{aligned}\mathcal{V}_1 \;=\; \{&\theta^S,\ \operatorname{grad}\theta^S,\ \theta^G,\ \operatorname{grad}\theta^G,\ n^G,\ \operatorname{grad} n^G,\ \rho^{SR},\ \operatorname{grad}\rho^{SR},\\ &\rho^{GR},\ \operatorname{grad}\rho^{GR},\ \mathbf{F}_S,\ \operatorname{Grad}_S\mathbf{F}_S,\ \mathbf{F}_G,\ \operatorname{Grad}_G\mathbf{F}_G,\ \overset{\prime}{\mathbf{x}}_G,\ \operatorname{Grad}\overset{\prime}{\mathbf{x}}_G\}\,.\end{aligned} \tag{3.35}$$

Further simplifications of $\mathcal{V}_1$ arise from the exclusion of mass exchanges and the consideration of the symmetry properties of the isotropic fluid, cf., e. g., Ehlers [31]. Since the deformation gradient of an isotropic fluid is defined as

$$\mathbf{F}_G = (\det\mathbf{F}_G)^{1/3}\,\mathbf{I}, \tag{3.36}$$

$\mathbf{F}_G$ must be substituted by $\det\mathbf{F}_G$ or through n^G and ρ^{GR}, respectively, where mass exchanges are excluded.

Using the *principle of frame indifference*, it can be shown (cf., e. g., Ehlers [31]) that the fluid velocity $\overset{\prime}{\mathbf{x}}_G$ can be replaced by the seepage velocity $\mathbf{w}_G$. In addition, $\operatorname{Grad}_G\overset{\prime}{\mathbf{x}}_G$, which describes the viscous behavior of the fluid, has to be substituted by the rate of deformation tensor $\mathbf{D}_G$. Thus, (3.35) reduces to

$$\begin{aligned}\mathcal{V}_2 \;=\; \{&\theta^S,\ \operatorname{grad}\theta^S,\ \theta^G,\ \operatorname{grad}\theta^G,\ n^G,\ \operatorname{grad} n^G,\ \rho^{SR},\ \operatorname{grad}\rho^{SR},\\ &\rho^{GR},\ \operatorname{grad}\rho^{GR},\ \mathbf{F}_S,\ \operatorname{Grad}_S\mathbf{F}_S,\ \mathbf{w}_G,\ \mathbf{D}_G\}\,.\end{aligned} \tag{3.37}$$

Furthermore, it was already found out in (3.29) that the material density of the thermoelastic solid constituent is determined by the deformation gradient of the solid. Following this, ρ^{SR} and, as a consequence, grad ρ^{SR} loose the character of independent variables and have to be crossed out from the set of constitutive variables $\mathcal{V}_2$. On the other hand, by use of the relationship (3.28), the saturation condition (3.11) can be put alternatively into the form

$$n^G = 1 - n_{0S}^S\,(\det \mathbf{F}_{S_m})^{-1} \tag{3.38}$$

so that also n^G and $\operatorname{grad} n^G$ cannot be considered as independent variables anymore. They are additionally dropped from $\mathcal{V}_2$. Following this, the set of constitutive variables governing the non-isothermal biphasic model under consideration is finally identified as

$$\mathcal{S} = \{\theta^S,\ \operatorname{grad}\theta^S,\ \theta^G,\ \operatorname{grad}\theta^G,\ \rho^{GR},\ \operatorname{grad}\rho^{GR},\ \mathbf{F}_S,\ \operatorname{Grad}_S \mathbf{F}_S,\ \mathbf{w}_G,\ \mathbf{D}_G\}\,. \tag{3.39}$$

It is pointed out that the presence of $\mathbf{F}_S$ in the variable set above implies the consideration of a general nonlinear elastic solid constituent. For a solid material with infinitesimal strains, the deformation gradient $\mathbf{F}_S$ can be replaced in (3.39) by the linearized strain tensor $\boldsymbol{\varepsilon}_S$, cf. Subsection 3.2.1.

3.2 Evaluation of the entropy inequality

The evaluation of the entropy inequality in this section is based on the remarks in Ehlers [31]. Therein, the entropy inequality is evaluated in accordance with the work by de Boer and Ehlers [16], Bowen [19] and Coleman and Noll [21].

For the evaluation of the inequality under consideration, a general nonlinear elastic solid constituent is considered at first. Subsequently, the corresponding thermodynamic potentials for a solid material with small strains are briefly discussed, cf. Subsection 3.2.1.

Further thermodynamic restrictions, which are required in order to formulate constitutive equations, are obtained by evaluating the dissipation inequality around the equilibrium state. This is justified, since *slow* thermodynamic processes are assumed to take place. In the model under consideration, small gradients, small velocities and also a small temperature difference exist between the constituents, cf. Chapter 1.

Preliminaries. Based on the principle of *equipresence*, it is assumed (cf., e. g., Ehlers [28, 31]) that the elements summarized in $\mathcal{R}$ can depend on the same set $\mathcal{S}$ of constitutive variables, i. e.

$$\mathcal{R} :=\ \mathcal{R}(\mathcal{S})\,. \tag{3.40}$$

Proceeding from this assumption, the combination of (3.33), (3.39) and (3.40) yields

$$\begin{aligned} &\{\psi^S,\ \psi^G,\ \mathbf{T}_E^S,\ \mathbf{T}_E^G,\ \hat{\mathbf{p}}_E^G,\ \hat{\varepsilon}^G,\ \mathbf{q}^S,\ \mathbf{q}^G\} = \\ &= \mathcal{R}\,\{\theta^S,\ \operatorname{grad}\theta^S,\ \theta^G,\ \operatorname{grad}\theta^G,\ \rho^{GR},\ \operatorname{grad}\rho^{GR},\ \mathbf{F}_S,\ \operatorname{Grad}_S \mathbf{F}_S,\ \mathbf{w}_G,\ \mathbf{D}_G\}\,. \end{aligned} \tag{3.41}$$

Furthermore, one presumes on the basis of the principle of *phase separation* (cf. Ehlers [26]) that the free energy ψ^α of a given constituent φ^α only depends on the variables included in the processes by φ^α. Thus,

$$\begin{aligned} \psi^S &:= \psi^S(\mathbf{F}_S,\ \operatorname{Grad}_S \mathbf{F}_S,\ \theta^S,\ \operatorname{grad}\theta^S)\,, \\ \psi^G &:= \psi^G(\rho^{GR},\ \operatorname{grad}\rho^{GR},\ \mathbf{w}_G,\ \mathbf{D}_G,\ \theta^G,\ \operatorname{grad}\theta^G)\,, \end{aligned} \tag{3.42}$$

where, using (2.28), the respective partial time derivatives read

$$
\begin{aligned}
(\psi^S)'_S &= \frac{\partial\,\psi^S}{\partial\,\mathbf{F}_S}\mathbf{F}_S^T\cdot\mathbf{L}_S + \frac{\partial\,\psi^S}{\partial\,\mathrm{Grad}_S\,\mathbf{F}_S}\cdot(\mathrm{Grad}_S\,\mathbf{F}_S)'_S + \\
&\quad + \frac{\partial\,\psi^S}{\partial\,\theta^S}(\theta^S)'_S + \frac{\partial\,\psi^S}{\partial\,(\mathrm{grad}\,\theta^S)}\cdot(\mathrm{grad}\theta^S)'_S\,, \\
(\psi^G)'_G &= \frac{\partial\,\psi^G}{\partial\,\rho^{GR}}(\rho^{GR})'_G + \frac{\partial\,\psi^G}{\partial\,\mathrm{grad}\,\rho^{GR}}\cdot(\mathrm{grad}\,\rho^{GR})'_G + \\
&\quad + \frac{\partial\,\psi^G}{\partial\,\mathbf{w}_G}\cdot(\mathbf{w}_G)'_G + \frac{\partial\,\psi^G}{\partial\,\mathbf{D}_G}\cdot(\mathbf{D}_G)'_G + \\
&\quad + \frac{\partial\,\psi^G}{\partial\,\theta^G}(\theta^G)'_G + \frac{\partial\,\psi^G}{\partial\,(\mathrm{grad}\,\theta^G)}\cdot(\mathrm{grad}\theta^G)'_G\,.
\end{aligned}
\tag{3.43}
$$

Considering (3.43), the determining entropy inequality (3.18) reads

$$
\begin{aligned}
&\left(\mathbf{T}_E^S - n^S\rho^{SR}\,\frac{\partial\,\psi^S}{\partial\,\mathbf{F}_S}\mathbf{F}_S^T\right)\cdot\mathbf{L}_S - n^S\rho^{SR}\,\frac{\partial\,\psi^S}{\partial\,\mathrm{Grad}_S\,\mathbf{F}_S}\cdot(\mathrm{Grad}_S\,\mathbf{F}_S)'_S - \\
&- n^S\rho^{SR}\left(\eta_E^S + \frac{\partial\,\psi^S}{\partial\,\theta^S}\right)(\theta^S)'_S - n^S\rho^{SR}\,\frac{\partial\,\psi^S}{\partial\,(\mathrm{grad}\,\theta^S)}\cdot(\mathrm{grad}\,\theta^S)'_S + \\
&+ n^G\left(\frac{1}{\rho^{GR}}\,\Lambda - \frac{\theta^S}{\theta^G}\rho^{GR}\,\frac{\partial\,\psi^G}{\partial\,\rho^{GR}}\right)(\rho^{GR})'_G - \frac{\theta^S}{\theta^G}\,n^G\rho^{GR}\,\frac{\partial\,\psi^G}{\partial\,\mathbf{w}_G}\cdot(\mathbf{w}_G)'_G - \\
&- \frac{\theta^S}{\theta^G}\,n^G\rho^{GR}\,\frac{\partial\,\psi^G}{\partial\,\mathbf{D}_G}\cdot(\mathbf{D}_G)'_G - \frac{\theta^S}{\theta^G}\,n^G\rho^{GR}\,\frac{\partial\,\psi^G}{\partial\,\mathrm{grad}\,\rho^{GR}}\cdot(\mathrm{grad}\,\rho^{GR})'_G - \\
&- \frac{\theta^S}{\theta^G}\,n^G\rho^{GR}\left(\eta^G + \frac{\partial\,\psi^G}{\partial\,\theta^G}\right)(\theta^G)'_G - \frac{\theta^S}{\theta^G}\,n^G\rho^{GR}\,\frac{\partial\,\psi^G}{\partial\,(\mathrm{grad}\theta^G)}\cdot(\mathrm{grad}\,\theta^G)'_G + \\
&+ \frac{\theta^S}{\theta^G}\,\mathbf{T}_E^G\cdot\mathbf{L}_G + \hat{\varepsilon}^G\left(\frac{\theta^S}{\theta^G} - 1\right) - \hat{\mathbf{p}}_E^G\cdot\mathbf{w}_G - \frac{1}{\theta^S}\,\mathbf{q}^S\cdot\mathrm{grad}\theta^S - \\
&- \frac{\theta^S}{(\theta^G)^2}\,\mathbf{q}^G\cdot\mathrm{grad}\theta^G \geq 0\,.
\end{aligned}
\tag{3.44}
$$

3.2.1 Thermodynamic potentials

According to the principle of the entropy evaluation (cf., e. g., Ehlers [31]), the inequality (3.44) must be fulfilled for arbitrary values of the *free parameters* $\mathbf{L}_S$, $(\mathrm{Grad}_S\,\mathbf{F}_S)'_S$, $(\theta^S)'_S$, $(\mathrm{grad}\,\theta^S)'_S$, $(\rho^{GR})'_G$, $(\mathbf{w}_G)'_G$, $(\mathbf{D}_G)'_G$, $(\mathrm{grad}\,\rho^{GR})'_G$, $(\theta^G)'_G$ and $(\mathrm{grad}\,\theta^G)'_G$. In order to satisfy this requirement, the necessary and sufficient constraints are well-defined through

$$
\begin{array}{rclcrcl}
\left(\mathbf{T}^S_E - n^S\rho^{SR}\,\dfrac{\partial\,\psi^S}{\partial \mathbf{F}_S}\mathbf{F}^T_S\right) & = & \mathbf{0} & \Longrightarrow & \mathbf{T}^S_E & = & n^S\rho^{SR}\,\dfrac{\partial\,\psi^S}{\partial\,\mathbf{F}_S}\mathbf{F}^T_S\,,\\[2ex]
\dfrac{\partial\,\psi^S}{\partial\,\mathrm{Grad}_S\,\mathbf{F}_S} & = & \overset{3}{\mathbf{0}}\,, & & & & \\[2ex]
\left(\eta^S_E + \dfrac{\partial\,\psi^S}{\partial\,\theta^S}\right) & = & 0 & \Longrightarrow & \eta^S_E & = & -\,\dfrac{\partial\,\psi^S}{\partial\,\theta^S}\,,\\[2ex]
\dfrac{\partial\,\psi^S}{\partial\,(\mathrm{grad}\,\theta^S)} & = & \mathbf{0}\,, & & & & \\[2ex]
\left(\dfrac{1}{\rho^{GR}}\,\Lambda - \dfrac{\theta^S}{\theta^G}\rho^{GR}\dfrac{\partial\,\psi^F}{\partial\,\rho^{GR}}\right) & = & 0 & \Longrightarrow & \Lambda & = & \dfrac{\theta^S}{\theta^G}(\rho^{GR})^2\dfrac{\partial\,\psi^G}{\partial\,\rho^{GR}}\,,\\[2ex]
\dfrac{\partial\,\psi^G}{\mathbf{w}_G} & = & \mathbf{0}\,, & & & & \\[2ex]
\dfrac{\partial\,\psi^G}{\partial\,\mathbf{D}_G} & = & \mathbf{0}\,, & & & & \\[2ex]
\dfrac{\partial\,\psi^G}{\mathrm{grad}\,\rho^{GR}} & = & \mathbf{0}\,, & & & & \\[2ex]
\left(\eta^G + \dfrac{\partial\,\psi^G}{\partial\,\theta^G}\right) & = & 0 & \Longrightarrow & \eta^G & = & -\,\dfrac{\partial\,\psi^G}{\partial\,\theta^G}\,,\\[2ex]
\dfrac{\partial\,\psi^G}{\partial\,(\mathrm{grad}\,\theta^G)} & = & \mathbf{0} & & & &
\end{array}
\tag{3.45}
$$

and

$$
\begin{aligned}
\mathcal{D} = {} & \frac{\theta^S}{\theta^G}\,\mathbf{T}^G_E\cdot\mathbf{L}_G + \frac{1}{\theta^G}\,\hat{\varepsilon}^G(\theta^S - \theta^G) - \hat{\mathbf{p}}^G_E\cdot\mathbf{w}_G - \\
& -\frac{1}{\theta^G}\left(\frac{\theta^G}{\theta^S}\,\mathbf{q}^S\cdot\mathrm{grad}\,\theta^S + \frac{\theta^S}{\theta^G}\,\mathbf{q}^G\cdot\mathrm{grad}\,\theta^G\right) \geq 0\,,
\end{aligned}
\tag{3.46}
$$

which represents the *dissipation inequality.*

Evidently, the conclusions listed in (3.45) reveal the actual dependency of the free energies ψ^S and ψ^G. It is now obvious that

$$
\begin{aligned}
\psi^S &= \psi^S(\mathbf{F}_S,\ \theta^S) \qquad \text{and}\\
\psi^G &= \psi^G(\rho^{GR},\ \theta^G)\,.
\end{aligned}
\tag{3.47}
$$

Furthermore, since $\mathbf{T}_E^S$ and η_E^S are expressed through potentials of the solid free energy, they must consequently depend on the same variables like ψ^S, i. e.,

$$\begin{aligned} \mathbf{T}_E^S &= \mathbf{T}_E^S(\mathbf{F}_S,\ \theta^S)\,, \\ \eta_E^S &= \eta_E^S(\mathbf{F}_S,\ \theta^S)\,. \end{aligned} \tag{3.48}$$

For the gas constituent, it follows analogously that

$$\begin{aligned} \eta^G &= \eta^G(\rho^{GR},\ \theta^G)\,, \\ \Lambda &= \Lambda(\rho^{GR},\ \theta^S,\ \theta^G)\,. \end{aligned} \tag{3.49}$$

The thermodynamic potentials obtained in $(3.45)_1$, $(3.45)_3$, $(3.45)_5$ and $(3.45)_9$ will be used in Section 3.3 in order to determine the solid *extra* stress as well as the entropies of both constituents.

The special case of small strains. The solid constituent under consideration is assumed to undergo small deformations, i. e.,

$$\begin{aligned} \mathbf{x} &\approx \mathbf{X}_S\,, \\ \operatorname{grad}\mathbf{u}_S &\approx \operatorname{Grad}_S\mathbf{u}_S\,, \\ \operatorname{div}\mathbf{u}_S &\approx \operatorname{Div}_S\mathbf{u}_S\,. \end{aligned} \tag{3.50}$$

The respective definitions of the gradients and divergence terms in (3.50) are given in Chapter 1 and Appendix B.

Furthermore, proceeding from small strains, linearized quantities have to be considered also for the stress as well as the strain tensors of the solid skeleton. In addition, the deformation gradient $\mathbf{F}_S$ can be substituted in (3.39) by the linearized strain tensor $\boldsymbol{\varepsilon}_S$ with

$$\mathbf{D}_{S_{lin}} = (\boldsymbol{\varepsilon}_S)'_S\,. \tag{3.51}$$

Following the aforementioned assumptions, the evaluation of the entropy inequality yields, instead of $(3.45)_1$, the thermodynamic potential

$$\left(\boldsymbol{\sigma}_E^S - n^S\rho^{SR}\,\frac{\partial\,\psi_{lin}^S}{\partial\boldsymbol{\varepsilon}_S}\right) = \mathbf{0} \qquad \Longrightarrow \qquad \boldsymbol{\sigma}_E^S = n^S\rho^{SR}\,\frac{\partial\,\psi_{lin}^S}{\partial\,\boldsymbol{\varepsilon}_S} \tag{3.52}$$

with the linearized stress tensor

$$\mathbf{T}_{E_{lin}}^S = \boldsymbol{\sigma}_E^S\,. \tag{3.53}$$

As a result of (3.52), one obtains

$$\begin{aligned} \psi_{lin}^S &= \psi_{lin}^S(\boldsymbol{\varepsilon}_S,\ \theta^S)\,, \\ \boldsymbol{\sigma}_E^S &= \boldsymbol{\sigma}_E^S(\boldsymbol{\varepsilon}_S,\ \theta^S)\,, \\ \eta_{E_{lin}}^S &= \eta_{E_{lin}}^S(\boldsymbol{\varepsilon}_S,\ \theta^S)\,. \end{aligned} \tag{3.54}$$

Note that the consideration of small strains for the solid constituent exerts only influences on the quantities related to $\boldsymbol{\sigma}_E^S$. Thus, the remainder of the conclusions obtained in (3.45) remains valid further on.

3.2.2 Restrictions around the equilibrium state

In this subsection, thermodynamic restrictions will be determined, which are necessary in order to formulate appropriate constitutive equations for the response functions included in the dissipation inequality $\mathcal{D}$ (3.46). In analogy to Ehlers [31], the respective response functions will be decomposed in equilibrium and non-equilibrium parts, where the latter will be linearized around the equilibrium state.

Preliminaries. It can be shown that, for non-polar constituents, the stress tensor $\mathbf{T}^\alpha$ is a symmetric tensor, cf., e. g., Ehlers [28, 32] or Hassanizadeh and Gray [46]. As a result of this fact and considering (2.32), one obtains

$$\mathbf{T}^\alpha \cdot \mathbf{L}_\alpha = \mathbf{T}^\alpha \cdot \mathbf{D}_\alpha \,. \tag{3.55}$$

Consequently, the spatial velocity gradient $\mathbf{L}_G$ of the gas can be replaced in the dissipation inequality (3.46). Thus,

$$\begin{aligned} \mathcal{D} = \; & \frac{\theta^S}{\theta^G}\,\mathbf{T}^G_E \cdot \mathbf{D}_G + \frac{1}{\theta^G}\,\hat{\varepsilon}^G(\theta^S - \theta^G) - \hat{\mathbf{p}}^G_E \cdot \mathbf{w}_G - \\ & -\frac{1}{\theta^G}\left(\frac{\theta^G}{\theta^S}\,\mathbf{q}^S \cdot \operatorname{grad}\theta^S + \frac{\theta^S}{\theta^G}\,\mathbf{q}^G \cdot \operatorname{grad}\theta^G\right) \geq 0\,. \end{aligned} \tag{3.56}$$

Therein, the following response functions have to be determined

$$\{\mathbf{T}^G_E,\ \hat{\mathbf{p}}^G_E,\ \hat{\varepsilon}^G,\ \mathbf{q}^S,\ \mathbf{q}^G\} =: \Upsilon(\mathcal{S}) \tag{3.57}$$

with

$$\mathcal{S} = \{\theta^S,\ \operatorname{grad}\theta^S,\ \theta^G,\ \operatorname{grad}\theta^G,\ \rho^{GR},\ \operatorname{grad}\rho^{GR},\ \mathbf{F}_S,\ \operatorname{Grad}_S\mathbf{F}_S,\ \mathbf{w}_G,\ \mathbf{D}_G\}\,. \tag{3.58}$$

The additive decomposition of the dissipation inequality. Proceeding from the remarks discussed in Ehlers [31], the dissipation inequality as well as the response functions can be decomposed additively into an equilibrium and a non-equilibrium part

$$\mathcal{D}(\mathcal{S}) = \mathcal{D}_0(\mathcal{S}_0) + \mathcal{D}_n(\mathcal{S})\,, \tag{3.59}$$

where

$$\mathcal{D}_0(\mathcal{S}_0) = 0 \quad \text{and} \quad \mathcal{D}_n(\mathcal{S}_0) = 0\,. \tag{3.60}$$

For the dissipation inequality, one obtains

$$\begin{aligned} \mathcal{D}_n(\mathcal{S}) = \; & \frac{\theta^S}{\theta^G}\,\mathbf{T}^G_E \cdot \mathbf{D}_G + \frac{1}{\theta^G}\,\hat{\varepsilon}^G(\theta^S - \theta^G) - \hat{\mathbf{p}}^G_E \cdot \mathbf{w}_G - \\ & -\frac{1}{\theta^G}\left(\frac{\theta^G}{\theta^S}\,\mathbf{q}^S \cdot \operatorname{grad}\theta^S + \frac{\theta^S}{\theta^G}\,\mathbf{q}^G \cdot \operatorname{grad}\theta^G\right) \geq 0\,. \end{aligned} \tag{3.61}$$

For the response functions, it follows analogously that

$$
\begin{aligned}
\mathbf{T}^G_E(\mathcal{S}) &= \mathbf{T}^G_{E_n}(\mathcal{S})\,,\\
\hat{\varepsilon}^G(\mathcal{S}) &= \hat{\varepsilon}^G_n(\mathcal{S})\,,\\
\hat{\mathbf{p}}^G_E(\mathcal{S}) &= \hat{\mathbf{p}}^G_{E_n}(\mathcal{S})\,,\\
\mathbf{q}^S(\mathcal{S}) &= \mathbf{q}^S_n(\mathcal{S})\,,\\
\mathbf{q}^G(\mathcal{S}) &= \mathbf{q}^G_n(\mathcal{S})\,.
\end{aligned}
\tag{3.62}
$$

The quantities in (3.62) will be linearized around the thermodynamic equilibrium state, which is given by

$$
\begin{aligned}
\mathcal{S}_0 \;=\; &\{\theta^S = \theta,\ \operatorname{grad}\theta^S = \mathbf{0},\ \theta^G = \theta,\ \operatorname{grad}\theta^G = \mathbf{0},\ \rho^{GR},\ \operatorname{grad}\rho^{GR},\ \mathbf{F}_S,\\
&\operatorname{Grad}_S \mathbf{F}_S,\ \mathbf{w}_G = \mathbf{0},\ \mathbf{D}_G = \mathbf{0}\}\,.
\end{aligned}
\tag{3.63}
$$

For the linearization of the corresponding quantities, *Taylor series* will be expanded around the point $\mathcal{S} = \mathcal{S}_0$. Therein, the quantities in (3.62) may be expanded with respect to the initial values of the parameters $\mathbf{D}_G$, θ^S, θ^G, $\mathbf{w}_G$, $\operatorname{grad}\theta^S$ and $\operatorname{grad}\theta^G$, where the series have to be truncated after the first order terms.

It is however pointed out that not all of the mathematically possible dependencies of the response functions must necessarily have a physical relevance. When investigating a physical process, one has to estimate, according to the problem on hand, which dependencies really are present. Irrelevant dependencies can be neglected. Concerning the problem under study, some constitutive assumptions will be made in the following.

Constitutive assumptions. Based on the *principle of phase separation*, it is assumed that response functions of each constituent φ^α depend on constitutive variables, which only belong to φ^α. On the other hand, for the interaction quantities, $\hat{\varepsilon}^G$ and $\hat{\mathbf{p}}^G_E$, only the dependencies of the so-called interaction variables, namely, $(\theta^S - \theta^G)$ and $\mathbf{w}_G$, are considered. It is additionally postulated that the interaction quantity $\hat{\varepsilon}^G$, which represents a thermal measure, only depend on *caloric* interaction variables. Unlike this, $\hat{\mathbf{p}}^G_E$, which embodies mechanical interaction effects, is assumed to depend only on kinematical interaction variables.

Furthermore, with regard to the well-known *Fourier*'s law for the heat conduction (cf., e. g., Grigull [43]), the respective heat flux vectors are assumed only to depend on their own temperature gradients, whereas the remaining response functions are postulated not to be influenced by these variables.

Concerning the quantity $\mathbf{T}^G_E$, the well-known constitutive relation, stemming from the classical mechanics for single-phasic fluids (cf., e. g., Ehlers [33]), is considered. Therein, $\mathbf{T}^G_E$ is understood as the fluid friction stress, where the friction effects are related to the rate of deformation tensor $\mathbf{D}_G$.

Following the aforementioned constitutive assumptions, one obtains

$$
\begin{aligned}
\hat{\mathbf{T}}_E^G &:= \hat{\mathbf{T}}_E^G\,(\mathbf{D}_G)\,, \\
\hat{\varepsilon}^G &:= \hat{\varepsilon}^G\,(\theta^S,\ \theta^G)\,, \\
\hat{\mathbf{p}}_E^G &:= \hat{\mathbf{p}}_E^G\,(\mathbf{w}_G)\,, \\
\mathbf{q}^S &:= \mathbf{q}^S\,(\,\mathrm{grad}\,\theta^S\,)\,, \\
\mathbf{q}^G &:= \mathbf{q}^G\,(\,\mathrm{grad}\,\theta^G\,)\,,
\end{aligned}
\tag{3.64}
$$

which leads to the respective linearizations:

$$
\begin{aligned}
\mathbf{T}_{E_n}^G(\mathcal{S}) &= \mathbf{T}_{E_n}^G(\mathcal{S}_0) + \frac{\partial\,\mathbf{T}_{E_n}^G}{\partial\,\mathbf{D}_G}\Big|_{\mathcal{S}_0}\mathbf{D}_G\,, \\
\hat{\varepsilon}_n^G(\mathcal{S}) &= \hat{\varepsilon}_n^G(\mathcal{S}_0) + \frac{\partial\,\hat{\varepsilon}_n^G}{\partial\,\theta^S}\Big|_{\mathcal{S}_0}(\theta^S-\theta) + \frac{\partial\,\hat{\varepsilon}_n^G}{\partial\,\theta^G}\Big|_{\mathcal{S}_0}(\theta^G-\theta)\,, \\
\hat{\mathbf{p}}_{E_n}^G(\mathcal{S}) &= \hat{\mathbf{p}}_{E_n}^G(\mathcal{S}_0) + \frac{\partial\,\hat{\mathbf{p}}_{E_n}^G}{\partial\,\mathbf{w}_G}\Big|_{\mathcal{S}_0}\mathbf{w}_G\,, \\
\mathbf{q}_n^S(\mathcal{S}) &= \mathbf{q}_n^S(\mathcal{S}_0) + \frac{\partial\,\mathbf{q}_n^S}{\partial\,\mathrm{grad}\,\theta^S}\Big|_{\mathcal{S}_0}\mathrm{grad}\,\theta^S\,, \\
\mathbf{q}_n^G(\mathcal{S}) &= \mathbf{q}_n^G(\mathcal{S}_0) + \frac{\partial\,\mathbf{q}_n^G}{\partial\,\mathrm{grad}\,\theta^G}\Big|_{\mathcal{S}_0}\mathrm{grad}\,\theta^G\,.
\end{aligned}
\tag{3.65}
$$

For the initial state of the quantities in (3.65), it is postulated (cf. Ehlers [31]) that

$$
\begin{aligned}
\mathbf{T}_{E_n}^G(\mathcal{S}_0) &= \mathbf{0}\,, \\
\hat{\varepsilon}_n^G(\mathcal{S}_0) &= 0\,, \\
\hat{\mathbf{p}}_{E_n}^G(\mathcal{S}_0) &= \mathbf{0}\,, \\
\mathbf{q}_n^S(\mathcal{S}_0) &= \mathbf{0}\,, \\
\mathbf{q}_n^G(\mathcal{S}_0) &= \mathbf{0}\,.
\end{aligned}
\tag{3.66}
$$

Thus, the *Taylor expansions* in (3.65) reduce to

$$
\begin{aligned}
\mathbf{T}^G_{E_n}(\mathcal{S}) &= \overset{4}{\mathbf{Z}}_D \, \mathbf{D}_G \,, \\
\hat{\varepsilon}^G_n(\mathcal{S}) &= k^\varepsilon_{\theta^S}(\theta^S - \theta) \,+\, k^\varepsilon_{\theta^G}(\theta^G - \theta) \,, \\
\hat{\mathbf{p}}^G_{E_n}(\mathcal{S}) &= \mathbf{S}_w \mathbf{w}_G \,, \\
\mathbf{q}^S_n(\mathcal{S}) &= \mathbf{K}^S_{\theta^S} \operatorname{grad} \theta^S \,, \\
\mathbf{q}^G_n(\mathcal{S}) &= \mathbf{K}^G_{\theta^G} \operatorname{grad} \theta^G \,,
\end{aligned}
\tag{3.67}
$$

where the following substitutions have been used:

$$
\begin{aligned}
\overset{4}{\mathbf{Z}}_D &= \frac{\partial \, \mathbf{T}^G_{E_n}}{\partial \, \mathbf{D}_G} \Big|_{\mathcal{S}_0} \,, \\
k^\varepsilon_{\theta^S} &= \frac{\partial \, \hat{\varepsilon}^G_n}{\partial \, \theta^S} \Big|_{\mathcal{S}_0} \,, \\
k^\varepsilon_{\theta^G} &= \frac{\partial \, \hat{\varepsilon}^G_n}{\partial \, \theta^G} \Big|_{\mathcal{S}_0} \,, \\
\mathbf{S}_w &= \frac{\partial \, \hat{\mathbf{p}}^G_{E_n}}{\partial \, \mathbf{w}_G} \Big|_{\mathcal{S}_0} \,, \\
\mathbf{K}^S_{\theta^S} &= \frac{\partial \, \mathbf{q}^S_n}{\partial \operatorname{grad} \theta^S} \Big|_{\mathcal{S}_0} \,, \\
\mathbf{K}^G_{\theta^G} &= \frac{\partial \, \mathbf{q}^G_n}{\partial \operatorname{grad} \theta^G} \Big|_{\mathcal{S}_0} \,.
\end{aligned}
\tag{3.68}
$$

Recall that, neglecting mass productions, the total energy interaction between two constituents consists of the direct energy production, also to be understood as the *caloric interaction*, and of an additional part, which can be interpreted as the heat exchange due to friction effects, cf. relation $(2.41)_3$. In addition, from the fundamentals of heat transfer, it is well known that the driving force for the *caloric interaction* between to bodies is given by the temperature difference between them, cf., e. g., Grigull [43]. As a result of this fact, the change in $\hat{\varepsilon}^G$ with respect to θ^S must be equivalent to the negative change of $\hat{\varepsilon}^G$ with respect to θ^G. Thus, it follows

$$
k^\varepsilon_{\theta^S} = -k^\varepsilon_{\theta^G} \,. \tag{3.69}
$$

Considering (3.69), the insertion of (3.68) into (3.61) yields

$$
\begin{aligned}
\mathcal{D}_n(\mathcal{S}) = \; & \frac{\theta^S}{\theta^G}\,(\overset{4}{\mathbf{Z}}_G\;\;\mathbf{D}_G)\cdot\mathbf{D}_G + \frac{1}{\theta^G}\,k^{\varepsilon}_{\theta^S}\,(\theta^S-\theta^G)^2 - \\
& -(\mathbf{S}_w\;\mathbf{w}_G)\cdot\mathbf{w}_G - \frac{1}{\theta^G}\left[\frac{\theta^G}{\theta^S}\,(\mathbf{K}^S_{\theta^S}\;\operatorname{grad}\theta^S)\cdot\operatorname{grad}\theta^S + \right. \\
& \left. + \frac{\theta^S}{\theta^G}\,(\mathbf{K}^G_{\theta^G}\;\operatorname{grad}\theta^G)\cdot\operatorname{grad}\theta^G\right] \geq 0\,.
\end{aligned}
\tag{3.70}
$$

In order to satisfy (3.70) sufficiently, it must be ensured that each term of this inequality separately is restricted to positive values. This requirement yields

$$
\begin{aligned}
\overset{4}{\mathbf{Z}}_G \;&\rightsquigarrow\; \text{positive definite}\,,\\
-\mathbf{S}_w \;&\rightsquigarrow\; \text{positive definite}\,,\\
-\mathbf{K}^S_{\theta^S} \;&\rightsquigarrow\; \text{positive definite}\,,\\
-\mathbf{K}^G_{\theta^G} \;&\rightsquigarrow\; \text{positive definite}\,,\\
k^{\varepsilon}_{\theta^S} \;&>\; 0\,.
\end{aligned}
\tag{3.71}
$$

Consequences from the restrictions. Considering (3.62) and (3.69), the insertion of (3.71) into the corresponding quantities in (3.67) leads to the constitutive equations:

$$
\begin{aligned}
\mathbf{T}^G_E &= \overset{4}{\mathbf{Z}}_G\;\;\mathbf{D}_G\,,\\
\hat{\varepsilon}^G &= k^{\varepsilon}_{\theta}\,(\theta^S-\theta^G)\,,\\
\hat{\mathbf{p}}^G_E &= -\mathbf{S}_w\;\mathbf{w}_G\,,\\
\mathbf{q}^S &= -\mathbf{K}^S_{\theta^S}\;\operatorname{grad}\theta^S\,,\\
\mathbf{q}^G &= -\mathbf{K}^G_{\theta^G}\;\operatorname{grad}\theta^G\,.
\end{aligned}
\tag{3.72}
$$

In $(3.72)_1$, $\overset{4}{\mathbf{Z}}_G$ can be understood as the viscosity tensor of fourth order for micro-fluids, for which the well-known constitutive approach (cf., e. g., Ehlers [33]) is introduced via

$$
\overset{4}{\mathbf{Z}}_G = 2\,\mu^G\,(\mathbf{I}\otimes\mathbf{I})^{\overset{23}{T}} + \lambda^G\,(\mathbf{I}\otimes\mathbf{I})\,.
\tag{3.73}
$$

Therein, μ^G and λ^G, respectively, are the partial shear viscosity and the material volumetric viscosity of the gas.

A corresponding approach for $\mathbf{S}_w$ in $(3.72)_3$ will be presented in Subsection 3.4.1. It will then be seen that $\mathbf{S}_w$ can be interpreted as a general permeability tensor.

Finally, k^{ε}_{θ} represents in $(3.72)_2$ the heat exchange coefficient with

$$k_\theta^\varepsilon \;:=\; k_{\theta S}^\varepsilon\,, \tag{3.74}$$

whereas $\mathbf{K}_{\theta S}^S$ and $\mathbf{K}_{\theta G}^G$ are the corresponding heat conduction tensors of second order in $(3.72)_4$ and $(3.72)_5$, respectively.

3.3 Consequences from thermodynamic potentials

After adequate approaches were formulated for the response functions in the preceding section, further quantities have still to be determined. This can be achieved by use of the thermodynamic potentials, which have been obtained in (3.45) and (3.52), respectively.

Note that a detailed derivation of the respective quantities represented in this section is given in Appendix B.

3.3.1 Total stress, total entropy and total interaction force

Proceeding from the *principle of phase separation*, it is generally assumed that the fluid constituent in multiphasic materials does not recognize the domain where it exists on and, consequently, the fluid behavior is independent from the fact, whether or not it is surrounded by a solid skeleton, cf. Ehlers [26]. As a result of this assumption, some relations from the classical mechanics of single-phasic fluids can be postulated *a priori* for the fluid phase in coupled solid-fluid problems. One of these postulations is the relationship between the effective gas pressure and the free energy ψ^G, viz.:

$$p^{GR} = (\rho^{GR})^2 \frac{\partial \psi^G}{\partial \rho^{GR}}\,, \tag{3.75}$$

which results from the entropy evaluation of an one-component compressible fluid, cf., e. g., Altenbach and Altenbach [1].

Taking advantage of (3.75), the *Lagrange*an multiplier Λ can be determined from the thermodynamic potential $(3.45)_5$ and reads

$$\Lambda = \frac{\theta^S}{\theta^G}\, p^{GR}\,. \tag{3.76}$$

Inserting (3.76) into (3.19), one obtains

$$\begin{aligned}
\mathbf{T}^S &= -\,n^S\,\frac{\theta^S}{\theta^G}\,p^{GR}\,\mathbf{I} + \mathbf{T}^S_E\,,\\
\mathbf{T}^G &= -\,n^G\,p^{GR}\,\mathbf{I} + \mathbf{T}^G_E\,,\\
\eta^S &= \frac{\theta^S}{\theta^G}\,p^{GR}\,\frac{1}{(\rho^{SR})^2}\,\frac{\partial \rho^{SR}}{\partial\,\theta^S} + \eta^S_E\,,\\
\hat{\mathbf{p}}^G &= \frac{\theta^S}{\theta^G}\,p^{GR}\,\mathrm{grad}\,n^G + \hat{\mathbf{p}}^G_E\,.
\end{aligned} \tag{3.77}$$

3.3.2 Specific heat

The specific heat has to be understood as the quantity of heat required per unit mass per degree rise in temperature. According to the fundamental principles of thermodynamics (cf., e. g., Baehr [3]), this quantity is postulated via

$$C_V^\alpha = \frac{\partial\,\varepsilon^\alpha}{\partial\,\theta^\alpha}\,. \tag{3.78}$$

$(\cdot)_V$ denotes that C_V^α is measured at constant volume. Substituting the internal energy ε^α by the free *Helmholtz* energy from (2.44), the potential above can also be expressed as

$$C_V^\alpha = \frac{\partial\,(\psi^\alpha + \theta^\alpha \eta^\alpha)}{\partial\,\theta^\alpha}\quad . \tag{3.79}$$

Furthermore, taking advantage of the thermodynamic potentials $(3.45)_3$ or $(3.45)_9$, respectively, the specific heat at constant volume alternatively yields for each constituent

$$C_V^\alpha = -\frac{\partial^2\,\psi^\alpha}{\partial\,(\theta^\alpha)^2}\,\theta^\alpha\,. \tag{3.80}$$

3.3.3 Free energy of the gas constituent

The compressible fluid constituent under consideration is presumed to be an ideal gas. The free energy ψ^G is defined (B.48) via

$$\psi^G = \bar{R}^G\,\theta^G \ln \rho^{GR} - C_V^G\,(\theta^G \ln \theta^G - \theta^G)\,, \tag{3.81}$$

with $\bar{R}^G$ being the specific gas constant.

3.3.4 Gas density

Taking advantage of relation (3.81) and the thermodynamic potential (3.75), one obtains for the effective gas density

$$\rho^{GR} = \frac{p^{GR}}{\bar{R}^G\,\theta^G}\,. \tag{3.82}$$

3.3.5 Entropy function of the gas constituent

Once ψ^G is given, one obtains the gas entropy by use of the thermodynamic potential $(3.45)_9$ as

$$\eta^G = -\bar{R}^G \ln \rho^{GR} + C_V^G \ln \theta^G\,. \tag{3.83}$$

3.3.6 Free energy of the solid constituent

Non-linear solid energy. Considering $(3.48)_1$, the stored strain energy of a thermoelastic solid constituent is postulated by Ehlers [33], where an extension of the *Simo-Pister* law is given for a non-linear thermoelastic model via

$$\begin{aligned}\rho_{0S}^S\,\psi^S(I_c,\ III_c,\ \theta^S) = \\ &\tfrac{1}{2}\,\mu^S\,(\ I_c - 3\ ) + (\ m^S\Delta\theta^S - \mu^S\ )\ \ln\,(\det\mathbf{C}_S)^{\frac{1}{2}} + \\ &+\tfrac{1}{2}\,\lambda^S\left[\ln(\det\mathbf{C}_S)^{\frac{1}{2}}\right]^2 - \rho_{0S}^S\,C_V^S\left(\theta^S\,\ln\frac{\theta^S}{\theta_{0S}^S} - \Delta\theta^S\right).\end{aligned} \tag{3.84}$$

Therein, m^S represents the stress-temperature modulus given by

$$m^S = -(2\mu^S + 3\lambda^S)\alpha^S \quad ; \quad \mu^S\,,\lambda^S\ :\ \textit{Lamé}\ \text{constants}\,. \tag{3.85}$$

Furthermore, I_c and III_c are the well-known first and third *principle invariants* of $\mathbf{C}_S$, which are defined as

$$\begin{aligned} I_c &= \mathbf{C}_S\cdot\mathbf{I}\,, \\ III_c &= \det\mathbf{C}_S\,. \end{aligned} \tag{3.86}$$

Linear solid energy. The solid stored energy for infinitesimal strains $(3.54)_1$ can be obtained from (3.84) by use of standard linearization procedures so that

$$\begin{aligned}\rho_{0S}^S\,\psi_{lin}^S(\boldsymbol{\varepsilon}_S,\theta^S) = {}& \mu^S\boldsymbol{\varepsilon}_S\cdot\boldsymbol{\varepsilon}_S + \tfrac{1}{2}\lambda^S(\boldsymbol{\varepsilon}_S\cdot\mathbf{I})^2 + m^S\,\Delta\theta^S\,\boldsymbol{\varepsilon}_S\cdot\mathbf{I} - \\ &-\rho_{0S}^S\ C_V^S\left(\theta^S\ln\frac{\theta^S}{\theta_0^S} - \Delta\theta^S\right).\end{aligned} \tag{3.87}$$

Therein, $\boldsymbol{\varepsilon}_S$ can be gained from the *Green-Lagrange*an strain tensor $\mathbf{E}_S$ from (2.26) through a linearization and has the form

$$\boldsymbol{\varepsilon}_{\boldsymbol{S}} = \tfrac{1}{2}(\,\mathrm{Grad}\mathbf{u}_S + \mathrm{Grad}^T\mathbf{u}_S\,)\,. \tag{3.88}$$

3.3.7 Thermoelastic stress

Non-linear solid stress tensor. Considering the thermodynamic potential $(3.45)_1$, the solid stress tensor $\mathbf{T}_E^S$ can be given (B.34) through the differentiation of the solid stored energy (3.84). Thus,

$$\begin{aligned}\mathbf{T}_E^S &= (\det\mathbf{F}_S)^{-1}\,[\,\mu^S\,(\mathbf{B}_S - \mathbf{I}\,) + m^S\,\Delta\theta^S\,\mathbf{I} + \lambda^S\ln(\det\mathbf{F}_S)\,\mathbf{I}\,] \\ &= (\det\mathbf{F}_S)^{-1}\,\boldsymbol{\tau}_E^S\end{aligned} \tag{3.89}$$

with $\boldsymbol{\tau}_E^S$ as the *Kirchhoff* stress tensor from (2.35).

Linear solid stress tensor. In analogy to (3.89), the linear stress tensor $\boldsymbol{\sigma}_E^S$ can be determined from (3.52) and (3.87), which yields

$$\boldsymbol{\sigma}_E^S = 2\,\mu^S\,\boldsymbol{\varepsilon}_S + \lambda^S\,(\,\boldsymbol{\varepsilon}_S\cdot\mathbf{I}\,)\,\mathbf{I} + m^S\,\Delta\theta^S\,\mathbf{I}\,. \tag{3.90}$$

3.3.8 Entropy function of the solid constituent

The solid extra entropies η_E^S and $\eta_{E_{lin}}^S$ can be gained from the solid energy functions (3.84) or (3.87), respectively, where the thermodynamic potential $(3.45)_3$ has to be used. The total entropies η^S and η_{lin}^S result then from $(3.77)_3$.

Non-linear solid entropy. The total entropy function for a non-linear solid constituent is derived in (B.39) and reads

$$\eta^S = -\frac{3\alpha^S\,\theta^S}{\rho_{0S}^{SR}\,\theta^G}\,p^{GR}\,e^{3\,\alpha^S\,\Delta\theta^S} + C_V^S\ln\frac{\theta^S}{\theta_{0S}^S} - \frac{1}{\rho_{0S}^S}\,m^S\ln\left(\det\mathbf{F}_S\right). \tag{3.91}$$

Linear solid entropy. In analogy to (3.91), one obtains (B.41) for the linear entropy function

$$\eta_{lin}^S = -\frac{3\alpha^S\,\theta^S}{\rho_{0S}^{SR}\,\theta^G}\,p^{GR}\,e^{3\,\alpha^S\,\Delta\theta^S} + C_V^S\ln\frac{\theta^S}{\theta_{0S}^S} - \frac{1}{\rho^S}\,m^S\,\boldsymbol{\varepsilon}_S\cdot\mathbf{I}\,. \tag{3.92}$$

3.4 The quasi-static formulation

In terms of the subsequent numerical computation of the model under study, the solid displacement $\mathbf{u}_S$, the real gas pressure p^{GR}, the velocity $\overset{\prime}{\mathbf{x}}_G$ of the gas as well as the respective temperature fields θ^S and θ^G have to be considered as unknown field variables, cf. Chapter 1. However, using (2.14), the seepage velocity $\mathbf{w}_G$ is introduced as an independent field variable instead of $\overset{\prime}{\mathbf{x}}_G$.

Once the determining set of the independent field variables is defined, the corresponding field equations can then be gained from the kinematics, the balance relations and the constitutive equations of the model. After suitable constitutive approaches were formulated in the preceding sections, the system of equations can now be assembled.

For the dynamic formulation of the problem under study, the corresponding equations, five in number, can be given, firstly, by the sum of the solid and gas momentum balance equations, secondly, by the gas mass balance equation, thirdly, by the gas momentum balance equation, fourthly, by the energy balance equation of the solid and, finally, by the energy balance equation of the gas.

However, proceeding from small velocities and lingering flow conditions in the model under consideration, only the quasi-static formulation of the problem is treated in the present work. Thus, the accelerations are assumed to be negligible, i. e.

$$\overset{\prime\prime}{\mathbf{x}}_S = \overset{\prime\prime}{\mathbf{x}}_G = \mathbf{0}\,. \tag{3.93}$$

It will be shown in Subsection 3.4.1 that the seepage velocity can be identified through a constitutive equation when quasi-static processes are described. As a consequence, $\mathbf{w}_G$ loses its independent character and has hence to be dropped from the set of unknown variables. The system of equations is then reduced to four, namely, the mixture momentum balance equation, the gas mass balance equation, the energy balance equation of the solid and the energy balance equation of the gas. The momentum balance equation of gas will be used in order to determine the constitutive equation for $\mathbf{w}_G$.

In Subsection 3.4.2, the set of the determining equations is given in the strong formulation. The weak formulation of these equations, based on the Finite Element Method (FEM), is then represented in Subsection 3.4.3. The detailed derivation of the corresponding equations can be found in Appendix B.

Note that small strains are assumed for the solid constituent under consideration so that the corresponding linear quantities are used in this section. However, for the sake of clarity, $(\cdot)_{lin}$ will be omitted.

Preliminaries. Before the corresponding field equations will be derived, some relations are better discussed in advance. At first, the solid velocity can be expressed by use of (2.13), which yields

$$\overset{\prime}{\mathbf{x}}_S = (\mathbf{u}_S)'_S + \underbrace{(\mathbf{X}_S)'_S}_{\mathbf{0}}\,. \tag{3.94}$$

Concerning the time derivatives of the gas density and the gas volume fraction, respectively, one can express these quantities with respect to the solid skeleton. To this end, the consideration of (2.14) and (2.21) yields

$$\begin{aligned} (\rho^G)'_G &= (\rho^G)'_S + \operatorname{grad}\rho^G \cdot \mathbf{w}_G\,, \\ (n^G)'_G &= (n^G)'_S + \operatorname{grad} n^G \cdot \mathbf{w}_G\,. \end{aligned} \tag{3.95}$$

Finally, taking note of the fact that both constituents are governed by the same gravitation field, it follows that

$$\mathbf{b}^G = \mathbf{b}^S = \mathbf{b}\,. \tag{3.96}$$

3.4.1 A Darcy-like approach

In this subsection, the momentum balance equation of the gas will be used in order to find a constitutive relation for the seepage velocity $\mathbf{w}_G$. For quasi-static processes (B.57), the momentum balance equation reads

$$\begin{aligned} &\operatorname{div}\mathbf{T}^G_E - p^{GR}\operatorname{grad} n^G - n^G\operatorname{grad} p^{GR} + \\ &+ \frac{\theta^S}{\theta^G}\, p^{GR}\operatorname{grad} n^G + \hat{\mathbf{p}}^G_E + n^G\rho^{GR}\mathbf{b}^G = \mathbf{0}\,. \end{aligned} \tag{3.97}$$

Inserting $(3.72)_3$, (3.97) can be rewritten as

$$\mathbf{S}_w \mathbf{w}_G \,=\, \operatorname{div} \mathbf{T}^G_E \,+\, p^{GR} \operatorname{grad} n^G \left(\frac{\theta^S}{\theta^G} \,-\, 1 \right) \,-\, n^G \operatorname{grad} p^{GR} \,+\, n^G \rho^{GR} \mathbf{b}^G \,. \qquad (3.98)$$

This equation represents the momentum balance of the gas constituent for quasi-static processes at *non-isothermal* conditions. However, neglecting the friction stress $\mathbf{T}^G_E$ and assuming *isothermal* conditions, (3.98) must result in the well-known *Darcy* law, which embodies an empirical expression for the fluid flow through a porous material. In order to achieve this, it turns immediately out that the following relation must apply:

$$\mathbf{S}_w \,=\, (n^G)^2 \, \mu^{GR} \, (\mathbf{K}^{\mathbf{S}})^{-1} \,. \qquad (3.99)$$

Therein, $\mathbf{K}^S$ represents the intrinsic permeability of the solid skeleton.

Reinserting (3.99) into (3.98) and neglecting $\mathbf{T}^G_E$, a new relation is found for the seepage velocity for quasi-static processes at *non-isothermal* conditions via

$$n^G \, \mathbf{w}_G = - \, \frac{1}{\mu^{GR}} \, \mathbf{K}^{\mathbf{S}} \left[\operatorname{grad} p^{GR} \,-\, \rho^{GR} \, \mathbf{b}^G \,+\, \frac{1}{n^G} \, p^{GR} \operatorname{grad} n^G \left(1 \,-\, \frac{\theta^S}{\theta^G} \right) \right] . \qquad (3.100)$$

This equation can be reduced for isothermal processes to the classical *Darcy* law (cf., e. g., Helmig [49])

$$n^G \, \mathbf{w}_G \,=\, - \, \frac{1}{\mu^{GR}} \, \mathbf{K}^{\mathbf{S}} \, (\operatorname{grad} p^{GR} \,-\, \rho^{GR} \, \mathbf{b}^G) \qquad (3.101)$$

and has thus to be understood as an extended *Darcy* approach for non-isothermal processes. It is pointed out that the seepage velocity is expressed in (3.100) with the aid of the pressure gradient, which means that the independent variable $\mathbf{w}_G$ can now be determined through an another independent variable p^{GR} and becomes thus an dependent variable.

Finally, note that, given (3.99), the equation $(3.72)_3$ can be rewritten as

$$\hat{\mathbf{p}}^G_E \,=\, - \, (n^G)^2 \, \mu^{GR} \, (\mathbf{K}^{\mathbf{S}})^{-1} \, \mathbf{w}_G \,. \qquad (3.102)$$

3.4.2 The strong formulation of the determining equations

Proceeding from the determining independent variables $\mathbf{u}_S, p^{GR}, \theta^S$ and θ^G for the quasi-static formulation of the non-isothermal biphasic model to be studied, the governing field equations can be taken from (B.53), (B.61), (B.70) and (B.80). Note that $\hat{\varepsilon}^S$ is substituted through (3.5) and $(3.77)_4$.

Mixture momentum balance equation:

$$\begin{aligned} &\operatorname{div} \left(\boldsymbol{\sigma}^S_E \,-\, n^S \, \frac{\theta^S}{\theta^G} \, p^{GR} \, \mathbf{I} \,+\, \mathbf{T}^G_E \,-\, n^G \, p^{GR} \, \mathbf{I} \right) \,+ \\ &+ (\, n^S \, \rho^{SR} \,+\, n^G \, \rho^{GR} \,) \, \mathbf{b} \,=\, \mathbf{0} \,. \end{aligned} \qquad (3.103)$$

Mass balance equation of the gas constituent:

$$\begin{aligned}
&\frac{n^G}{\bar{R}^G\,\theta^G}\,(p^{GR})'_S \,-\, \frac{n^G}{\bar{R}^G\,(\theta^G)^2}\,p^{GR}\,(\theta^G)'_S \,+\, \mathrm{div}\,(n^G\,\rho^{GR}\,\mathbf{w}_G)\,+ \\
&+n^G\,\rho^{GR}\,\mathrm{div}\,(\mathbf{u}_S)'_S \,-\, (n^S)'_S\,\rho^{GR} \,=\, 0\,,
\end{aligned} \tag{3.104}$$

Energy balance equation of the gas constituent:

$$\begin{aligned}
&-\,n^G\,\rho^{GR}\,C_V^G\,(\theta^G)'_S \,-\, n^G\,\rho^{GR}\,C_V^G\,\mathrm{grad}\,\theta^G\cdot\mathbf{w}_G \,+\, n^G\,(p^{GR})'_S\,- \\
&-\frac{n^G}{\theta^G}\,p^{GR}\,(\theta^G)'_S \,+\, n^G\,\mathrm{grad}\,p^{GR}\cdot\mathbf{w}_G \,-\, \frac{n^G}{\theta^G}\,p^{GR}\,\mathrm{grad}\,\theta^G\cdot\mathbf{w}_G\,+ \\
&+p^{GR}\,\mathrm{grad}\,n^G\cdot\mathbf{w}_G \,-\, p^{GR}\,(n^S)'_S \,+\, \mathbf{T}_E^G\cdot\mathbf{D}_G \,-\, \mathrm{div}\,\mathbf{q}^G\,+ \\
&+n^G\,\rho^{GR}\,r^G \,+\, \hat{\varepsilon}^G \,=\, 0\,,
\end{aligned} \tag{3.105}$$

Energy balance equation of the solid constituent:

$$\begin{aligned}
&3\,\alpha^S\,n^S\,\frac{\theta^S}{\theta^G}\,p^{GR}\,\Big[2\,(\theta^S)'_S \,-\, \frac{\theta^S}{\theta^G}\,(\theta^G)'_S \,+\, \frac{1}{p^{GR}}\,\theta^S\,(p^{GR})'_S\,+ \\
&+3\,\alpha^S\,\theta^S\,(\theta^S)'_S\Big] \,-\, n^S\,\rho^{SR}\,C_V^S\,(\theta^S)'_S \,+\, \theta^S\,m^S\,\mathbf{I}\cdot(\boldsymbol{\varepsilon}_S)'_S\,+ \\
&+n^S\,\rho^{SR}\,r^S \,-\, n^S\,\frac{\theta^S}{\theta^G}\,p^{GR}\,\mathbf{I}\cdot(\boldsymbol{\varepsilon}_S)'_S \,-\, \mathrm{div}\,\mathbf{q}^S \,-\, \hat{\varepsilon}^G\,- \\
&-\,\frac{\theta^S}{\theta^G}\,p^{GR}\,\mathrm{grad}\,n^G\cdot\mathbf{w}_G \,-\, \hat{\mathbf{p}}_E^G\cdot\mathbf{w}_G = 0\,.
\end{aligned} \tag{3.106}$$

3.4.3 The weak formulation

Concerning the foundations of the numerical analysis, reference should be made to, e. g., Axelsson and Barker [2], Schwarz [67] or Zienkiewicz and Taylor [83]. The numerical realization of the problem on hand is based on the weak formulation of the determining field equations in Subsection 3.4.2.

In order to obtain the weak form of (3.103), (3.104), (3.105) and (3.106), respectively, the standard *Galerkin* procedure (*Bubnov-Galerkin*) is utilized, cf., e. g., Schwarz [67]. Therein, the corresponding equations are multiplied by the so-called test functions, which in turn are introduced as virtual quantities. The test function $\delta \mathbf{u}_S$ applied to the mixture momentum balance can be understood as a virtual displacement, whereas δp^{GR} included in the gas mass balance equation represents a virtual pressure. In analogy, $\delta\theta^S$ and $\delta\theta^G$, respectively, can be interpreted as virtual temperatures. Furthermore, after the test functions are applied to the respective equations, the subsequent integration over the control space Ω yields the corresponding weak forms.

It is pointed out that the spatial discretization (cf., e. g., Schwarz [67]) of the equations is based on the quadratic shape functions for the solid displacement $\mathbf{u}_S$, whereas the remainder of the independent fields is described by linear shape functions. The primary variables of the quasi-static problem are thus given in the spatial discretization, via

$$
\begin{aligned}
\mathbf{u}_S^h(\mathbf{x}, t) &= \sum_{i=1}^{N} \mathcal{G}_i(\mathbf{x})\, \mathbf{u}_S^i(t)\,, \\
p^{GRh}(\mathbf{x}, t) &= \sum_{i=1}^{M} \mathcal{H}_i(\mathbf{x})\, p^{GRi}(t)\,, \\
\theta^{Sh}(\mathbf{x}, t) &= \sum_{i=1}^{M} \mathcal{H}_i(\mathbf{x})\, \theta^{Si}(t)\,, \\
\theta^{Gh}(\mathbf{x}, t) &= \sum_{i=1}^{M} \mathcal{H}_i(\mathbf{x})\, \theta^{Gi}(t)\,.
\end{aligned}
\tag{3.107}
$$

As is seen in (3.107), the respective quantities $(\cdot)^h$ are spatially discretized by use of a quadratic shape function, $\mathcal{G}_i$ at the node i for all N nodes, or a linear shape function, $\mathcal{H}_i$ at the node i related only to corner nodes M. Note that the corresponding test functions have to be discretized in an analogous manner. The insertion of the semi-discrete model, i. e. discretized in space but not in time, into the weak formulation of the corresponding equations yields a system of Differential-Algebraic Equations (DAE).

Furthermore, constituting the weak forms of the equations, it can be seen in (B.83), (B.87) and (B.89) that some divergence terms can be reformulated. Therein, surface integrals are created, which enable the definition of the corresponding boundary conditions for the model under consideration.

The respective weak formulations are obtained as follows:

Mixture momentum balance equation in weak form:

$$\begin{aligned}
\int\limits_{\Gamma_t} \bar{\mathbf{t}} \cdot \delta \mathbf{u}_S \, \mathrm{d}a + \int\limits_{\Omega} (n^S \rho^{SR} + n^G \rho^{GR}) \, \mathbf{b} \cdot \delta \mathbf{u}_S \, \mathrm{d}v = \\
= \int\limits_{\Omega} \boldsymbol{\sigma}_E^S \cdot \operatorname{grad} \delta \mathbf{u}_S \, \mathrm{d}v - \\
- \int\limits_{\Omega} n^S \frac{\theta^S}{\theta^G} p^{GR} \mathbf{I} \cdot \operatorname{grad} \delta \mathbf{u}_S \, \mathrm{d}v - \\
- \int\limits_{\Omega} n^G p^{GR} \mathbf{I} \cdot \operatorname{grad} \delta \mathbf{u}_S \, \mathrm{d}v + \\
+ \int\limits_{\Omega} \mathbf{T}_E^G \cdot \operatorname{grad} \delta \mathbf{u}_S \, \mathrm{d}v \, ,
\end{aligned} \tag{3.108}$$

with $\bar{\mathbf{t}}$ being the external load vector acting on the *Neumann* boundary Γ_t (B.83) defined as

$$\bar{\mathbf{t}} = \left(\boldsymbol{\sigma}_E^S - n^S \frac{\theta^S}{\theta^G} p^{GR} \mathbf{I} + \mathbf{T}_E^G - n^G p^{GR} \mathbf{I} \right) \mathbf{n} \, . \tag{3.109}$$

Mass balance equation of the gas constituent in weak form:

$$\begin{aligned}
- \int\limits_{\Gamma_v} \delta p^{GR} \, \bar{v} \, \mathrm{d}a + \int\limits_{\Omega} \frac{1}{\mu^{GR}} (\rho^{GR})^2 (\mathbf{K}_S \, \mathbf{b}^G) \cdot \operatorname{grad} \delta p^{GR} \, \mathrm{d}v = \\
= \int\limits_{\Omega} \frac{n^G}{\bar{R}^G \theta^G} (p^{GR})'_S \, \delta p^{GR} \, \mathrm{d}v - \\
- \int\limits_{\Omega} \frac{n^G}{\bar{R}^G (\theta^G)^2} p^{GR} (\theta^G)'_S \, \delta p^{GR} \, \mathrm{d}v + \\
+ \int\limits_{\Omega} \frac{1}{\mu^{GR}} \rho^{GR} (\mathbf{K}_S \operatorname{grad} p^{GR}) \cdot \operatorname{grad} \delta p^{GR} \, \mathrm{d}v + \\
+ \int\limits_{\Omega} \frac{1}{n^G \mu^{GR}} \rho^{GR} p^{GR} \left(1 - \frac{\theta^S}{\theta^G} \right) (\mathbf{K}_S \operatorname{grad} n^G) \cdot \operatorname{grad} \delta p^{GR} \, \mathrm{d}v + \\
+ \int\limits_{\Omega} n^G \rho^{GR} \operatorname{div} (\mathbf{u}_S)'_S \, \delta p^{GR} \, \mathrm{d}v - \\
- \int\limits_{\Omega} (n^S)'_S \, \rho^{GR} \, \delta p^{GR} \, \mathrm{d}v
\end{aligned} \tag{3.110}$$

with $\bar{v}$ as the efflux of the gas through the *Neumann* boundary Γ_v (B.87), identified as

$$\bar{v} = n^G \rho^{GR} \mathbf{w}_G \cdot \mathbf{n} \, . \tag{3.111}$$

Energy balance equation of the gas constituent in weak form:

$$
\begin{aligned}
\int\limits_{\Gamma_{q^G}} \delta\theta^G\, \bar{q}^{\,G}\, \mathrm{d}a \;-\; \int\limits_{\Omega} n^G\, \rho^{GR}\, r^G\, \delta\theta^G\;\, \mathrm{d}v \;=\; & \\
= -\int\limits_{\Omega} n^G\, \rho^{GR}\, C_V^G\, (\theta^G)'_S\, \delta\theta^G\;\, \mathrm{d}v\, - & \\
- \int\limits_{\Omega} n^G\, \rho^{GR}\, C_V^G\, \mathrm{grad}\, \theta^G \cdot \mathbf{w}_G\, \delta\theta^G\;\, \mathrm{d}v\, + & \\
+ \int\limits_{\Omega} n^G\, (p^{GR})'_S\, \delta\theta^G\;\, \mathrm{d}v\, - & \\
- \int\limits_{\Omega} \frac{n^G}{\theta^G}\, p^{GR}\, (\theta^G)'_S\, \delta\theta^G\;\, \mathrm{d}v\, + & \\
+ \int\limits_{\Omega} n^G\, \mathrm{grad}\, p^{GR} \cdot \mathbf{w}_G\, \delta\theta^G\;\, \mathrm{d}v\, - & \\
- \int\limits_{\Omega} \frac{n^G}{\theta^G}\, p^{GR}\, \mathrm{grad}\, \theta^G \cdot \mathbf{w}_G\, \delta\theta^G\;\, \mathrm{d}v\, + & \\
+ \int\limits_{\Omega} p^{GR}\, \mathrm{grad}\, n^G \cdot \mathbf{w}_G\, \delta\theta^G\;\, \mathrm{d}v\, - & \\
- \int\limits_{\Omega} p^{GR}\, (n^S)'_S\, \delta\theta^G\;\, \mathrm{d}v\, + & \\
+ \int\limits_{\Omega} \mathbf{T}_E^G \cdot \mathbf{D}_G\, \delta\theta^G\;\, \mathrm{d}v\, + & \\
+ \int\limits_{\Omega} \mathbf{q}^G \cdot \mathrm{grad}\, \delta\theta^G\, \mathrm{d}v\, + & \\
+ \int\limits_{\Omega} \hat{\varepsilon}^G\, \delta\theta^G\;\, \mathrm{d}v &
\end{aligned}
\tag{3.112}
$$

with $\bar{q}^{\,G}$ as the heat efflux of the gas through the *Neumann* boundary Γ_{q^G} (B.89), given by

$$
\bar{q}^{\,G} \;=\; \mathbf{q}^G \cdot \mathbf{n}\,. \tag{3.113}
$$

Energy balance equation of the solid constituent in weak form:

$$
\begin{aligned}
\int\limits_{\Gamma_{q^S}} \delta\theta^S \, \bar{q}^S \; \mathrm{d}a \; - \int\limits_{\Omega} n^S \rho^{SR} r^S \, \delta\theta^S \; \mathrm{d}v \; = \\
= & \int\limits_{\Omega} 6\,\alpha^S n^S \frac{\theta^S}{\theta^G} \, p^{GR} \, (\theta^S)'_S \, \delta\theta^S \; \mathrm{d}v \, - \\
& - \int\limits_{\Omega} 3\,\alpha^S n^S \left(\frac{\theta^S}{\theta^G}\right)^2 p^{GR} \, (\theta^G)'_S \, \delta\theta^S \; \mathrm{d}v \, + \\
& + \int\limits_{\Omega} 3\,\alpha^S n^S \frac{(\theta^S)^2}{\theta^G} \, (p^{GR})'_S \, \delta\theta^S \; \mathrm{d}v \, + \\
& + \int\limits_{\Omega} 9\, n^S \frac{(\alpha^S \theta^S)^2}{\theta^G} \, p^{GR} \, (\theta^S)'_S \, \delta\theta^S \; \mathrm{d}v \, - \\
& - \int\limits_{\Omega} n^S \rho^{SR} C_V^S \, (\theta^S)'_S \, \delta\theta^S \; \mathrm{d}v \, + \\
& + \int\limits_{\Omega} \theta^S m^S \, (\boldsymbol{\varepsilon}_S)'_S \cdot \mathbf{I} \, \delta\theta^S \; \mathrm{d}v \, - \\
& - \int\limits_{\Omega} n^S \frac{\theta^S}{\theta^G} \, p^{GR} \, (\boldsymbol{\varepsilon}_S)'_S \cdot \mathbf{I} \, \delta\theta^S \; \mathrm{d}v \, + \\
& + \int\limits_{\Omega} \mathbf{q}^S \cdot \operatorname{grad} \delta\theta^S \; \mathrm{d}v \, - \\
& - \int\limits_{\Omega} \hat{\varepsilon}^G \, \delta\theta^S \; \mathrm{d}v \, - \\
& - \int\limits_{\Omega} \frac{\theta^S}{\theta^G} \, p^{GR} \operatorname{grad} n^G \cdot \mathbf{w}_G \, \delta\theta^S \; \mathrm{d}v \, - \\
& - \int\limits_{\Omega} \hat{\mathbf{p}}_E^G \cdot \mathbf{w}_G \, \delta\theta^S \; \mathrm{d}v
\end{aligned}
\tag{3.114}
$$

with $\bar{q}^S$ as the heat efflux of the solid through the *Neumann* boundary Γ_{q^S} (B.89), given by

$$\bar{q}^{\,S} \, = \, \mathbf{q}^S \cdot \mathbf{n} \, . \tag{3.115}$$

The overall heat efflux $\bar{q}$ through the mixture surface is split up *a priori* with the aid of the volume fractions via

$$\bar{q} \, = \, \bar{q}^{\,S} \, + \, \bar{q}^{\,G} \, = \, n^S \, \bar{q} \, + \, n^G \, \bar{q} \, . \tag{3.116}$$

Note that the verification of this assumption can only be achieved by experiments.

Finally, it is noted that the following relations must be additionally considered in the weak form of the balance equations:

$$
\begin{aligned}
n^S &= n^S_{0S}\,(1 - \operatorname{div}\mathbf{u}_S)\,e^{3\,\alpha^S\,\Delta\theta^S}\,,\\
(n^S)'_S &= 3\,\alpha^S\,n^S_{0S}\,e^{3\,\alpha^S\,\Delta\theta^S}\left[(\theta^S)'_S\,-\,\operatorname{div}\mathbf{u}_S\,-\,\frac{1}{3\,\alpha^S}\operatorname{div}(\mathbf{u}_S)'_S\right]\,,\\
n^G &= 1\,-\,n^S\,,\\
\rho^{SR} &= \rho^{SR}_{0S}\,e^{-3\,\alpha^S\,\Delta\theta^S}\,,\\
\rho^{GR} &= \frac{p^{GR}}{\bar{R}^G\,\theta^G}\,,\\
\boldsymbol{\sigma}^S_E &= 2\,\mu^S\,\boldsymbol{\varepsilon}_S\,+\,\lambda^S\,(\,\boldsymbol{\varepsilon}_S\cdot\mathbf{I}\,)\,\mathbf{I}\,+\,m^S\,\Delta\theta^S\,\mathbf{I}\,,\\
\mathbf{T}^G_E &= 2\,\mu^G\,\mathbf{D}_G\,+\,\lambda^G\,(\,\mathbf{D}_G\cdot\mathbf{I}\,)\,\mathbf{I}\,,\\
\boldsymbol{\varepsilon}_{\boldsymbol{S}} &= \tfrac{1}{2}(\,\mathrm{Grad}\mathbf{u}_S+\mathrm{Grad}^T\mathbf{u}_S\,)\,,\\
m^S &= -\,(2\mu^S+3\lambda^S)\alpha^S\,,\\
(\boldsymbol{\varepsilon}_{\boldsymbol{S}})'_S &= \tfrac{1}{2}\,[\,\mathrm{Grad}\,(\mathbf{u}_S)'_S\,+\,\mathrm{Grad}^T\,(\mathbf{u}_S)'_S\,]\,,\\
(p^{GR})'_S &= \frac{\partial\,p^{GR}}{\partial\,t}\,+\,\operatorname{grad}p^{GR}\cdot(\mathbf{u}_S)'_S\,,\\
(\theta^S)'_S &= \frac{\partial\,\theta^S}{\partial\,t}\,+\,\operatorname{grad}\theta^S\cdot(\mathbf{u}_S)'_S\,,\\
(\theta^G)'_S &= \frac{\partial\,\theta^G}{\partial\,t}\,+\,\operatorname{grad}\theta^G\cdot(\mathbf{u}_S)'_S\,,\\
\mathbf{q}^S &= -\,\mathbf{K}^S_{\theta^S}\,\operatorname{grad}\theta^S\,,\\
\mathbf{q}^G &= -\,\mathbf{K}^G_{\theta^G}\,\operatorname{grad}\theta^G\,,\\
r^S &:= \text{here neglected}\,,\\
r^G &:= \text{here neglected}\,,\\
\hat{\varepsilon}^G &= k^e_\theta\,(\theta^S-\theta^G)\,,\\
\hat{\mathbf{p}}^G_E &= -\,(n^G)^2\mu^{GR}(\mathbf{K}^S)^{-1}\,\mathbf{w}_G\,,\\
n^G\,\mathbf{w}_G &= -\,\frac{1}{\mu^{GR}}\,\mathbf{K}^{\mathbf{S}}\left[\operatorname{grad}p^{GR}-\rho^{GR}\,\mathbf{b}^G+\frac{1}{n^G}\,p^{GR}\operatorname{grad}n^G\,\left(1-\frac{\theta^S}{\theta^G}\right)\right]\,.
\end{aligned}
\tag{3.117}
$$

For the sake of clearness, the initial and boundary conditions of the model under consideration in the quasi-static formulation are collected in the following:

Initial conditions:

$$\begin{aligned} \mathbf{u}_S(\mathbf{x},\,0) &= \mathbf{u}_{0S}(\mathbf{x})\,, \\ p^{GR}(\mathbf{x},\,0) &= p_0^{GR}(\mathbf{x})\,, \\ \theta^S(\mathbf{x},\,0) &= \theta_0^S(\mathbf{x})\,, \\ \theta^G(\mathbf{x},\,0) &= \theta_0^G(\mathbf{x})\,. \end{aligned} \tag{3.118}$$

Dirichlet boundary conditions:

$$\begin{aligned} &\mathbf{u}_S(\mathbf{x},\,t) && \text{for } \mathbf{x} \in \Gamma_u\,, \\ &p^{GR}(\mathbf{x},\,t) && \text{for } \mathbf{x} \in \Gamma_p\,, \\ &\theta^S(\mathbf{x},\,t) && \text{for } \mathbf{x} \in \Gamma_{\theta^S}\,, \\ &\theta^G(\mathbf{x},\,t) && \text{for } \mathbf{x} \in \Gamma_{\theta^G}\,. \end{aligned} \tag{3.119}$$

Neumann boundary conditions:

$$\begin{aligned} &\mathbf{t}(\mathbf{x},\,t) && \text{for } \mathbf{x} \in \Gamma_t\,, \\ &\bar{v}(\mathbf{x},\,t) && \text{for } \mathbf{x} \in \Gamma_v\,, \\ &\bar{q}^S(\mathbf{x},\,t) && \text{for } \mathbf{x} \in \Gamma_{q^S}\,, \\ &\bar{q}^{\,G}(\mathbf{x},\,t) && \text{for } \mathbf{x} \in \Gamma_{q^G}\,. \end{aligned} \tag{3.120}$$

Chapter 4: Material parameters

4.1 General framework

Before physical effects occurring in the construction under study can be computed by means of the developed model, the material parameters must be determined from experimental data. The parameters of the non-isothermal biphasic model under consideration are collected in the following table.

parameter	description
$\rho_{0S}^{SR}; \rho_{0G}^{GR}$	real initial densities
$n_{0S}^{S}; n_{0G}^{G}$	initial volume fractions
$\mathbf{K}_{0S}^{S}$	initial intrinsic permeability tensor of second order
$\mu^S; \lambda^S$	*Lamé* constants
α_{0S}^{S}	thermal expansion coefficient of the solid
μ_{0G}^{GR}	real initial viscosity parameter of the fluid
$\bar{R}^G$	specific gas constant
$C_{0V}^{S}; C_{0V}^{G}$	initial specific heat at constant volume
$\mathbf{K}_{0\theta^S}^{S}; \mathbf{K}_{0\theta^G}^{G}$	initial heat conduction tensors of second order
k_θ^ε	heat exchange coefficient

Table 4.1: Material parameters of the non-isothermal biphasic model.

Therein, $(\cdot)_0$ denotes the initial state of the quantities, since material parameters can vary during physical processes. For instance, the permeability of a porous material can change, if large deformations occur, cf. Eipper [37]. On the other hand, the viscosity parameter, the heat conduction as well as the thermal expansion coefficient can behave *temperature-dependent*.

It is however almost impossible to determine the whole set of the parameters simultaneously, in particular, since the processes under consideration take place strongly coupled. It is rather necessary to perform the experiments in such a way that the respective physical effects are decoupled and can thus be investigated as isolated processes. For instance, $\mathbf{K}_{0S}^{S}$, which represents a geometrical measure, can be accurately determined by an isothermal and slow flow-through experiment by use of an incompressible fluid. For a porous material with orthotropic permeability properties, $\mathbf{K}^S_{0S}$ has then the form

$$\mathbf{K}^S_{0S} = \begin{bmatrix} k^S_1 & 0 & 0 \\ 0 & k^S_2 & 0 \\ 0 & 0 & k^S_3 \end{bmatrix} (\mathbf{e}_i \otimes \mathbf{e}_j) \, . \tag{4.1}$$

In general, one can divide the model parameters to be studied into three groups. The parameters belonging to the first group are those to be determined from isolated processes such as $\mathbf{K}^S_{0S}$. The second group is represented by parameters, for which it is not necessary to proceed from the mixture model. They can be determined for each constituent separately. To this group belong μ^S, λ^S, α^S_{0S}, μ^{GR}_{0G}, $\bar{R}^G$, C^G_{0V}, C^S_{0V} and $\mathbf{K}^S_{0\theta^S}$. To this end, one benefits from the assumption that, e. g., the fluid density must be the same, irrespective from the fact whether or not the fluid is surrounded by a solid skeleton. It is however pointed out that the heat conduction coefficients of the solid constituent have then to be determined for an empty porous skeleton in a vacuum unit in order to avoid the influences of the ambient air existing in the pores.

The third group concerns those parameters, for which it is not possible to perform isolated physical processes. This problem exists, since there occur coupling phenomena with other physical effects, which cannot be deactivated. The heat conduction coefficient $\mathbf{K}^G_{0\theta^G}$ of the fluid constituent as well as the heat exchange coefficient k^ε_θ constitute the third group.

4.2 The heat conduction of the fluid constituent

It would be tempting to assume that the heat conduction of a fluid flowing through a porous material must behave identically as outside of that. However, it will be shown that there is in fact a difference. To illustrate how this difference is induced, attention must be paid to the microscopic pore structure, cf. Figure 4.1.

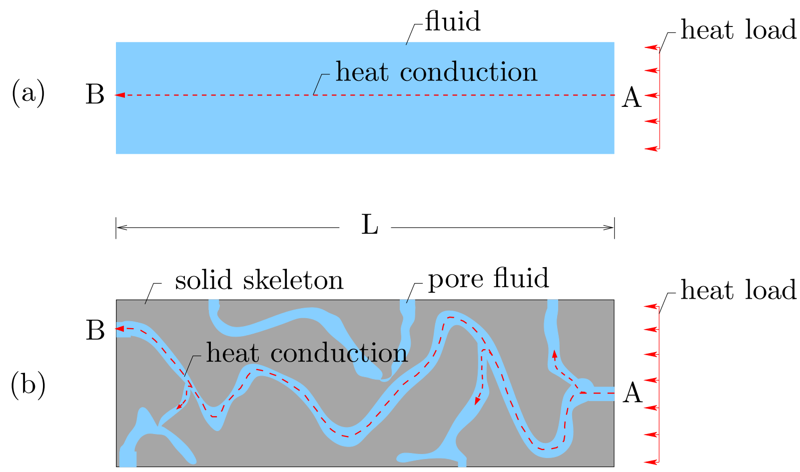

Figure 4.1: Heat conduction of the fluid constituent, (a) in a single phasic fluid and (b) in a pore-fluid surrounded by a solid skeleton.

Compared to Figure 4.1(a), the heat in Figure 4.1(b) will need a longer time to arrive at the point B, since it has to cover a longer microscopic distance. This holds, even if both models have the same macroscopic length L. In addition, due to the permanent heat exchange with the surrounding solid material, the heat conduction of the fluid in Figure 4.1(b) is perturbed. As a result of this fact, one should be aware of the inaccuracy of the measured value for the macroscopic heat conduction coefficient of the fluid constituent in multiphasic materials. Considering these inaccuracies, it seems to be reasonable to proceed from the real (microscopic) heat conduction coefficient for multiphasic materials. This is recommended, even though, due to the turtuosity, it holds that

$$\Big[\mathbf{K}^G_{0\theta^G}\Big]_{mic} \neq \Big[\mathbf{K}^G_{0\theta^G}\Big]_{mac} . \tag{4.2}$$

For an orthotropic heat conduction, one obtains

$$\mathbf{K}^\alpha_{\theta^\alpha} = \begin{bmatrix} k^\alpha_{q^1} & 0 & 0 \\ 0 & k^\alpha_{q^2} & 0 \\ 0 & 0 & k^\alpha_{q^3} \end{bmatrix} (\mathbf{e}_i \otimes \mathbf{e}_j) . \tag{4.3}$$

4.3 The heat exchange coefficient

Following the preceding remarks, except for k^ε_θ, the remainder of the material parameters can evidently be determined by the classical procedures.

In $(3.72)_2$, the following approach was found for the direct energy interaction of the gas constituent:

$$\hat{\varepsilon}^G = k^\varepsilon_\theta \, (\theta^S - \theta^G) . \tag{4.4}$$

Therein, k^ε_θ has the unit [W/K m^3]. This equation was formulated by considering the common approach for the heat exchange from the classical thermodynamics, namely,

$$\begin{aligned} q^{ex}_G &= k^{ex} \, (\theta^S - \theta^G) \quad \text{or} \\ q^{ex}_S &= k^{ex} \, (\theta^G - \theta^S) , \end{aligned} \tag{4.5}$$

respectively, where for k^{ex} the unit [W/K m^2] holds. It is by the way mentioned that relation (4.5) is based on *Newton*'s law of cooling, cf., e. g., Grigull [43]. Even if this equation, on the first view, seems to be identically to the approach found for $\hat{\varepsilon}^G$, a basic difference exists between the coefficients k^ε_θ and k^{ex}. The quantity q^{ex} contains the total heat exchange, which consists of two parts: the caloric heat exchange resulting purely from the temperature difference between two bodies and the heat production caused by frictional forces. The heat exchange coefficient k^{ex} must thus include also frictional effects. In the classical thermodynamics, this coefficient is in fact determined by use of the dimensionless *Nusselt number*, *Reynolds number* and *Prandtl number*, in which the influences of the fluid velocity and viscosity are considered, cf., e. g., Grigull [43] or Whitaker [82].

In order to utilize the classical way for the description of heat transfer phenomena, the shape and the size of the contact surface between two bodies, where the heat exchange takes place, must be known. However, the contact surface between the fluid phase and the solid skeleton in a multiphasic material is embodied through the internal microscopic pore surfaces, which are unknown. Note that k_θ^ε has been defined as a volumetric coefficient (4.4), for which the information about the internal microscopic geometry is not needed. In order to understand the physical meaning of k_θ^ε, attention must be paid to (3.5), which, by inserting relations $(3.77)_4$ and (3.102), yields

$$\hat{\varepsilon}^S = -\, k_\theta^\varepsilon\,(\theta^S - \theta^G) - \frac{\theta^S}{\theta^G}\,p^{GR}\mathrm{grad}\,n^G \cdot \mathbf{w}_G + (n^G)^2\,\mu^{GR}\,(\mathbf{K^S})^{-1}\,\mathbf{w}_G \cdot \mathbf{w}_G\,. \qquad (4.6)$$

As is seen in relation (4.6), the heat coefficient k_θ^ε is only related to the caloric heat exchange. Additional friction effects are considered separately in the last two terms of (4.6). Note that these terms are not coupled on any coefficients. Therein, the last term describes the frictional heat caused by the viscosity of the fluid constituent. The second term in (4.6) represents frictional heat arising from volume deformations. The physical meaning of this expression becomes more understandable, when therein relation (3.11) is considered, which leads to

$$\frac{\theta^S}{\theta^G}\,p^{GR}\mathrm{grad}\,n^G \cdot \mathbf{w}_G = -\frac{\theta^S}{\theta^G}\,p^{GR}\mathrm{grad}\,n^S \cdot \mathbf{w}_G\,. \qquad (4.7)$$

Looking at the right hand side of (4.7), one can easily imagine that a deformation of the solid skeleton along the stream line of the pore-fluid might cause frictional heat, cf. Figure 4.2.

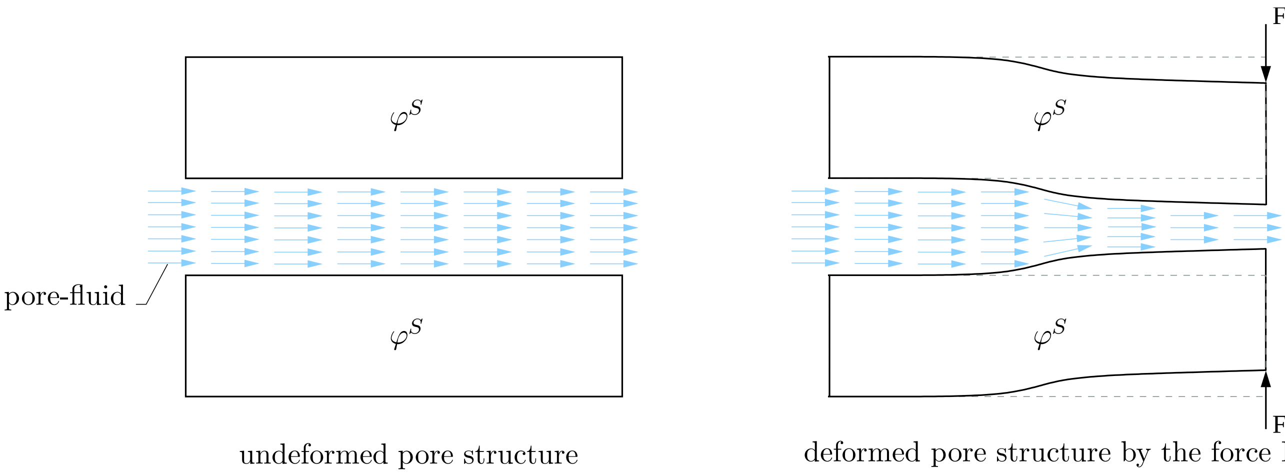

Figure 4.2: Frictional effect caused by deformations.

In order to determine the volumetric heat exchange coefficient k_θ^ε, an adequate experiment must be performed. It can be expected that this coefficient will depend on the heat conduction coefficient of the pore-fluid as well as on the internal geometrical parameters of the corresponding porous material to be studied. The biphasic model created can then be used for the simulation of the experimental results. Therein, k_θ^ε can be identified by means of standard *parameter identification* procedures. General remarks on *parameter identification* can be found, e. g., in Luenberger [55], Mahnken [56], Schwefel [68], Spellucci [71] or Thielecke [74].

Chapter 5: Numerical examples

Several experiments and simulations have to be performed in order to understand the strongly coupled physical effects occurring in the porous combustion chamber under consideration. The ultimate design of the construction will then result from numerous optimization computations, where the influences of different material parameters as well as boundary conditions must be investigated. The determination of the optimal overall design would however go beyond the scope of this work. The numerical simulations in this chapter analyze the most significant physical effects, which are essential for the design investigations of the effusion-cooled porous chamber. Therein, simplified geometries and boundary conditions are assumed.

When designing the porous chamber under study, the flow of the compressible coolant through the porous wall plays a major role. In the following examples, the attention is predominantly restricted to the influences of the non-isothermal conditions on the behavior of the gas flow. The distribution and the velocity of the compressible coolant through the porous wall are affected by thermal loads, the pressure level as well as by material parameters such as, e. g., the porosity and the permeability. Considering a two-dimensional model of a real testing chamber, these influences are shown at first qualitatively. The respective temperature and pressure effects are then extensively discussed in further simplified models.

5.1 Basic investigations

One of the major difficulties of the design investigations is the determination of the required length and the optimal run of the coolant distribution channels along the chamber contour. The run of a channel has to be designed in such a way that each point of the inner chamber contour is supplied by the necessary dosage of the coolant, cf. Chapter 1. The most important factors influencing the coolant flow are qualitatively investigated in the following.

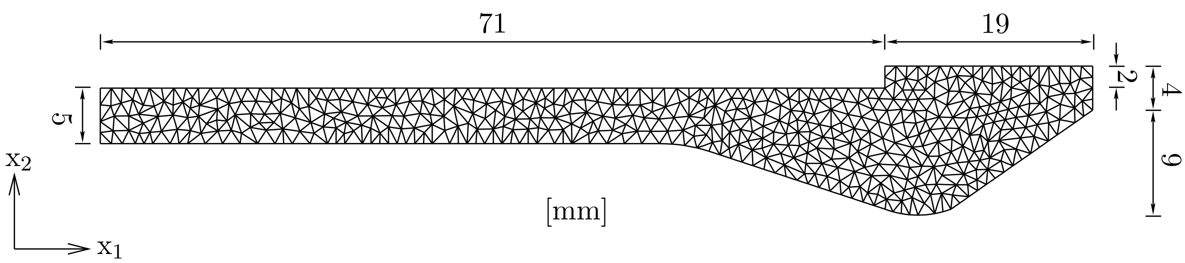

Figure 5.1: Discretized 2-d model of the porous liner along a channel.

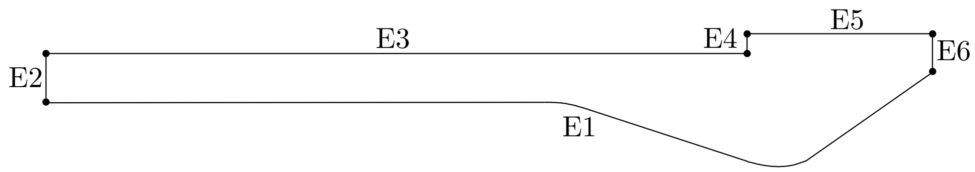

Figure 5.2: Numbering of the edges for the definition of boundary conditions.

In a first simulation, the influence of a temperature gradient on the behavior of the gas flow is shown. To this end, a two-dimensional model (cf. Figures 5.1 and 5.2) is calculated according to the simplified definitions given in Tables 5.1 and 5.2, respectively. The pressure level arising in a channel is compared between two different conditions. At first, an uniform temperature distribution is considered for the gas, whereas, in a next step, a simplified thermal boundary condition acts on the inner contour of the chamber.

initial conditions	$p_0 = 1\,\mathrm{bar}$ $\theta_0^S = 40\,\mathrm{K}$ $\theta_0^G = 40\,\mathrm{K}$
Dirichlet boundary conditions	$u_1\,(E2, E4, E6) = 0\,\mathrm{m}$ $u_2\,(E1, E3, E5) = 0\,\mathrm{m}$ $p\,(E1) = 1\,\mathrm{bar}$
Neumann boundary conditions	$\bar{v}\,(E3, E4) = 10\,\mathrm{kg/s\,m^2}$

Table 5.1: Initial and boundary conditions for the isothermal case.

initial conditions	$p_0 = 1\,\mathrm{bar}$ $\theta_0^S = 40\,\mathrm{K}$ $\theta_0^G = 40\,\mathrm{K}$
Dirichlet boundary conditions	$u_1\,(E2, E4, E6) = 0\,\mathrm{m}$ $u_2\,(E1, E3, E5) = 0\,\mathrm{m}$ $p\,(E1) = 1\,\mathrm{bar}$ $\theta^G\,(E3, E4) = 40\,\mathrm{K}$ $\theta^G\,(E1) = 500\,\mathrm{K}$
Neumann boundary conditions	$\bar{v}\,(E3, E4) = 10\,\mathrm{kg/s\,m^2}$

Table 5.2: Initial and boundary conditions for the non-isothermal case.

solid constituent	$n_{0S}^S = 0.85$	$[-]$
	$\rho_{0S}^{SR} = 2 \cdot 10^2$	$[\mathrm{kg/m^3}]$
	$\mu^S = 5.583 \cdot 10^6$	$[\mathrm{N/m^2}]$
	$\lambda^S = 8.375 \cdot 10^6$	$[\mathrm{N/m^2}]$
	$\alpha_{0S}^S = 0.0$	$[-]$
	$k_1^S = 4.0 \cdot 10^{-10}$	$[\mathrm{m^2}]$
	$k_2^S = 4.0 \cdot 10^{-10}$	$[\mathrm{m^2}]$
	$k_{q1}^S = 8.0$	$[\mathrm{W/m\,K}]$
	$k_{q2}^S = 15.0$	$[\mathrm{W/m\,K}]$
	$C_V^S = 1.850 \cdot 10^3$	$[\mathrm{Ws/kg\,K}]$
gas constituent	$\mu^{GR} = 8.7 \cdot 10^{-6}$	$[\mathrm{Ns/m^2}]$
	$\bar{R}^{GR} = 4.1248 \cdot 10^3$	$[\mathrm{Ws/kg\,K}]$
	$k_{q1}^G = 0.171$	$[\mathrm{W/m\,K}]$
	$k_{q2}^G = 0.171$	$[\mathrm{W/m\,K}]$
	$C_V^G = 1.013 \cdot 10^4$	$[\mathrm{Ws/kg\,K}]$
	$k_\theta^\varepsilon = 0.0$	$[\mathrm{W/m^3\,K}]$

Table 5.3: The arbitrary chosen set of material parameters.

The material parameters have been chosen as listed in Table 4.1. Note that the heat exchange coefficient k_θ^ε has been put to zero in order to exclude the caloric heat transfer between the solid skeleton and the gas. Heat exchange phenomena will be discussed separately in further numerical examples.

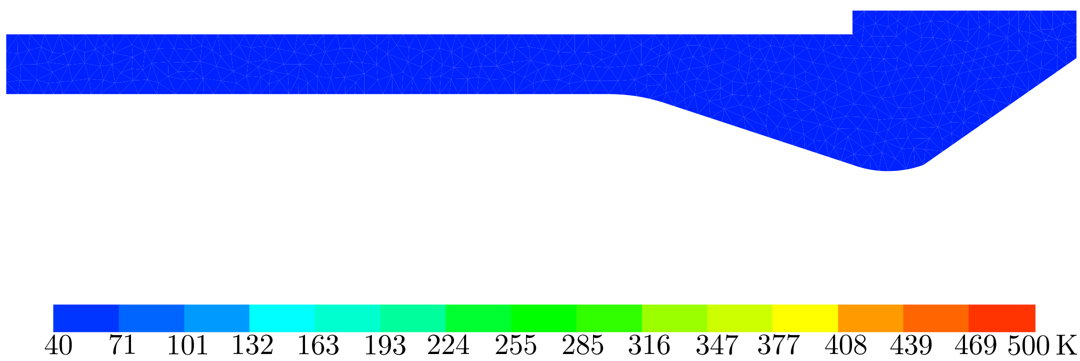

Figure 5.3: Isothermal distribution of the gas temperature.

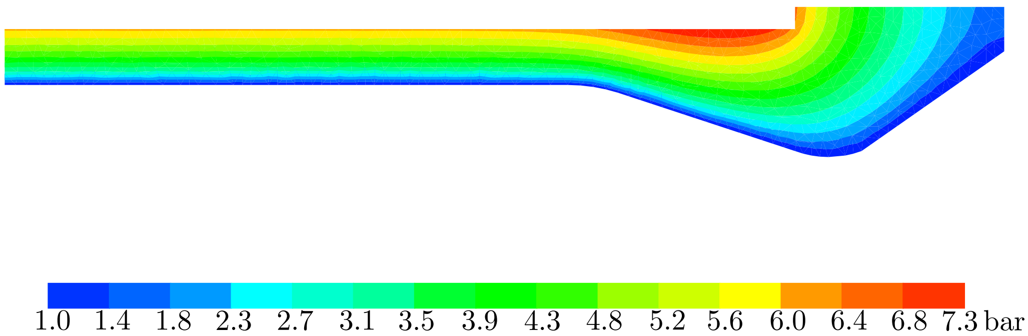

Figure 5.4: Pressure distribution according to the definitions in Table 5.1.

It can be seen in Figure 5.4 that the pressure of the compressible gas possesses a weak non-linear distribution. Note that the two-dimensional model is submitted to a uniform temperature, cf. Figure 5.3.

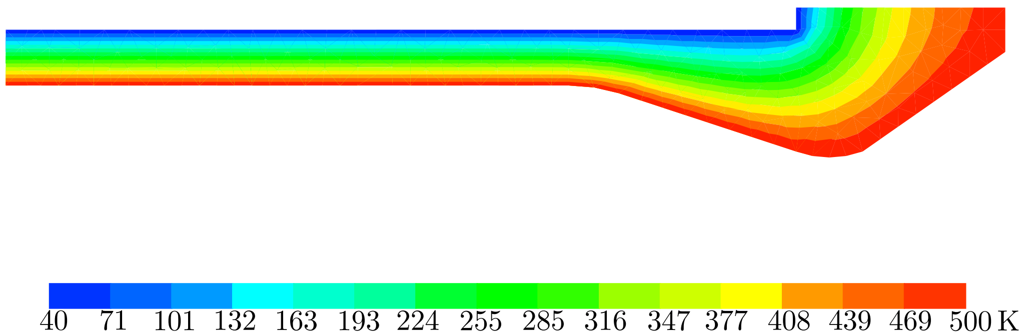

Figure 5.5: Non-isothermal distribution of the gas temperature according to the definitions in Table 5.2.

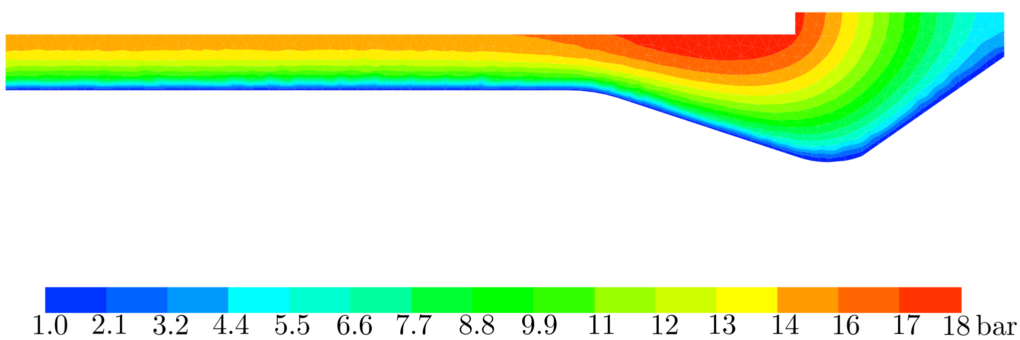

Figure 5.6: Pressure distribution according to the definitions in Table 5.2.

The thermal boundary definitions in Table 5.2 lead to the temperature distribution given in Figure 5.5. It can be observed that, in comparison to Figure 5.4, the non-linear distribution of the pressure occurs in a more pronounced manner, cf. Figure 5.6. The superposition of the pressure distribution along the edge E2 for both cases renders this effect more noticeable, cf. Figure 5.7.

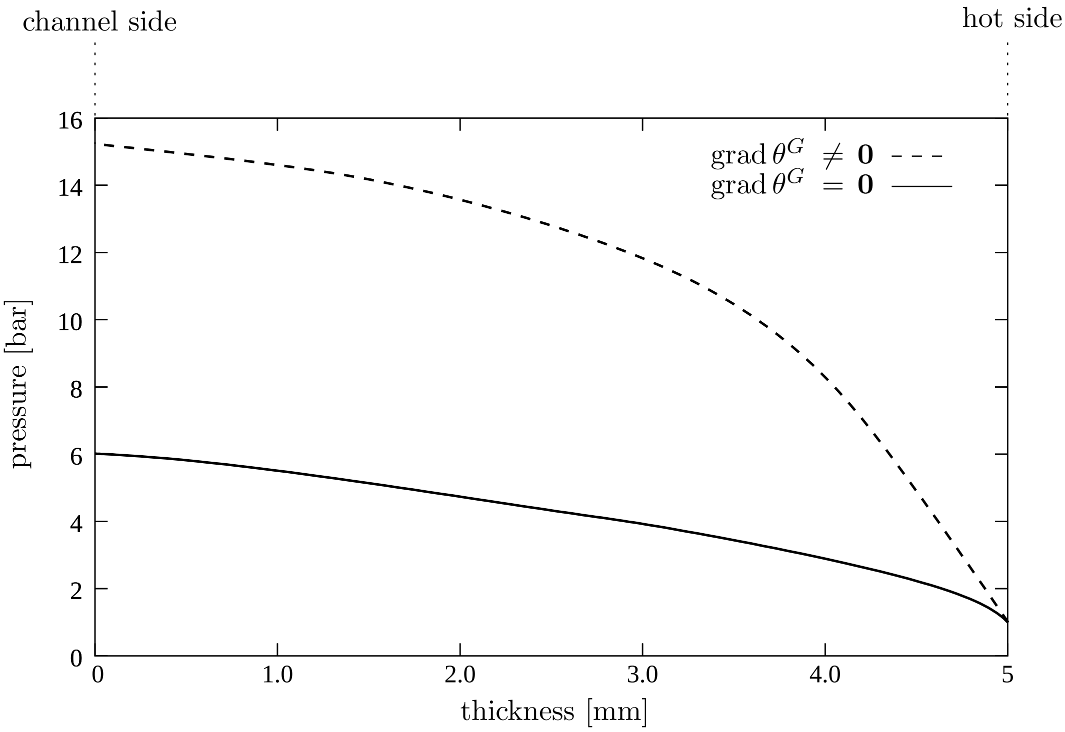

Figure 5.7: The distribution of the pressure along the edge E2.

As depicted in Figure 5.7, even the same mass flow rate is defined for both cases (cf. Tables 5.1 and 5.2), a higher pressure arise in the channel side when the given temperature gradient is considered. In order to understand this effect, attention must be paid to the definition of the specific mass flow rate (3.111). Considering the real gas law (3.2), relation (3.111) can be rewritten as

$$\bar{v} \;=\; \frac{p^{GR}}{\bar{R}^G\,\theta^G}\, n^F\,|\mathbf{w}_G| \qquad [\mathrm{kg/s\,m^2}]\,. \tag{5.1}$$

From (5.1), it becomes obvious that, keeping $\bar{v}$ constant, a rise in the gas temperature causes an increase in the pressure.

Furthermore, the run of the pressure along a channel (cf. Figure 5.8) is a consequence of the chosen pressure boundary condition along the edge E1, cf. Tables 5.1 and 5.2. Since an uniform pressure is defined along the inner contour, the pressure run along a channel is determined by the thickness of the porous wall. In comparison to the cylindrical section of the chamber, the fluid particles in the converging section have to cover a longer distance between a channel and the inner contour. This is at last the reason why the channel pressure increases toward the nozzle throat, cf. Figure 5.8.

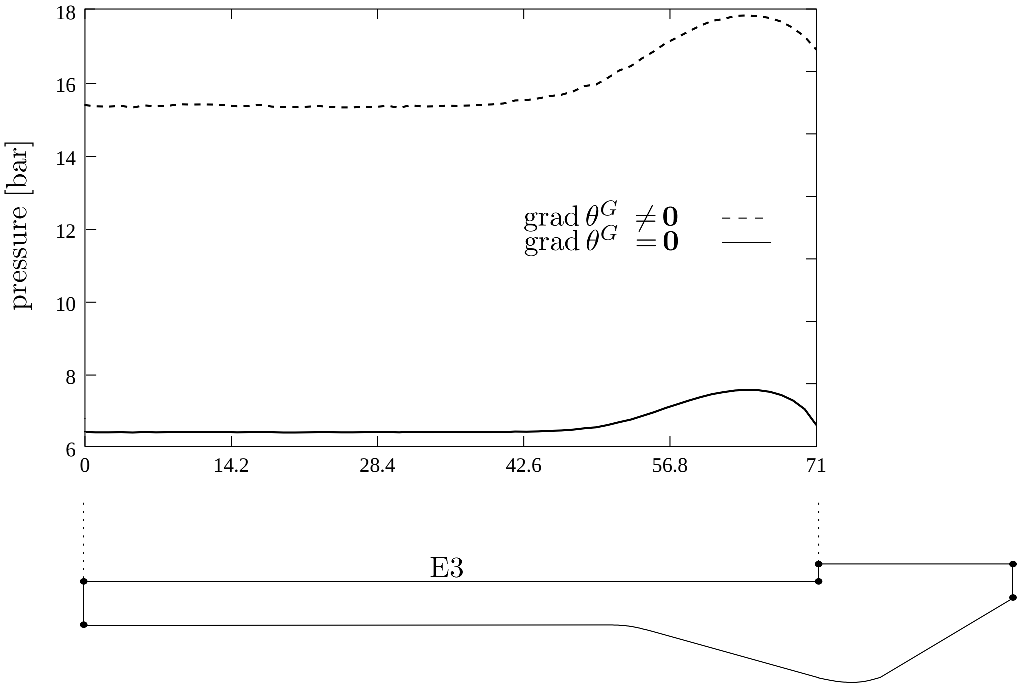

Figure 5.8: The distribution of the pressure along a channel (edge E3) according to the definitions in Tables 5.1 and 5.2, respectively.

The pressure run along a channel changes however, if a real pressure distribution (cf. Figure 1.9) is considered inside of the chamber. Figure 5.10 shows the run of the channel pressure according to the definitions in Table 5.4. For this simulation, an approximated real pressure distribution has been considered, cf. Figure 5.9.

initial conditions	$p_0 = 1\,\mathrm{bar}$ $\theta_0^S = 40\,\mathrm{K}$ $\theta_0^G = 40\,\mathrm{K}$
Dirichlet boundary conditions	$u_1\,(E2, E4, E6) = 0\,\mathrm{m}$ $u_2\,(E1, E3, E5) = 0\,\mathrm{m}$ $p\,(E1) =$ cf. Figure 5.9 $\theta^G\,(E3, E4) = 40\,\mathrm{K}$ $\theta^G\,(E1) = 500\,\mathrm{K}$
Neumann boundary conditions	$\bar{v}\,(E3, E4) = 6\,\mathrm{kg/s\,m^2}$

Table 5.4: Initial and boundary conditions for a combustion chamber at 30 bar.

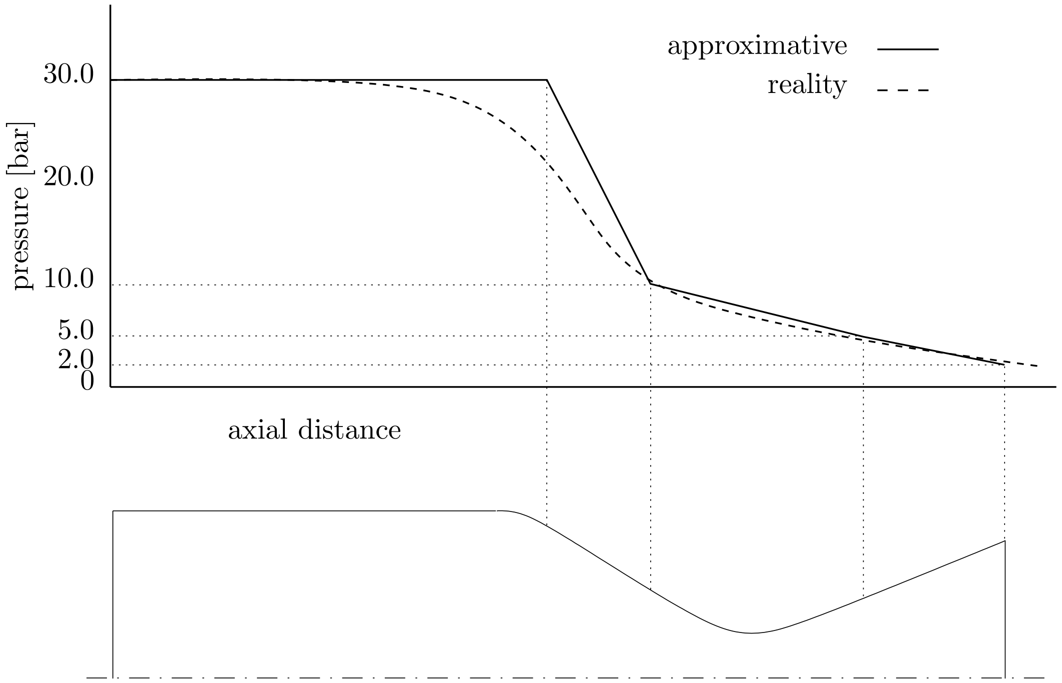

Figure 5.9: The approximated pressure distribution along the inner contour (edge E1) of a chamber with the operating pressure at 30 bar.

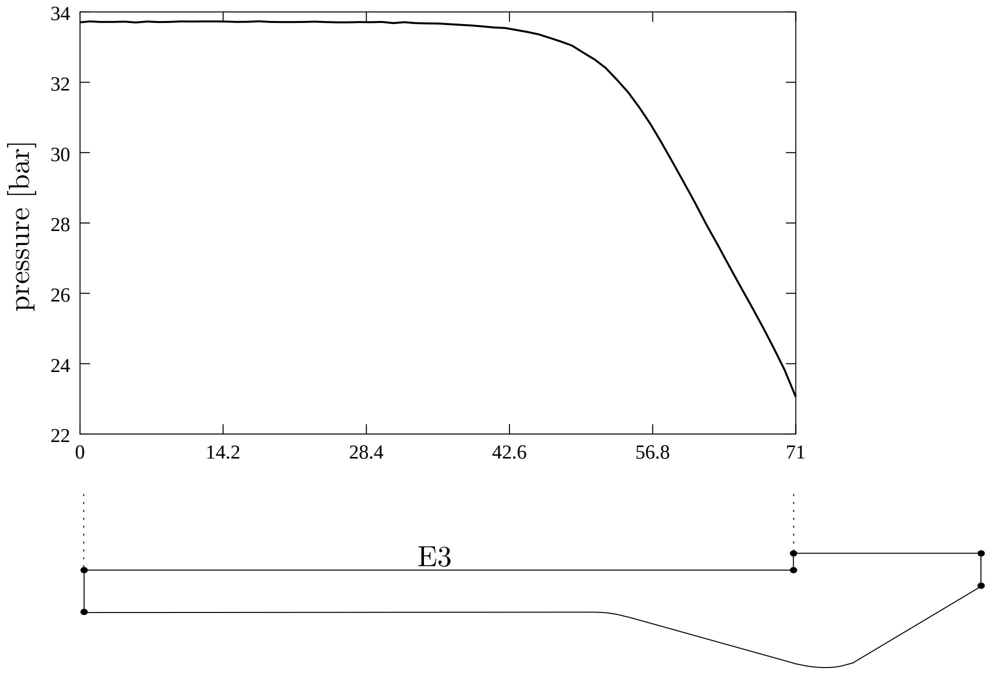

Figure 5.10: The distribution of the pressure along a channel (edge E3) according to the pressure boundary condition from Figure 5.9.

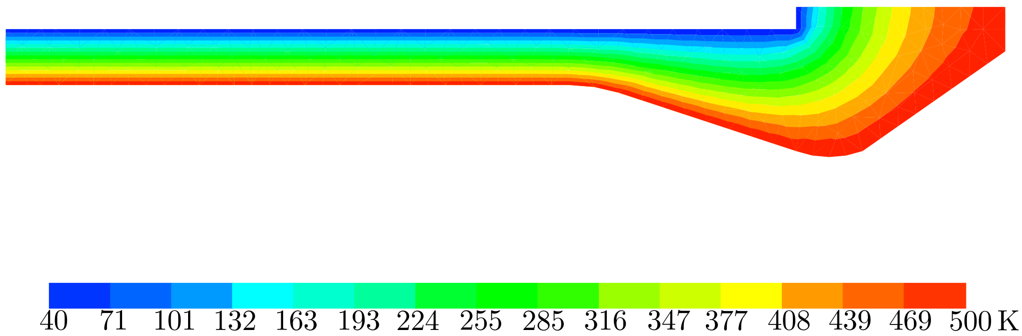

Figure 5.11: Non-isothermal distribution of the gas temperature according to the definitions in Table 5.4.

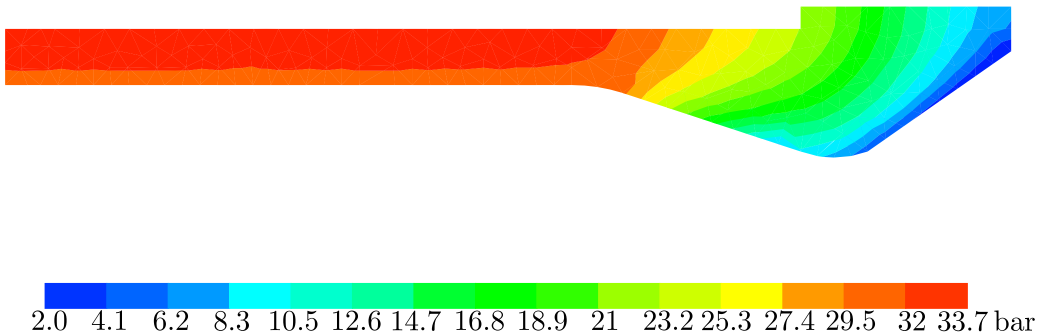

Figure 5.12: Pressure distribution according to the definitions in Table 5.4.

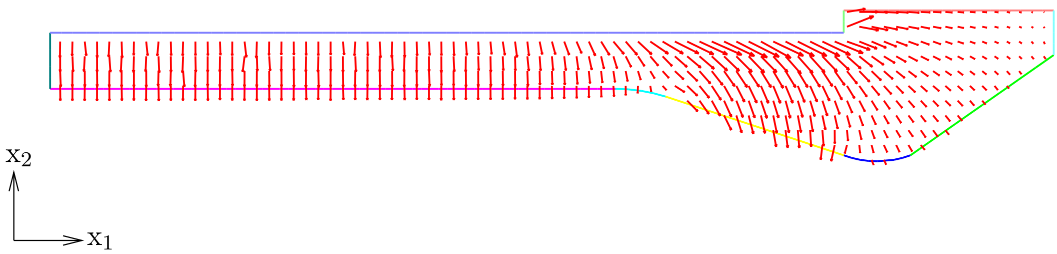

Figure 5.13: The distribution of the gas fluxes according to the pressure distribution in Figure 5.12.

In Figures 5.12 and 5.13, respectively, the pressure distribution and the corresponding distribution of the mass fluxes are represented. The qualitative distribution of the mass fluxes along the inner contour renders that the converging section of the chamber is not sufficiently supplied by the coolant. Proceeding from real temperature loads in a rocket combustion chamber (cf. Figure 1.8), twice as much coolant is necessary in the nozzle throat compared to the cylindrical section of the chamber. In order to accomplish this, it stands to reason that the variation of the permeability coefficients in x_1 and x_2-direction might be one of the possible measures.

The qualitative change in the distribution of the coolant fluxes, depending on different relations between k_1^S and k_2^S, is demonstrated in Figures 5.14 and 5.15. Note that the same definitions (cf. Table 5.4) have been considered for these simulations.

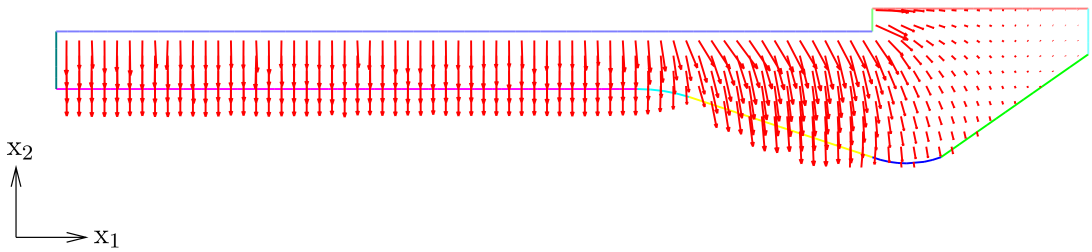

Figure 5.14: The distribution of the gas fluxes resulting from $k_1^S = 0.25\, k_2^S$.

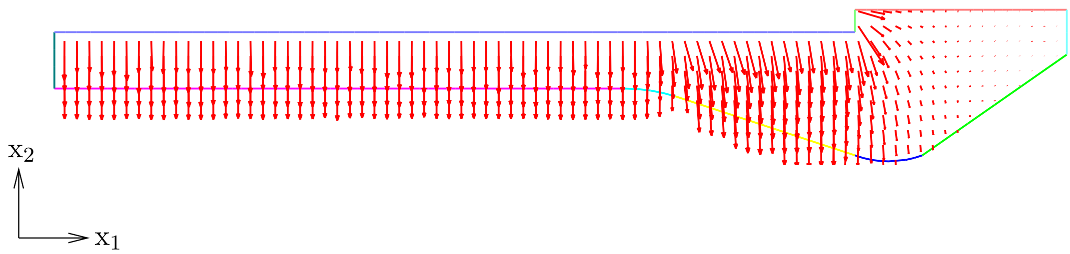

Figure 5.15: The distribution of the gas fluxes resulting from $k_1^S = 0.1\, k_2^S$.

Further changes in the distribution of the coolant along the inner contour can be achieved by varying the geometrical run of a channel, cf. Figure 5.16.

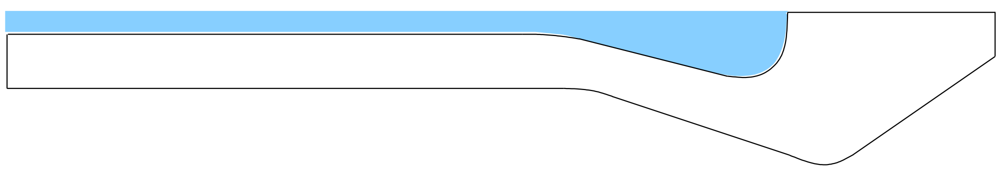

Figure 5.16: A possible adapted geometrical run of the channel.

In order to define the optimal run for the cooling channels, several influencing factors must still be investigated and understood. They will be discussed in the following by use of simplified models. First of all, the permeability coefficient of the porous material under consideration will be determined from real experimental data.

5.2 The numerical simulation of a flow-through experiment with gaseous hydrogen

As it was mentioned in the preceding chapter, material parameters can be determined from basic experiments. The permeability coefficient of the C/C material under consideration will be identified in the following by use of real test data stemming from experiments at the DLR. The experimental setup as well as the dimensions of the used specimen are depicted in Figure 5.17.

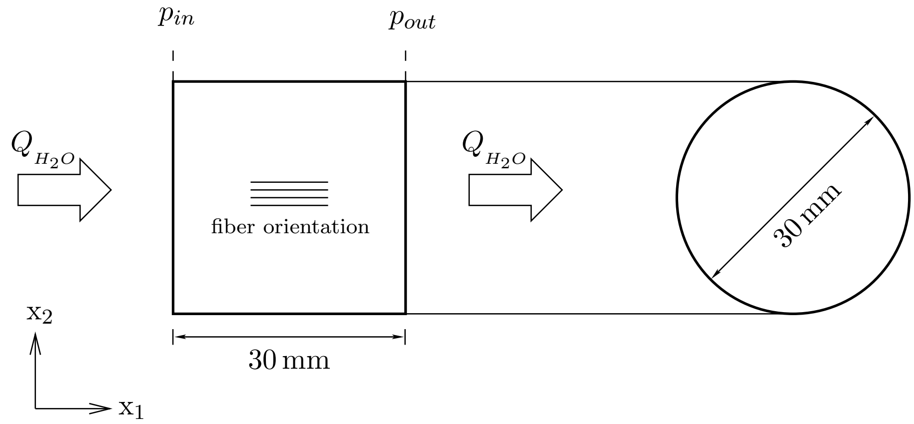

Figure 5.17: The setup of the flow-through experiment with H_2O.

In a first configuration, the specimen was flowed through by water on isothermal conditions. Therein, the inflow and the outflow pressure have been measured for different flow rates Q_{H_2O}, cf. Table 5.5.

	p_{in}	p_{out}	Δp	$\partial p/\partial x_1$	Q_{H_2O}	$n^w \mathbf{w}_{w_1}$
i	[bar]	[bar]	[bar]	[10^7 N/m^3]	[$10^{-6}\, m^3/s$]	[$10^{-3}\, m/s$]
1	2.80	1.1	1.70	0.58	2.7	3.8
2	5.03	1.1	3.93	1.3	5.2	7.3
3	9.97	1.1	8.87	3.0	9.2	13.0
4	12.4	1.1	11.3	3.8	11.5	16.3
5	15.0	1.1	13.9	4.6	13.2	18.7
6	17.6	1.1	16.5	5.5	15.6	22.0
7	20.2	1.1	19.1	6.4	16.7	23.6
8	22.5	1.1	21.4	7.2	18.6	26.3

Table 5.5: Test data from the flow-through experiment with H_2O.

The permeability coefficient can be determined through the classical *Darcy* law for isothermal processes. Neglecting volume forces and considering an one-dimensional flow, relation (3.100) can be rewritten for isothermal processes as

$$n^w \mathbf{w}_{w_1} = -\frac{k_1^S}{\mu^W}\frac{\partial}{\partial x_1}p\,. \tag{5.2}$$

The shear viscosity μ^W of water can be taken from the literature. For the average temperature of approx. 293 K, which was measured during the experiments, the shear viscosity amounts to $\mu^W \approx 0.00107\,\mathrm{Ns/m^2}$, cf., e. g., Grigull [43].

The permeability coefficient k_1^S can be determined by standard procedures of *parameter identification*. Considering the linear relationship between the pressure gradient and the velocity in (5.2), the *quadratic minimization* is used in order to minimize

$$\sum_{i=1}^{8}(m\,x_i + b - y_i)^2\,. \tag{5.3}$$

Incorporating the experimental data from Table 5.5 in the definition above and considering the given shear viscosity, the permeability coefficient is identified as $k_1^S \approx 3.6\cdot 10^{-13}\,\mathrm{m}^2$, cf. Figure 5.18.

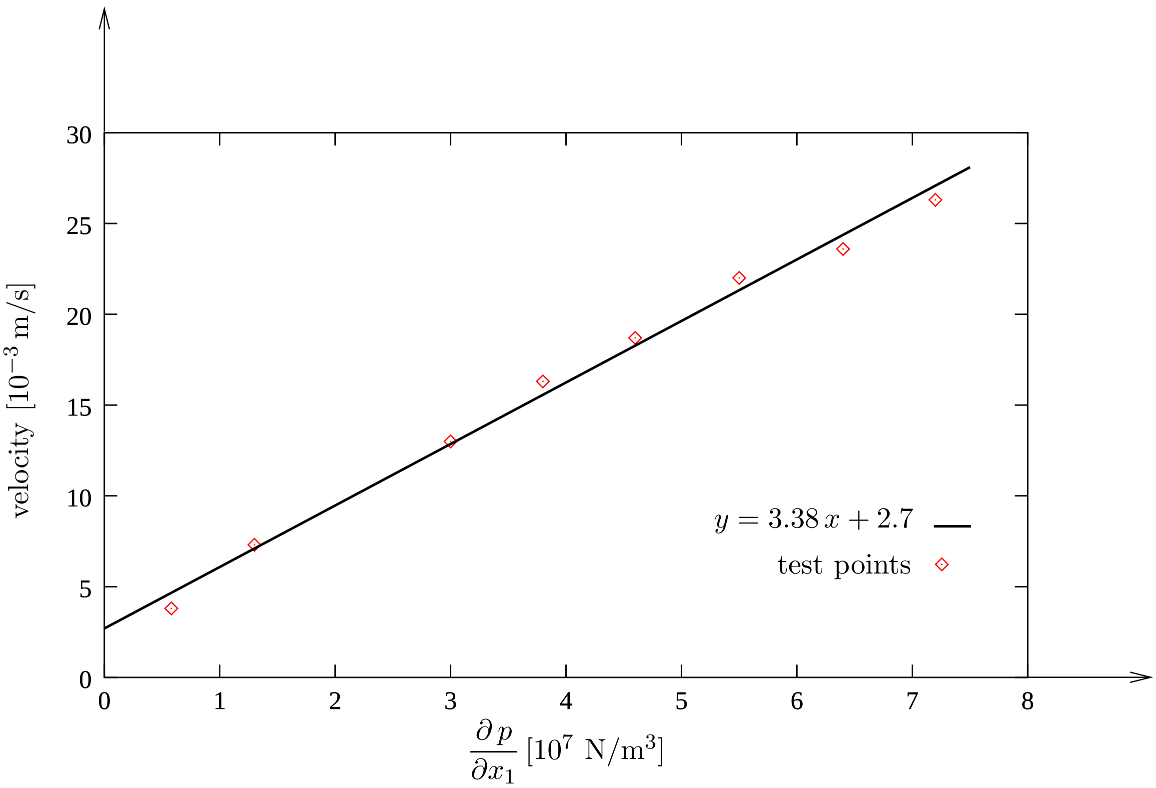

Figure 5.18: The optimized curve resulting from the *quadratic minimization* (5.3).

In a further step, the same experiment has been conducted by using gaseous hydrogen GH_2. In this configuration, the pressure was measured along the thickness of the specimen at four positions, cf. Figure 5.19. Moreover, the inflow and the outflow temperatures, $\theta_{in}^{H_2}$ and $\theta_{out}^{H_2}$, were measured additionally. This experiment has been performed at different pressure levels between 10 bar and 100 bar. In Table 5.6, the experimental data are given exemplarily at five different levels of the outflow pressure together with the corresponding mass flow rates.

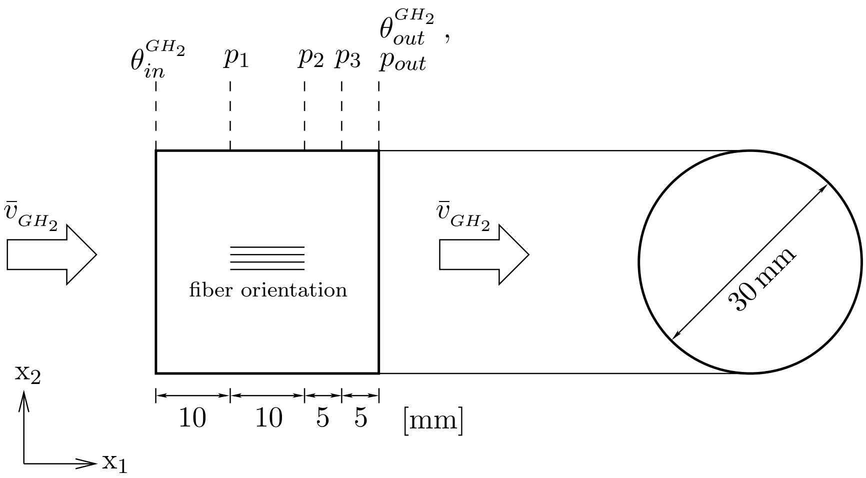

Figure 5.19: The setup of the flow-through experiment with GH_2.

After the permeability coefficient k_1^S has been determined from flow-through experiments with H_2O, the idea is now to consider this coefficient in order to simulate the experiments with GH_2. Therein, the respective mass flow rates and the corresponding outflow pressure values (cf. Table 5.6) will be used as boundary conditions. The numerically calculated pressure distributions over the thickness of the FE model (cf. Figure 5.20) will then be compared with the experimental pressure values p_1, p_2 and p_3.

$\theta_{in}^{GH_2}$	$\theta_{out}^{GH_2}$	p_1	p_2	p_3	p_{out}	$\bar{v}_{GH_2}$
[K]	[K]	[bar]	[bar]	[bar]	[bar]	[kg/s m^2]
286.9	287.3	44.6	42.0	41.1	39.5	3.4
287.0	287.5	41.1	36.5	34.9	31.8	4.6
286.8	287.6	37.9	31.1	28.5	23.3	5.5
286.7	287.6	36.4	28.4	25.3	18.4	5.8
286.4	287.4	35.5	26.8	23.2	14.6	6.1

Table 5.6: Test data from the flow-through experiment with GH_2.

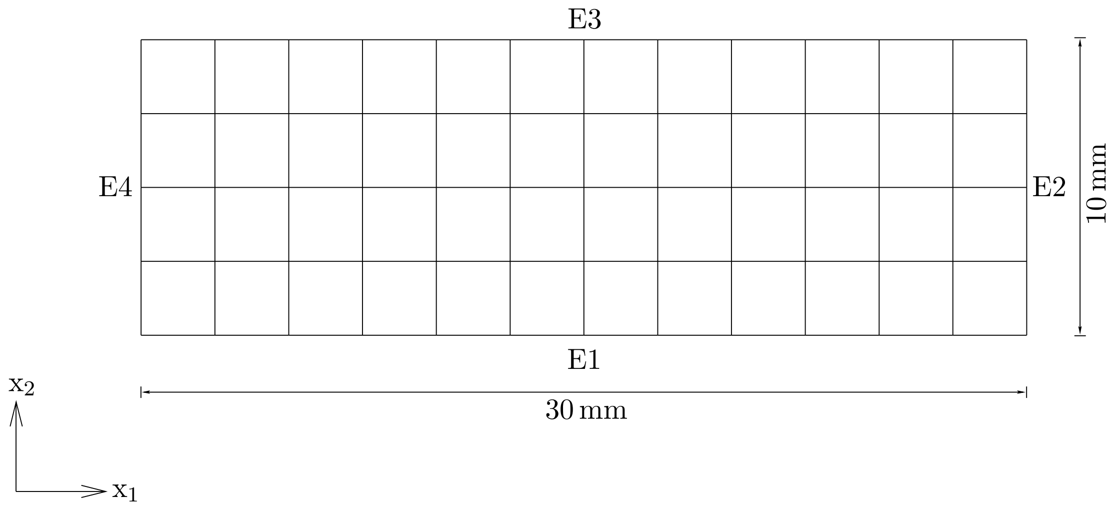

Figure 5.20: Simplified FE model for the simulation of the GH_2 flow through the C/C specimen in Figure 5.19.

The simulations are carried out according to the definitions given in Table 5.7. Note that, due to the evanescent variation in temperature between the inflow and the outflow (cf. Table 5.6), the model is calculated for the uniform temperature 287 K. Considering this temperature, the material parameters of GH_2 (cf. Table 5.8) have been taken from the literature, cf., e. g., Grigull [43] or VDI-Wärmeatlas [78].

Furthermore, it is pointed out that the determined coefficient k_1^S represents the permeability parallel to fiber direction. For the permeability coefficient perpendicular to fiber direction, the same value is considered in Table 5.8. This simplification has no influences on the one-dimensional flow in this simulation.

initial conditions	$p_0 = p_{out}$ (cf. Table 5.6) $\theta_0^S = \theta_0^G = 287\,\mathrm{K}$
Dirichlet boundary conditions	$u_1\,(E1, E3) = 0\,\mathrm{m}$ $u_2\,(E2, E4) = 0\,\mathrm{m}$ $p\,(E2) = p_{out}$ (cf. Table 5.6) $\theta^G\,(E2, E4) = 287\,\mathrm{K}$ $\theta^S\,(E2, E4) = 287\,\mathrm{K}$
Neumann boundary conditions	$\bar{v}\,(E4) = \bar{v}_{GH_2}$ (cf. Table 5.6)

Table 5.7: Initial and boundary conditions for the simulation of the flow-through experiments with GH_2.

solid constituent	$n_{0S}^S = 0.85$	$[-]$
	$\rho_{0S}^{SR} = 1.3 \cdot 10^3$	[kg/m^3]
	$\mu^S = 5.583 \cdot 10^6$	[N/m^2]
	$\lambda^S = 8.375 \cdot 10^6$	[N/m^2]
	$\alpha_{0S}^S = 0.0$	$[-]$
	$k_1^S = 3.6 \cdot 10^{-13}$	[m^2]
	$k_2^S = 3.6 \cdot 10^{-13}$	[m^2]
	$k_{q_1}^S = 15.0$	[W/m K]
	$k_{q_2}^S = 8.0$	[W/m K]
	$C_V^S = 1.850 \cdot 10^3$	[Ws/kg K]
gas constituent	$\mu^{GR} = 8.7 \cdot 10^{-6}$	[Ns/m^2]
	$\bar{R}^{GR} = 4.1248 \cdot 10^3$	[Ws/kg K]
	$k_{q_1}^G = 0.171$	[W/m K]
	$k_{q_2}^G = 0.171$	$[W/m\,K]$
	$C_V^G = 1.013 \cdot 10^4$	[Ws/kg K]
	$k_\theta^\varepsilon = 0.0$	[W/m^3 K]

Table 5.8: Material parameters for the flow-through experiment with GH_2.

The respective inflow pressure values p_{in} resulting from the simulations are listed in Table 5.6. In Figure 5.21, the nonlinear interrelationship between the mass-flow rate $\bar{v}_{GH_2}$ and the pressure difference Δp becomes evident.

$\bar{v}_{GH_2}$	p_{in}	p_{out}	Δp
[kg/s m^2]	[bar]	[bar]	[bar]
3.4	46.3	39.5	6.8
4.6	42.4	31.8	10.6
5.5	38.6	23.3	15.3
5.8	36.5	18.4	18.1
6.1	35.5	14.6	20.9

Table 5.9: The respective values for the inflow pressure p_{in} from numerical simulations.

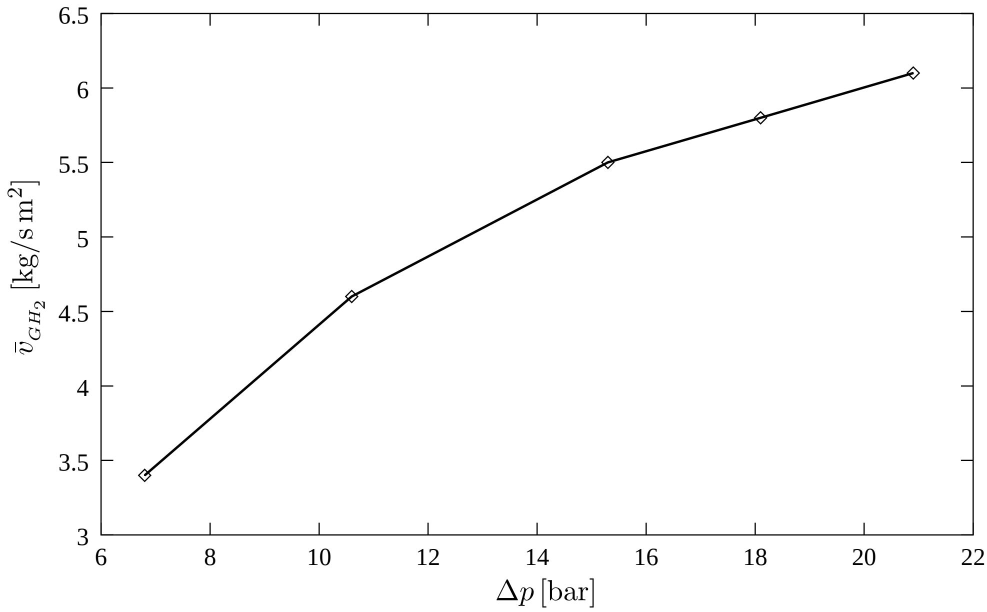

Figure 5.21: The nonlinear interrelationship between the mass flow rate and the pressure difference.

In order to understand the reasons of this phenomenon, attention must be paid again to relation (5.1), i. e.

$$\bar{v}_1 = -\frac{k_1^S}{\bar{R}^G\,\theta^G\,\mu^{GR}}\,p^{GR}\,\frac{\partial p^{GR}}{\partial x_1}\,. \tag{5.4}$$

Therein, the *Darcy* approach for isothermal processes from (3.100) has been inserted, whereas volume forces were neglected. Relation (5.4) reveals immediately the nonlinear interrelationship between $\bar{v}$ and p^{GR}. As is seen, the mass flow rate does not only depend on the pressure gradient but also on the level of the absolute pressure. This effect will be taken up again in Section 5.3.

$\bar{v}_{GH_2}$	Δp	p_1^{exp}	p_1^{sim}	$(p_1^{exp} - p_1^{sim})$	$(p_1^{exp} - p_1^{sim})/p_1^{exp}$
[kg/s m^2]	[bar]	[bar]	[bar]	[bar]	[%]
3.4	6.8	44.6	44.2	0.45	1.01
4.6	10.6	41.1	39.2	1.89	4.60
5.5	15.3	37.9	34.2	3.67	9.68
5.8	18.1	36.4	31.7	4.75	13.05
6.1	20.9	35.5	30.2	5.32	14.99

Table 5.10: The growth in the deviation between experiment and simulation by comparing the measured pressure p_1^{exp} with the corresponding value p_1^{sim} from the numerical calculation.

Furthermore, in Figures 5.22 and 5.23, respectively, the run of the pressure is diagrammed exemplarily for the pressure difference of 6.8 bar and 20.9 bar. Therein, the experimental data (p_1, p_2, p_3) have been taken from Table 5.6. It is seen that the higher the pressure difference grows, the larger is the deviation from the experimental data, cf. also Table 5.10. Note that the biphasic model under consideration has been formulated for quasi-static processes. Thus, the dynamic pressure, i. e.,

$$p_{dyn} = \rho^{GR} \, \frac{|\,\mathbf{w}_{G_1}\,|^2}{2}\,, \tag{5.5}$$

which results from the dynamic formulation of the momentum balance equation of the fluid phase (B.50), is not considered. As it can be observed in the general formulation of the dynamic pressure (5.5) (cf., e. g., Grigull [43]), the influence of p_{dyn} becomes however more noticeable, the higher the velocity $\mathbf{v}$ increases. This effect explains the growing deviation between the experiments and the simulations, since it can be shown that the velocities in fact increase with a growing pressure difference, cf. Figure 5.24.

It is pointed out that the processes occurring in the porous combustion chamber under study can be sufficiently described by using the quasi-static formulation of the biphasic model. If one purposes the dynamic formulation all the same, the numerical expenditure should be taken into consideration. This holds, since the seepage velocity must then be considered as an additional independent variable, cf. Section 3.4. Furthermore, the dynamic treatment of coupled solid-fluid problems implies numerical instabilities, cf., e. g., Danilov [22].

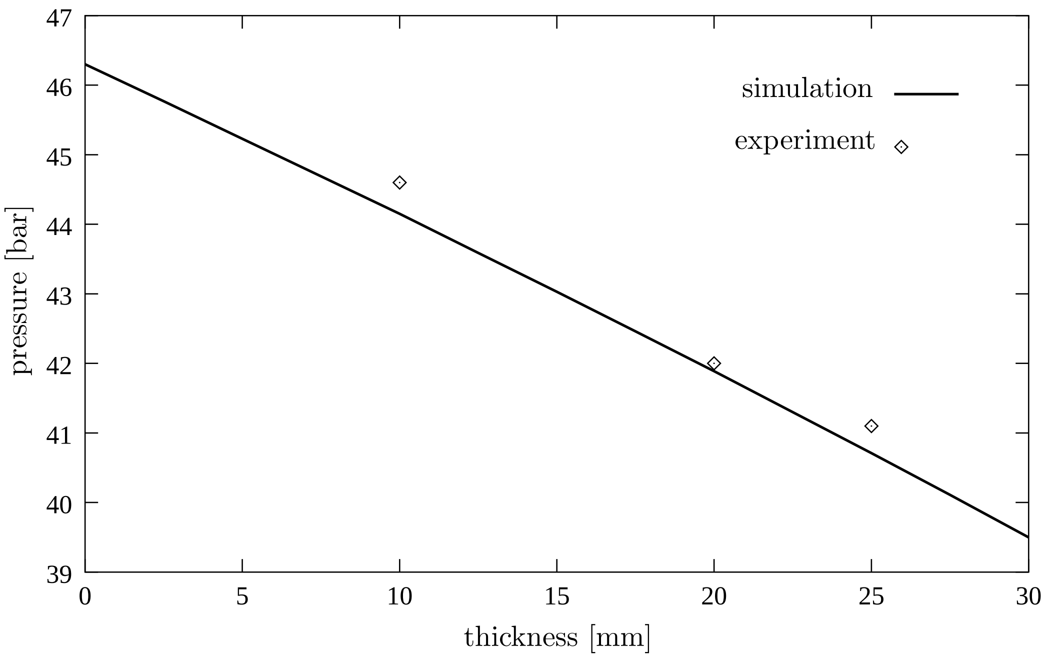

Figure 5.22: The comparison between the measured pressure and the simulated pressure distribution for Δp =6.8 bar, cf. Table 5.9.

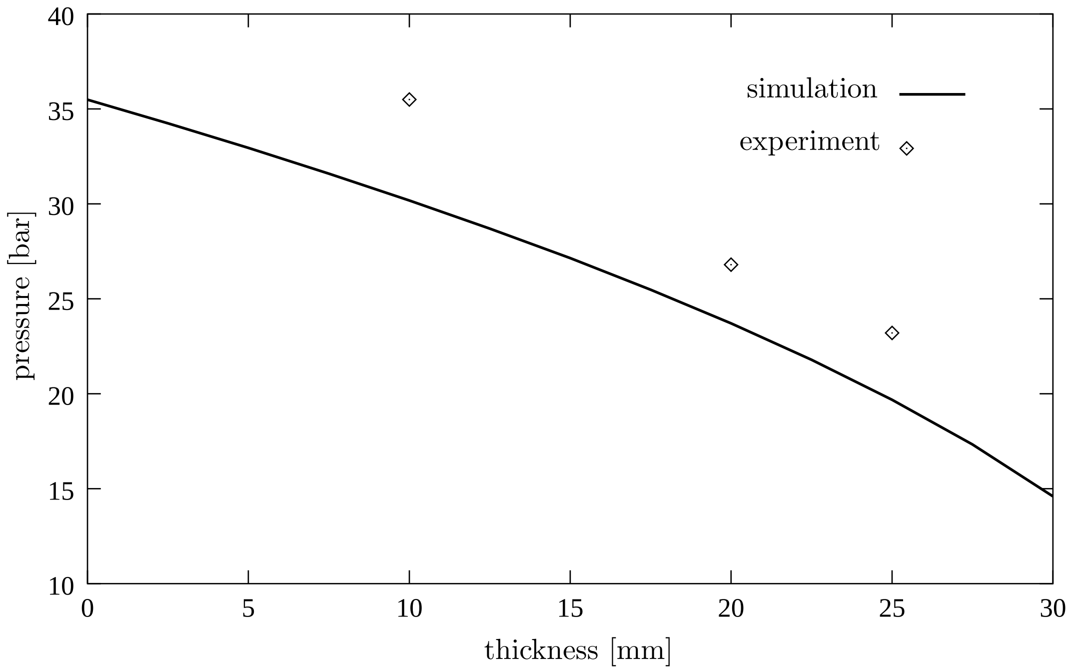

Figure 5.23: The comparison between the measured pressure and the simulated pressure distribution for Δp =20.9 bar, cf. Table 5.9.

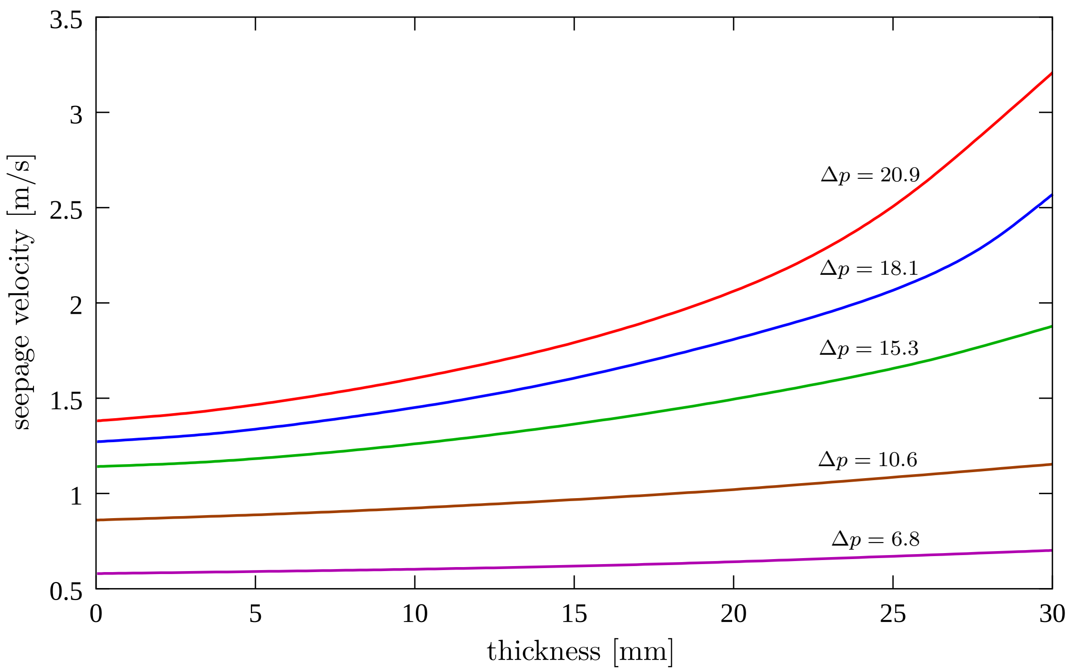

Figure 5.24: Seepage velocity of GH_2 vs. thickness of the model.

5.3 Temporal development of the supply pressure during transient conditions

The supply pressure in the coolant distribution channels, which is necessary in order to press a predefined dosage of the coolant through the porous wall of the combustion chamber, is generated automatically. This happens, since the coolant mass flow rate is kept constant, cf. Chapter 1. As was seen in preceding examples, the inflow pressure varies depending on the boundary conditions at the outflow side. Defining time dependent boundary conditions, the inflow pressure must thus change also during a simulation. One of these transient conditions occurring in a real combustion chamber is the ignition process. Therein, the pressure as well as the temperature rapidly increase in the combustion space within milliseconds, cf. Chapter 1.

In the following simulation, the temporal development of the supply pressure will be investigated during the ignition process. To this end, the simplified model from Figure 5.20 will be used. Concerning the material parameters, the same values are taken like in the preceding example, cf. Table 5.8. The boundary conditions are defined for this simulation according to Table 5.11. Note that also in this simulation the heat exchange coefficient is set to zero.

The boundary conditions are created for the following simulation in accordance to conditions occurring during a real ignition, cf. Figure 1.10. As depicted in Figure 5.25, the pressure as well as the gas temperature increase at the outflow side after 0.01 seconds to the operating conditions. Note that the operating pressure of 100 bar and the corresponding temperature of 2000 K represent arbitrary chosen values for this example.

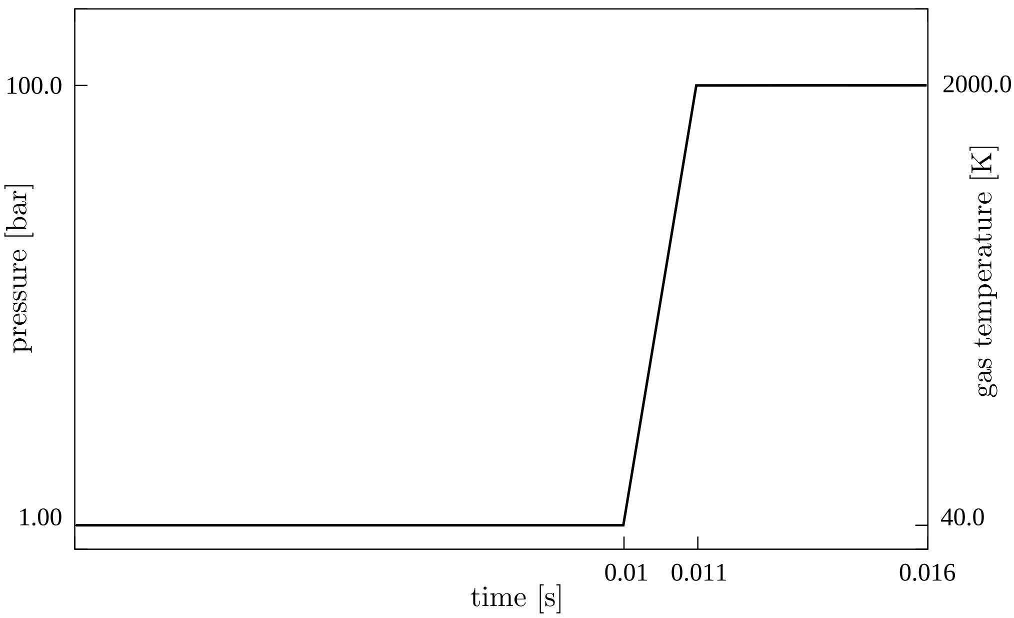

Figure 5.25: Time-dependent boundary conditions at the outflow side (edge E2) representing a simplified ignition process.

initial conditions	$p_0 = 1\,\text{bar}$ $\theta_0^S = \theta_0^G = 40\,\text{K}$
Dirichlet boundary conditions	$u_1\,(E1, E3) = 0\,\text{m}$ $u_2\,(E2, E4) = 0\,\text{m}$ $p\,(E2) =$ cf. Figure 5.25 $\theta^G\,(E2) =$ cf. Figure 5.25 $\theta^G\,(E4) = 40\,\text{K}$
Neumann boundary conditions	$\bar{v}\,(E4) = 5\,\text{kg/s}\,\text{m}^2$

Table 5.11: Initial and boundary conditions for the simulation of a simplified ignition process.

The ignition process is represented in this simulation by the fact that the outflow pressure increase within one millisecond from the ambient value of 1 bar to the operating pressure. On the other hand, the gas temperature rises during the same time from 40 K to 2000 K, cf. Figure 1.10.

The temporal development of the inflow pressure is diagrammed in Figure 5.26. Starting from the initial value of p_0 =1 bar (cf. Table 5.11), the inflow pressure reaches after 0.006 seconds the first stationary state at 11 bar. After the ignition, as the higher pressure of 100 bar exists at the outflow side, the inflow pressure arises to 100.5 bar.

The same mass flow rate, for which the pressure difference of Δp =10 bar is necessary before the ignition, can evidently be transported after the ignition by Δp =0.5 bar. This demonstrates the influence of the absolute pressure on the mass flow rate (5.4). The required pressure difference has been calculated for different values of the outflow pressure, cf. Table 5.12.

$\bar{v}_{GH_2}$	p_{in}	p_{out}	Δp
[kg/s m^2]	[bar]	[bar]	[bar]
5.0	22.7	20.0	2.7
5.0	51.1	50.0	1.1
5.0	80.7	80.0	0.7
5.0	100.5	100.0	0.5
5.0	200.3	200.0	0.3
5.0	250.2	250.0	0.2

Table 5.12: The required pressure difference for a constant mass flow rate depending on the absolute pressure.

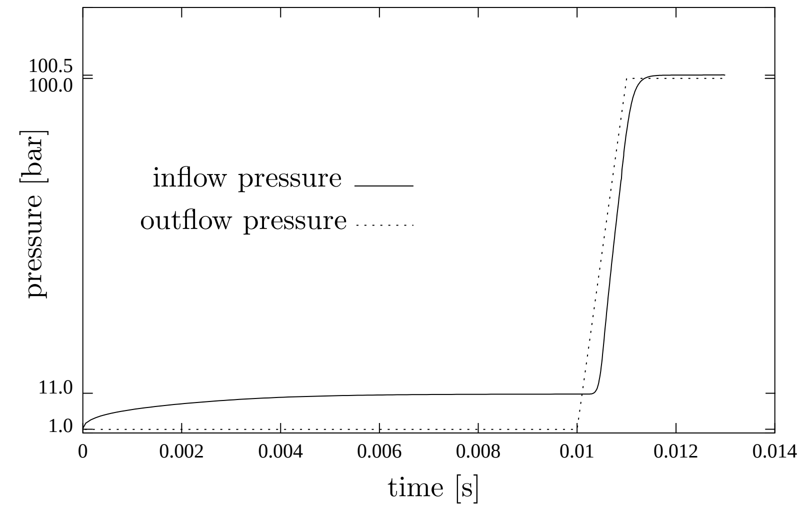

Figure 5.26: Temporal development of the inflow pressure according to the definitions in Table 5.11.

The nonlinear interrelationship between the pressure level and the arising pressure difference is depicted in Figure 5.27. In order to comprehend this effect, one should imagine the fluid particles as small packets, which are extremely compressed when a high pressure level exists. As a result, a minor pressure difference is needed in order to press the compressed packets through the microscopic pores of a porous material.

This phenomenon plays a major role for the design investigations of the construction under study. In particular, it justifies the quasi-static formulation of the problem on hand, since small pressure gradients and, as a consequence, small velocities can be assumed during the operation of the combustion chamber.

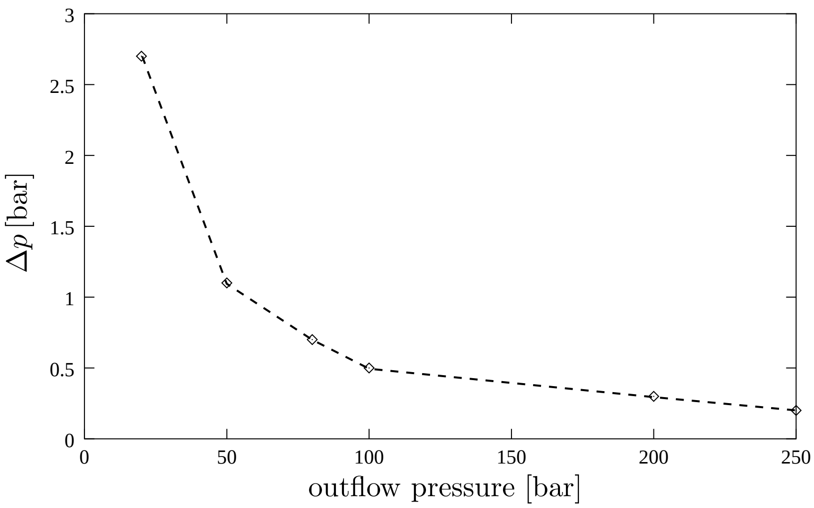

Figure 5.27: The required pressure difference for a constant mass flow rate depending on the pressure level.

5.4 Heat exchange phenomena

5.4.1 Caloric heat exchange

As was discussed in Chapter 4, heat exchange phenomena between the cooling gas and the solid skeleton can be caused by two different effects. Proceeding from a stagnant fluid, i. e. $\mathbf{w}_G = \mathbf{0}$, the heat exchange reduces to the caloric part, cf. relation (4.6). In a first simulation, the caloric heat exchange will be demonstrated in the following by means of a simplified model, cf. Figure 5.28.

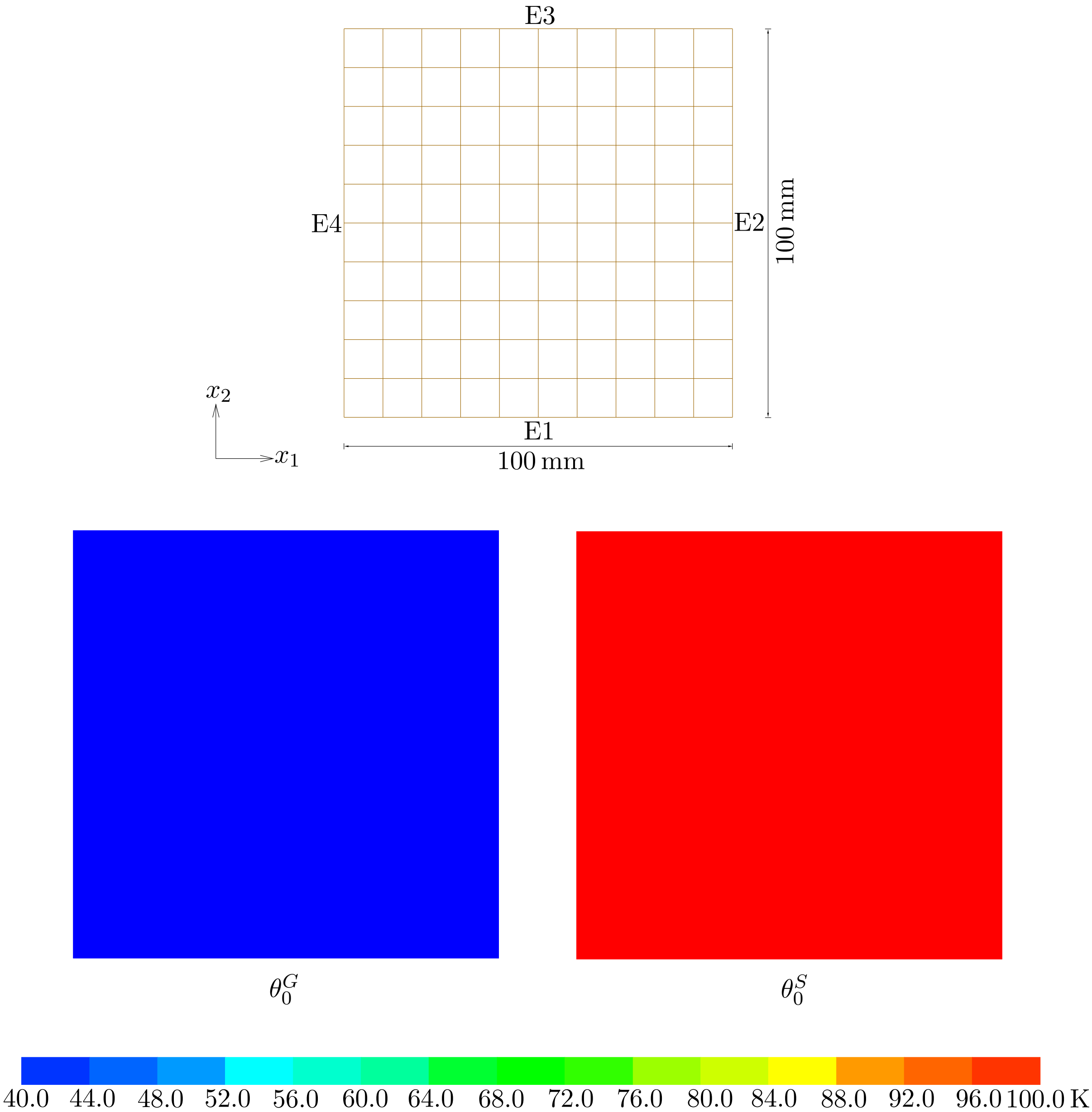

Figure 5.28: Simplified FE model for the simulation of the caloric heat exchange process.

It is pointed out that the volumetric heat exchange coefficient k_θ^ε represents one of the most important parameters and must be determined from experiments, cf. Chapter 4. For a first qualitative investigation, this coefficient is arbitrarily chosen as $k_\theta^\varepsilon = 100\,\mathrm{kW/m^3\,K}$. Except of this parameter, the remainder of the material parameters is taken for the following simulations from Table 5.8. Furthermore, the initial conditions are given in Table 5.13.

initial conditions	$p_0 = 1\,\mathrm{bar}$ $\theta_0^S = 100\,\mathrm{K}$ $\theta_0^G = 40\,\mathrm{K}$
Dirichlet boundary conditions	$u_1\,(E1, E3) = 0\,\mathrm{m}$ $u_2\,(E2, E4) = 0\,\mathrm{m}$
Neumann boundary conditions	–

Table 5.13: Initial and boundary conditions for the simulation of the heat exchange process.

In real processes, the heat transfer would take place between φ^S and φ^G until the equalization of the temperatures occurs. In Figure 5.29, the distribution of the temperature versus time is given for the solid and the fluid, respectively. Therein, the heat equalization occurs approximately after 0.05 seconds, where both constituents reach $\theta = 99.97\,\mathrm{K}$.

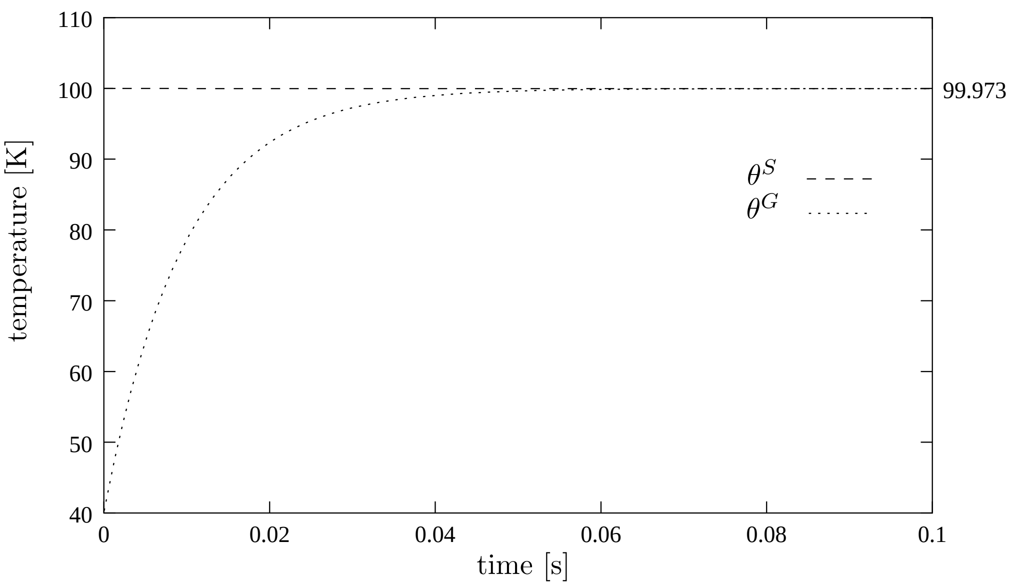

Figure 5.29: Heat exchange between φ^S and φ^G vs. time (heat equalization approx. after 0.05 seconds at $\theta = 99.973\,[K]$).

As is seen in Figure 5.29, the chosen parameters for this simulation lead to an inefficient cooling of the solid skeleton. At this point, it has to be investigated, which parameters significantly affect the cooling process. This is interesting, since a specific modification of some parameters can be made during the manufacturing of the porous material under consideration.

Proceeding from a stagnant fluid, the heat absorption behavior plays the major role on the heat transfer processes between φ^S and φ^G. In Figures 5.30 and 5.31, the temporal development of the solid temperature is given depending on different values for the solid density or the solid heat capacity, respectively. Note that these parameters are varied within a fairly realistic range.

However, looking at Figures 5.30 and 5.31, one observes that a variation in ρ^{SR} or C_V^S has an insignificant influence on the heat equalization level. Unlike this, it can be shown that the material gas density, which is defined through the ideal gas law (3.82), affects the heat equalization level stronger. Starting from the initial gas pressure $p_0 = 100\,\text{bar}$ instead of $p_0 = 1\,\text{bar}$, the solid and the gas constituent reach the temperature equalization approximately after 5 seconds at $\theta = 97\,\text{K}$, cf. Figure 5.32.

Finally, it is pointed out that the heat exchange coefficient does not influence the level of the temperature equalization, but only causes a temporal shift of this event, cf. Figures 5.33 and 5.34.

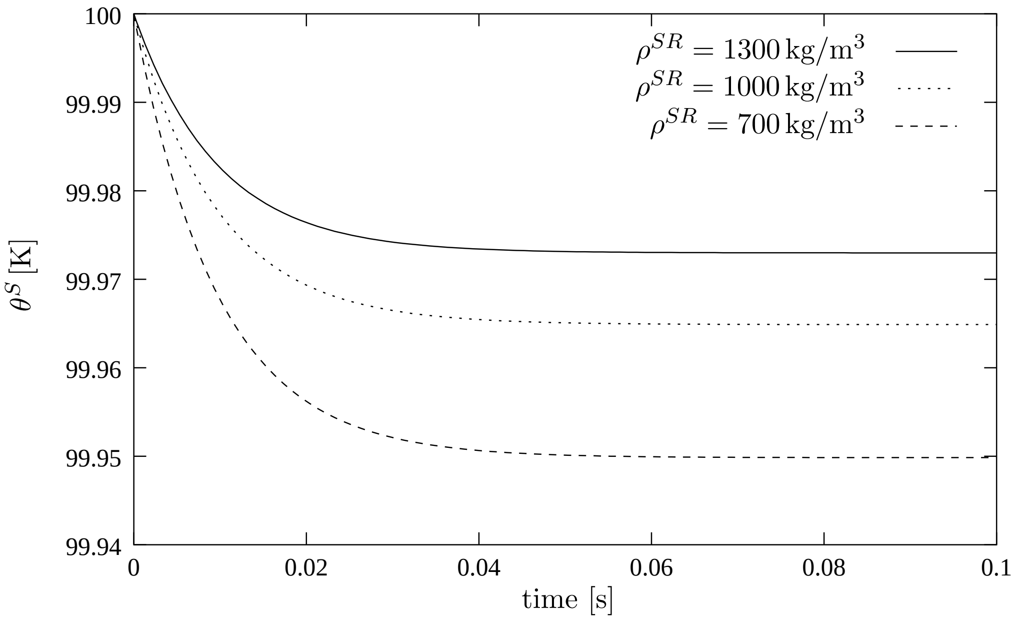

Figure 5.30: Temporal development of the solid temperature during the heat exchange process depending on different densities.

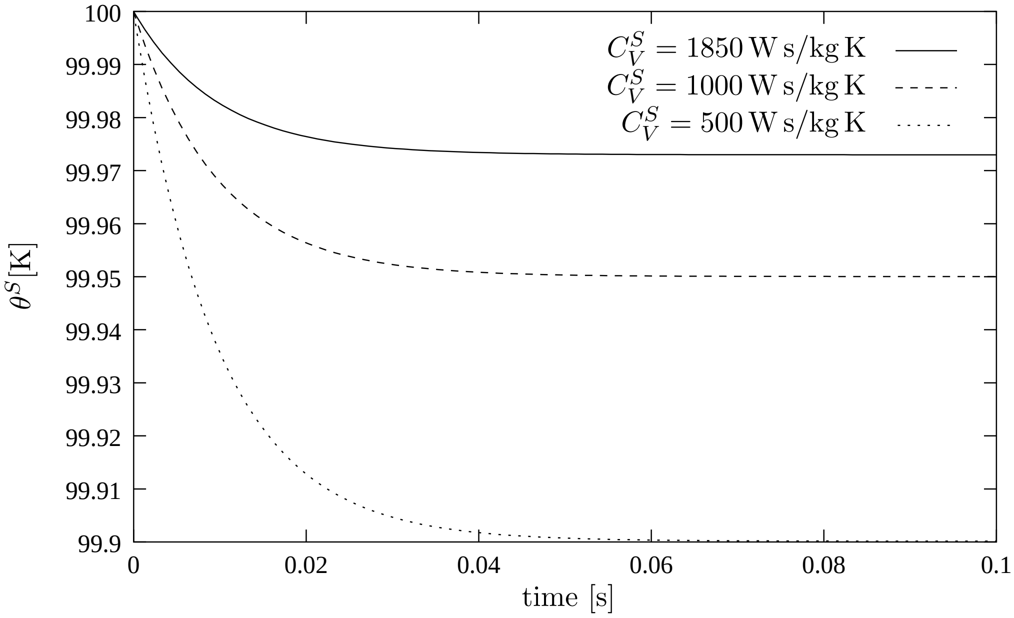

Figure 5.31: Temporal development of the solid temperature during the heat exchange process depending on different heat capacities.

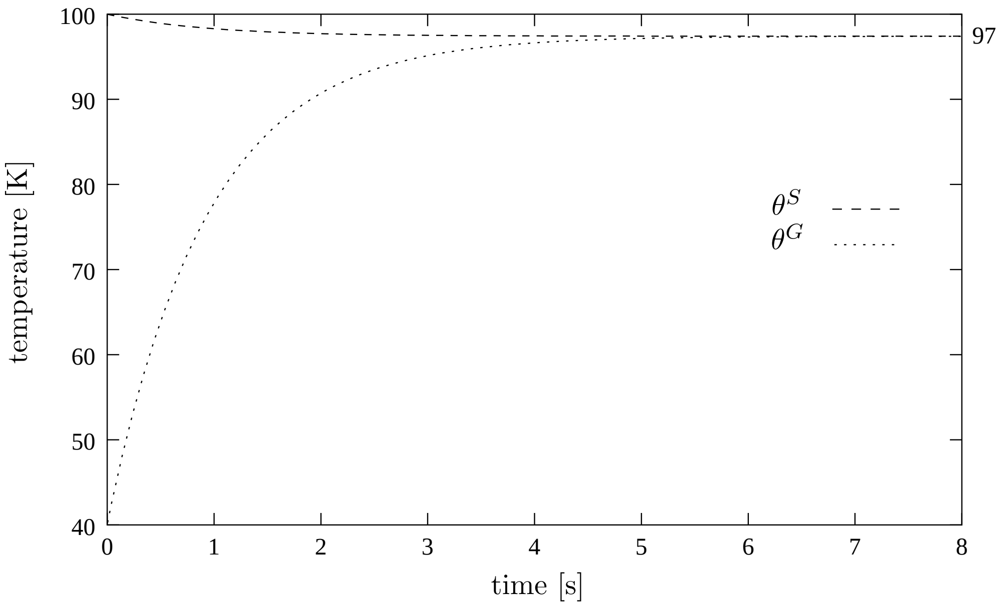

Figure 5.32: Heat equalization between φ^S and φ^G approx. after 5.0 seconds ; ($p_0 = 100\,\mathrm{bar}$, $k_\theta^\varepsilon = 100\,\mathrm{kW/m^3\,K}$).

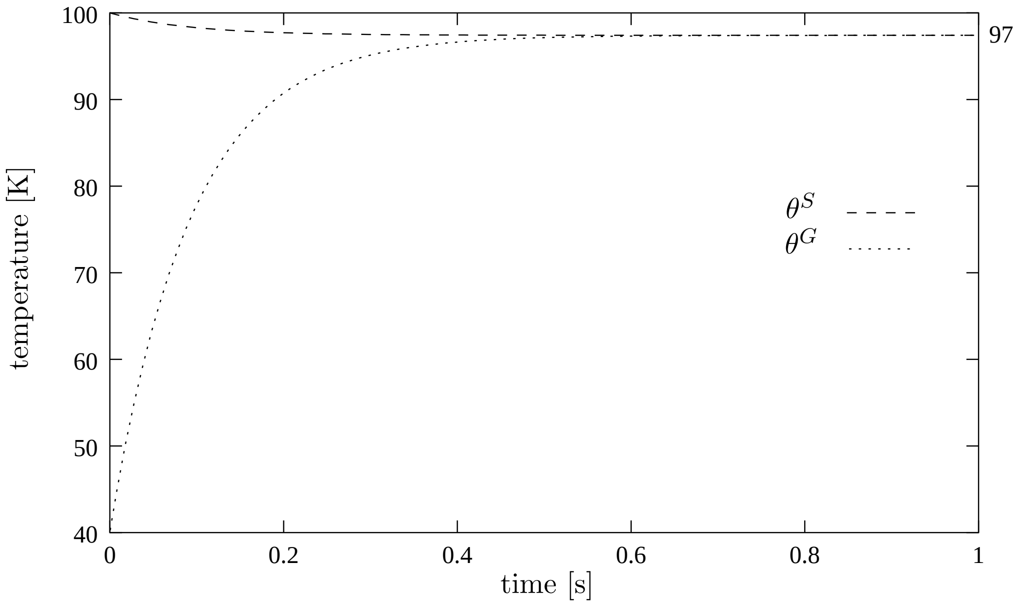

Figure 5.33: Heat equalization between φ^S and φ^G approx. after 0.5 seconds ; ($p_0 = 100\,\mathrm{bar}$, $k_\theta^\varepsilon = 1\,\mathrm{MW/m^3\,K}$).

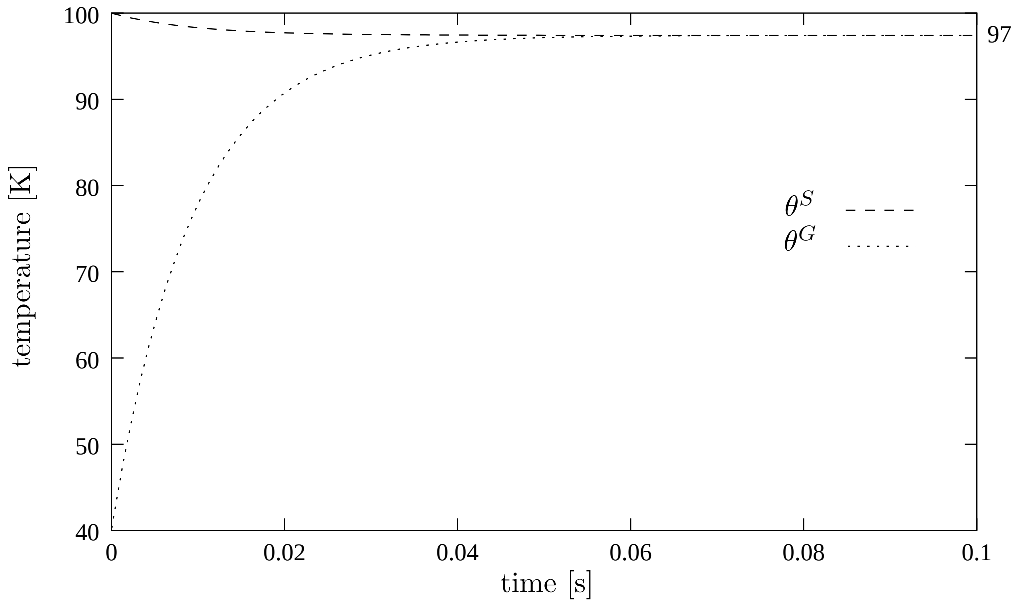

Figure 5.34: Heat equalization between φ^S and φ^G approx. after 0.05 seconds ; ($p_0 = 100\,\mathrm{bar}$, $k_\theta^\varepsilon = 10\,\mathrm{MW/m^3\,K}$).

5.4.2 The influence of the convective heat transfer

The basic effects on the caloric heat exchange demonstrated in the preceding subsection have been investigated for a stagnant pore-fluid. However, in order to understand the cooling phenomena in the porous combustion chamber under consideration, a flowing pore-fluid must be considered. Using the same FE model given in Figure 5.28, it will be seen that the convective heat transfer plays the major role on the cooling process. This holds, in particular, since in the real construction the coolant flows in the opposite direction to the heat load, cf. Figure 1.5.

The influence of the convective heat transfer becomes evident by considering a varying mass flow rate on the edge E4, whereas the heat load acting on the edge E2 is kept constant, cf. Figure 5.38. In the following simulations, the heat propagation in both constituents is shown depending on different values for $\bar{v}$. Comparing the temperature of the solid constituent at the edge E_2 (hot side) for different mass flow rates, one clearly recognizes the influence of the flowing coolant on the temperature distribution in φ^S . However, in order to have a reference solid temperature, the heat propagation is calculated in a first simulation by considering a stagnant fluid, cf. Figure 5.35 and Table 5.14. Note that the material parameters are taken from Table 5.8.

As is seen in Table 5.14, the heat load vector $\bar{q}$ is assumed only to act on the solid surface. This simplification is made, since it represents the worst case for the cooling of the solid skeleton.

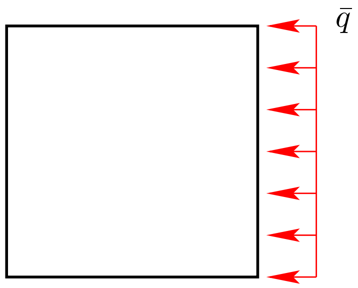

Figure 5.35: Heat load acting on the right edge of the biphasic model containing a stagnant pore-fluid.

initial conditions	$p_0 = 1\,\text{bar}$ $\theta_0^S = \theta_0^G = 40\,\text{K}$
Dirichlet boundary conditions	$u_1\,(E1, E3) = 0\,\text{m}$ $u_2\,(E2, E4) = 0\,\text{m}$
Neumann boundary conditions	$\bar{q}\,(E2) = \bar{q}^S\,(E2) = 2\,\text{MW/m}^2$

Table 5.14: Initial and boundary conditions for the simulation of the heat propagation by considering a stagnant fluid.

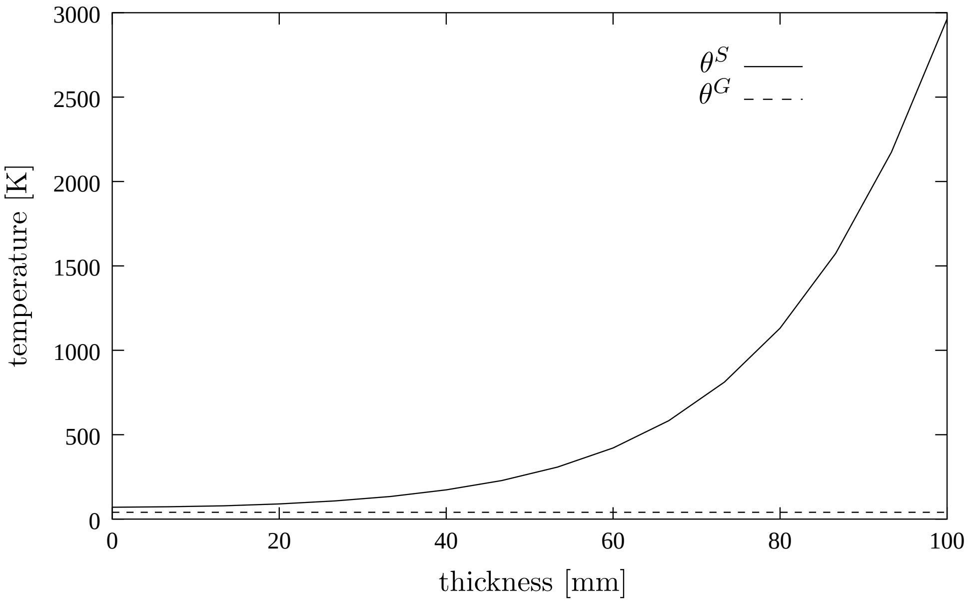

Figure 5.36: Temperature distribution along the edge E1 after 60 seconds with $\theta^S = 2963\,\mathrm{K}$ and $\theta^G = 40\,\mathrm{K}$ at E2 ; ($k^{\varepsilon}_{\theta} = 0\,\mathrm{kW/m^3\,K}$).

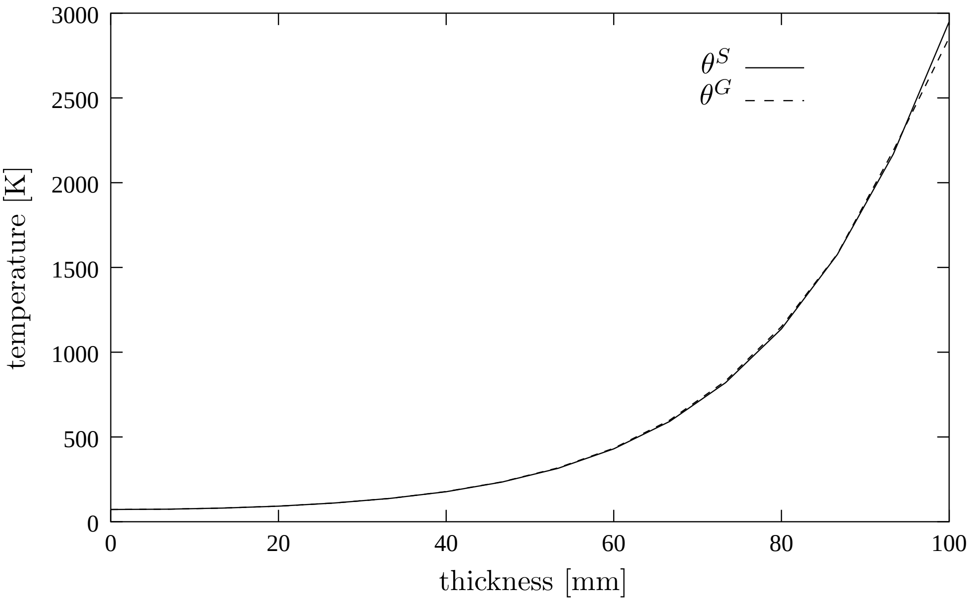

Figure 5.37: Temperature distribution along the edge E1 after 60 seconds with $\theta^S = 2949\,\mathrm{K}$ and $\theta^G = 2855\,\mathrm{K}$ at E2 ; ($k^{\varepsilon}_{\theta} = 100\,\mathrm{kW/m^3\,K}$).

As depicted in Figure 5.37, the solid temperature at the edge E2 amounts to $\theta^S = 2949\,\mathrm{K}$. It is now to investigate how this temperature changes depending on different mass flow rates, cf. Table 5.15.

In a first configuration, the mass flow rate is varied between $\bar{v} = 490\,\mathrm{g/s\,m^2}$ and $\bar{v} = 600\,\mathrm{g/s\,m^2}$, cf. Figure 5.39. Therein, it can be observed that the higher the mass flow rate is considered, the stronger is the cooling effect.

It is however pointed out that an arbitrary increase in the mass flow rate might also entail the reverse effect, cf. Figure 5.40. In order to understand this phenomenon, attention must be paid again to relation (4.6). Looking at the last two terms of this relation, it turns immediately out that the solid constituent additionally is heated up by frictional effects. This occurs in a pronounced manner, if high velocities exist. In Figures 5.41 and 5.42, the temperature distribution of the constituents is given for different mass flow rates along the edge E1 of the model. The corresponding velocities are represented in Figure 5.43. Note that in all of the following numerical results, $k_\theta^\varepsilon = 100\,\mathrm{kW/m^3\,K}$ has been considered.

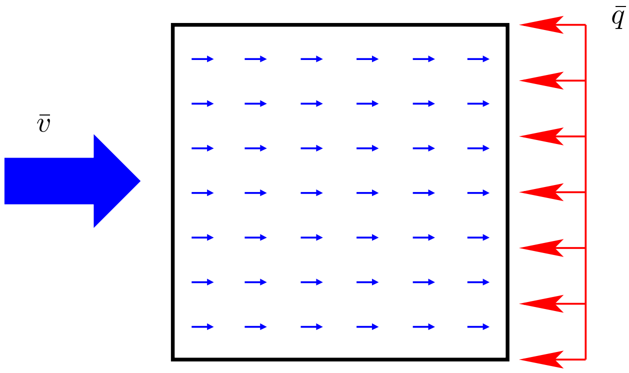

Figure 5.38: Heat load acting on the right edge of the biphasic model and a fluid mass flow rate flowing in the opposite direction.

initial conditions	$p_0 = 1\,\mathrm{bar}$ $\theta_0^S = \theta_0^G = 40\,\mathrm{K}$
Dirichlet boundary conditions	$u_1\,(E1, E3) = 0\,\mathrm{m}$ $u_2\,(E2, E4) = 0\,\mathrm{m}$ $p\,(E2) = 1\,\mathrm{bar}$ $\theta^G\,(E4) = 40\,\mathrm{K}$
Neumann boundary conditions	$\bar{q}\,(E2) = \bar{q}^S\,(E2) = 2\,\mathrm{MW/m^2}$ $\bar{v}\,(E4) = \text{variable}\,[\mathrm{kg/s\,m^2}]$

Table 5.15: Initial and boundary conditions for the simulation of the convective heat exchange.

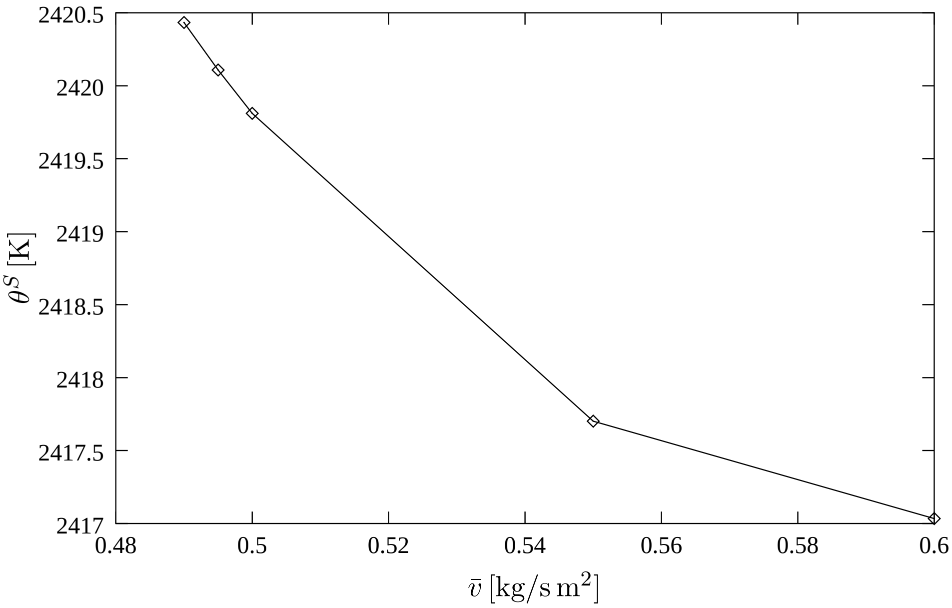

Figure 5.39: Solid temperature at the edge E2 after 240 seconds depending on different mass flow rates.

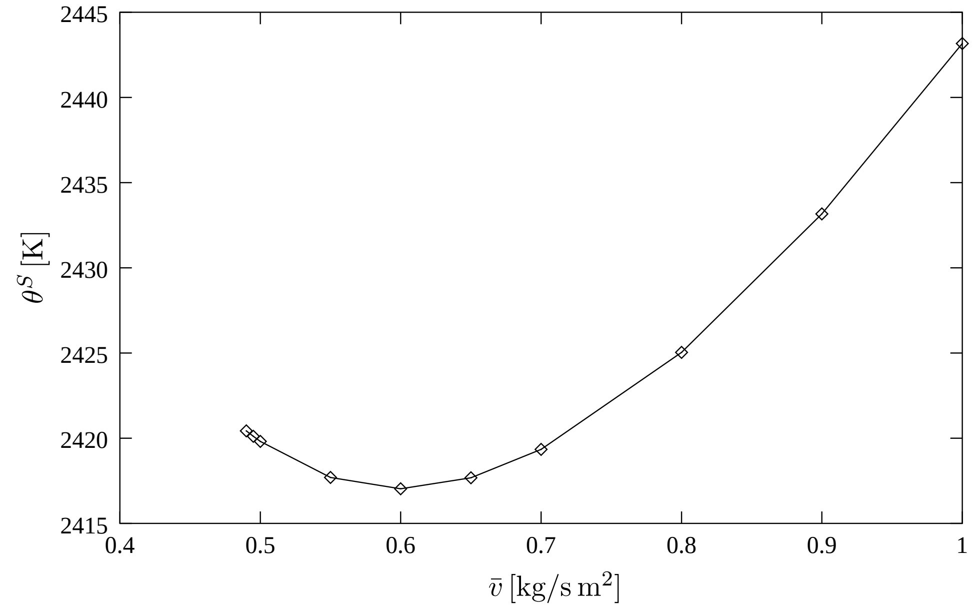

Figure 5.40: Solid temperature at the edge E2 after 240 seconds depending on different mass flow rates; the influence of the predominant frictional heat.

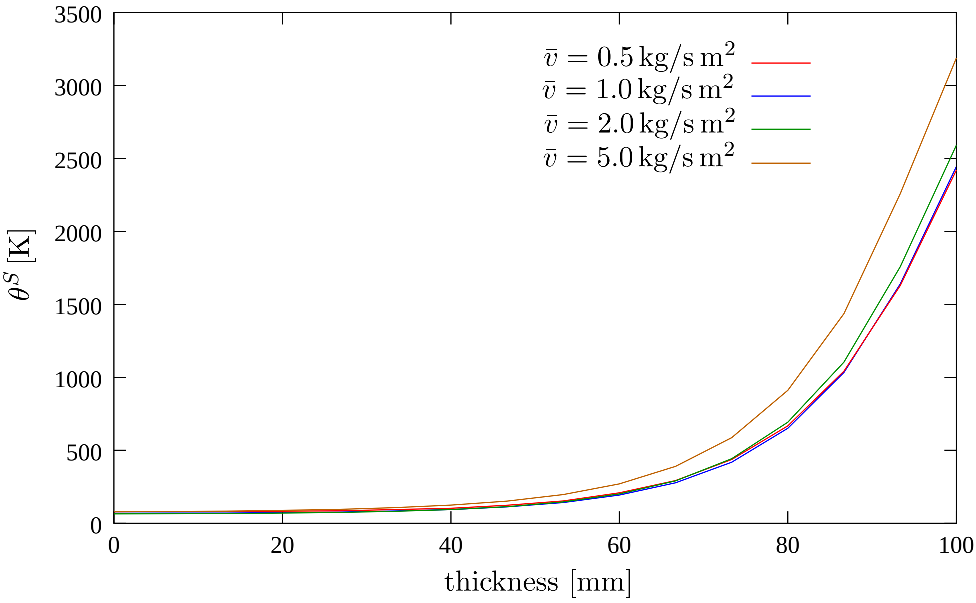

Figure 5.41: Distribution of the solid temperature along the edge E1 after 240 seconds for different mass flow rates.

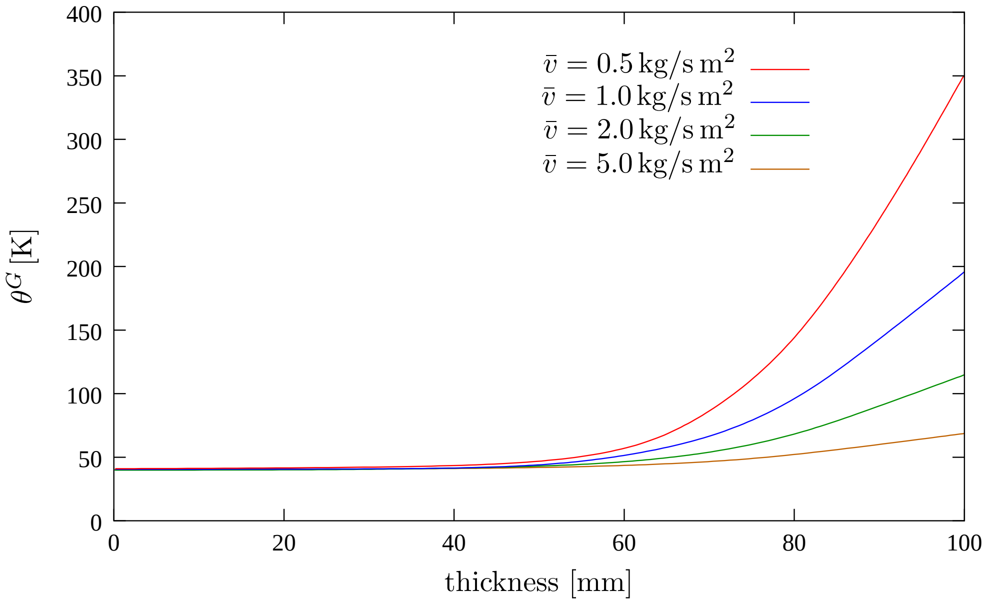

Figure 5.42: Distribution of the gas temperature along the edge E1 after 240 seconds for different mass flow rates.

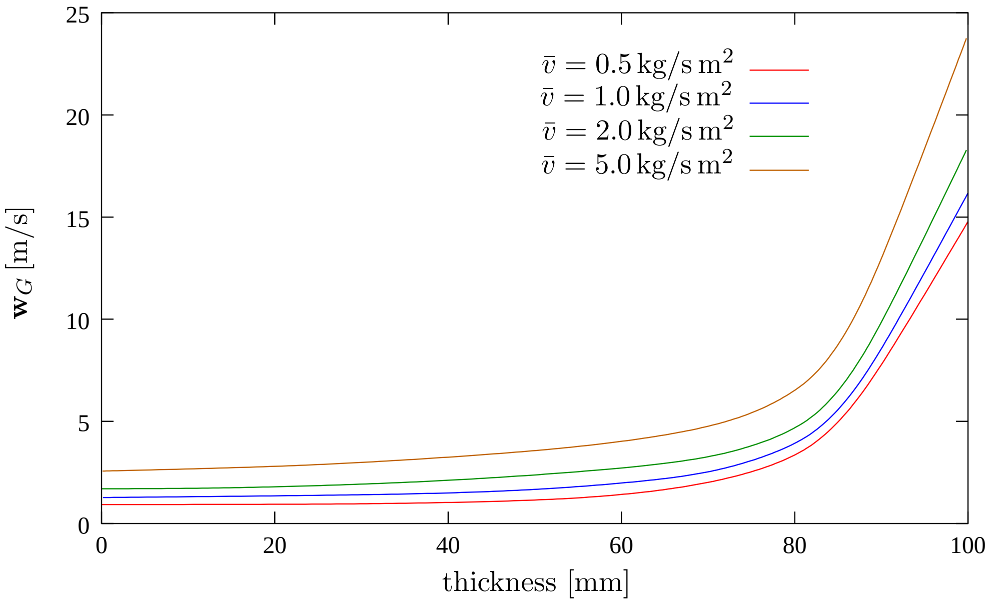

Figure 5.43: Distribution of the gas velocity along the edge E1 after 240 seconds for different mass flow rates.

As was expected, the gas velocity increases when a higher mass flow rate has to be pressed through the porous material, cf. Figure 5.43.

The preceding findings reveal that the required coolant mass flow rate for a real *effusion*-cooled construction must be determined by optimization calculations. This is necessary, since the solid temperature limit could be exceeded at the hot side, if the coolant is underdosed, on the one hand. On the other hand, an additional thermal increase occurs due to high velocities by oversupplying the porous construction with the coolant.

At this point, it should be pointed out that the presence of the *cooling film* (cf. Chapter 1) has been completely neglected in the numerical examples in this chapter. Nevertheless, several physical effects have been demonstrated qualitatively. It is however seen that large differences exist between the temperatures θ^S and θ^G, when the influence of the *cooling film* is not considered.

Finally, the influence of the heat conduction of the solid constituent will be discussed in a closing simulation. This is useful, since the heat conduction behavior of the solid material under consideration can be modified during the manufacturing. In Figures 5.45 and 5.44, the distribution of the solid temperature is represented for different heat conductions. Therein, it appears that, considering smaller values for the heat conduction, the heat propagation is reduced, whereas the corresponding surface temperature increases.

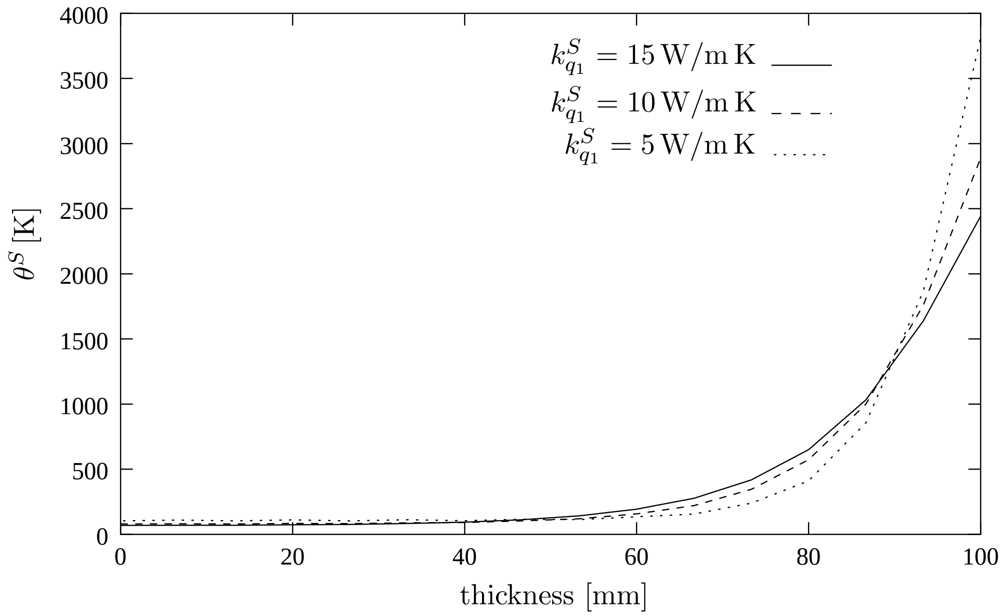

Figure 5.44: Distribution of the solid temperature after 240 seconds depending on different values for the heat conduction.

Note that the heat load acting on the edge E2 (cf. Table 5.15) has been assumed to be constant. This is however a simplification, since, in a real construction, the heat load acting on a surface is a time-dependent value. This quantity actually results from the interaction with the corresponding surface temperature at each point of time, cf., e. g., Schaefer [66]. For a precise investigation of the heat transfer phenomena under consideration, it is hence recommended to couple the numerical boundary layer simulations of the *cooling film*, e. g., with the aid of the numerical tool TDK, with the FE tool PANDAS used as solver for the model under study.

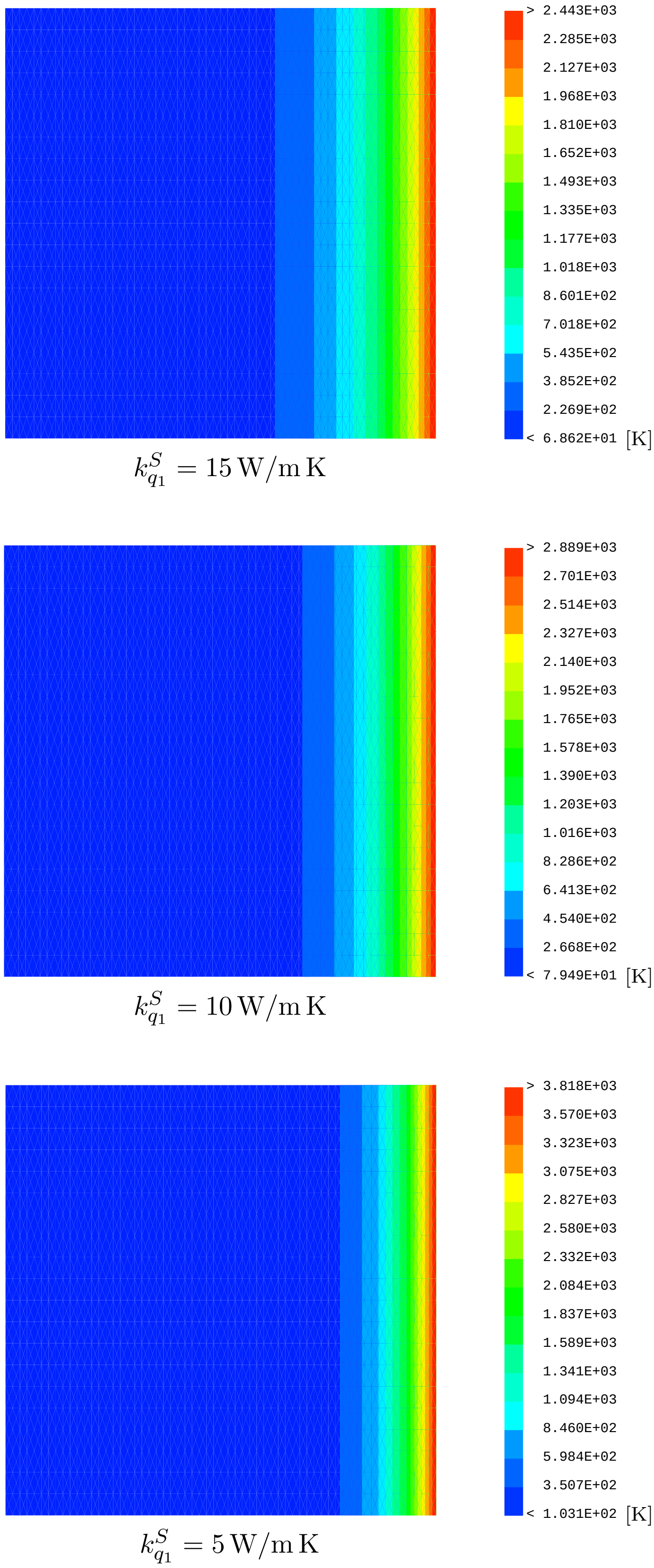

Figure 5.45: Distribution of the solid temperature after 240 seconds depending on different values for the heat conduction.

Chapter 6: Summary and outlook

6.1 Summary

In this work, a biphasic model consisting of a thermoelastic solid material and a compressible gas with separate temperature fields has been formulated on the basis of the TPM. The development of this model and the subsequent implementation of the corresponding system of equations in the FE solver PANDAS aimed at giving a serviceable tool in order to analyze and to understand the strongly coupled physical effects occurring in the porous liner of the combustion chamber under consideration. To this end, all required relations have been obtained from the evaluation of the entropy inequality, which was modified by a new constraint evolving from the saturation condition.

Because of the presence of the so-called *cooling film*, which protects the surface of the construction from excessive heat transfer, small temperature differences have been assumed between the gas and the solid skeleton inside of the porous material.

Considering the fact that, additionally to the deformation and the temperature of the solid material, also the pressure, the velocity as well as the temperature of the gas have to be determined as unknown field variables, a system of equations consisting of five balance relations was needed. However, for quasi-static processes, a constitutive equation could be formulated for the seepage velocity so that it has been crossed out from the set of the unknown variables. The number of equations was thus reduced to four. The numerical realization of the quasi-static problem is based on the Finite Element Method by use of a standard *Galerkin* procedure.

Concerning material parameters of the model, it was remarked that, except for the heat exchange coefficient, the remainder of the parameters can be adequately determined by performing basic experiments in such a manner that coupled effects are excluded. The determination of the heat exchange coefficient as the only unknown parameter must then be conducted by means of standard *parameter identification* procedures.

The numerical examples presented in this thesis have been restricted to the demonstration of some carefully selected physical effects, which are of utmost significance for the construction under study.

6.2 Outlook

As was remarked before, material parameters have still to be determined in order to simulate physical processes realistically. To this end, the required experimental data will be gained from divers ongoing experiments being performed at the DLR. The results of these investigations will be separately published within the framework of future reports.

Furthermore, in order to consider dynamic processes, where, additionally, acceleration effects are included, the FE package PANDAS must be extended by stable *explicit* time integration strategies, cf., e. g., Danilov [22].

The reliability of the model created must be verified by numerous experiments.

Appendix A: Vector and tensor calculus

(cf. de Boer [12])

Notation:

$$
\begin{aligned}
\{\alpha,\,\beta\} \in\ \mathbb{R} &\ :\ \text{real scalar values}\\
\{\mathbf{a},\,\mathbf{b},\,\mathbf{c},\,\mathbf{u},\,\mathbf{v},\,\mathbf{w}\} \in\ \mathcal{V}^3 &\ :\ \text{vectors in three-dimensional Euclidean space}\\
\{\mathbf{A},\,\mathbf{B},\,\mathbf{C},\,\mathbf{S},\,\mathbf{T}\} &\ :\ \text{tensors of second order}\\
\mathbf{x} &\ :\ \text{actual position vector}\\
\mathbf{X} &\ :\ \text{reference position vector}\\
\mathbf{I} &\ :\ \text{identity tensor}\\
\phi(\,\cdot\,) &\ :\ \text{scalar-valued function of } (\,\cdot\,)\\
\mathbf{v}(\,\cdot\,) &\ :\ \text{vector-valued function of } (\,\cdot\,)\\
\mathbf{T}(\,\cdot\,) &\ :\ \text{tensor-valued function of } (\,\cdot\,)
\end{aligned}
\tag{A.1}
$$

Vector calculus:

Multiplication of a vector with a scalar quantity

$$
\begin{aligned}
1\,\mathbf{v} &= \mathbf{v} && :\ 1\text{: identity } (-1\text{: inverse) element}\\
\alpha\,(\beta\,\mathbf{v}) &= (\alpha\,\beta)\,\mathbf{v} && :\ \text{associative law}\\
(\alpha+\beta)\,\mathbf{v} &= \alpha\,\mathbf{v}+\beta\,\mathbf{v} && :\ \text{distributive law (addition of scalars)}\\
\alpha\,(\mathbf{v}+\mathbf{w}) &= \alpha\,\mathbf{v}+\alpha\,\mathbf{w} && :\ \text{distributive law (addition of vectors)}\\
\alpha\,\mathbf{v} &= \mathbf{v}\,\alpha && :\ \text{commutative law}
\end{aligned}
\tag{A.2}
$$

Scalar product of vectors

$$
\begin{aligned}
\mathbf{u}\cdot\mathbf{v} &= \mathbf{v}\cdot\mathbf{u} && :\ \text{commutative law}\\
\mathbf{u}\cdot(\mathbf{v}+\mathbf{w}) &= \mathbf{u}\cdot\mathbf{v}+\mathbf{u}\cdot\mathbf{w} && :\ \text{distributive law}\\
\alpha\,(\mathbf{u}\cdot\mathbf{v}) &= \mathbf{u}\cdot(\alpha\,\mathbf{v}) = (\alpha\,\mathbf{u})\cdot\mathbf{v} && :\ \text{associative law}
\end{aligned}
\tag{A.3}
$$

Vector or cross product (outer product) of vectors

$$
\begin{aligned}
\mathbf{a}\times\mathbf{b} &= \mathbf{c} && :\ \text{result is a vector}\\
\mathbf{u}\times\mathbf{v} &= -\mathbf{v}\times\mathbf{u} && :\ \text{no commutative law}\\
\mathbf{u}\times(\mathbf{v}+\mathbf{w}) &= \mathbf{u}\times\mathbf{v}+\mathbf{u}\times\mathbf{w} && :\ \text{distributive law}\\
\alpha\,(\mathbf{u}\times\mathbf{v}) &= (\alpha\,\mathbf{u})\times\mathbf{v} = \mathbf{u}\times(\alpha\,\mathbf{v}) && :\ \text{associative law}
\end{aligned}
\tag{A.4}
$$

Tensor calculus:

Dyadic product

$$\mathbf{T} = \mathbf{a} \otimes \mathbf{b} \;\; : \;\; \in \; \mathcal{V}^3 \otimes \mathcal{V}^3 \text{ (dyadic product space)} \tag{A.5}$$

Multiplication of tensors by a scalar

$$\begin{aligned}
1\,\mathbf{A} &= \mathbf{A} && : 1 \;:\; \text{identical } (-1\text{: inverse) element} \\
\alpha\,(\beta\,\mathbf{A}) &= (\alpha\,\beta)\,\mathbf{A} && : \text{associative law} \\
(\alpha + \beta)\,\mathbf{A} &= \alpha\,\mathbf{A} + \beta\,\mathbf{A} && : \text{distributive law} \\
\alpha\,(\mathbf{A} + \mathbf{B}) &= \alpha\,\mathbf{A} + \alpha\,\mathbf{B} && : \text{distributive law} \\
\alpha\,\mathbf{A} &= \mathbf{A}\,\alpha && : \text{commutative law}
\end{aligned} \tag{A.6}$$

Linear mapping between tensor and vector

$$\begin{aligned}
\mathbf{A}\,(\mathbf{u} + \mathbf{v}) &= \mathbf{A}\,\mathbf{u} + \mathbf{A}\,\mathbf{v} && : \text{distributive law} \\
\mathbf{A}\,(\alpha\,\mathbf{u}) &= \alpha(\mathbf{A}\,\mathbf{u}) && : \text{associative law} \\
(\mathbf{A} + \mathbf{B})\,\mathbf{u} &= \mathbf{A}\,\mathbf{u} + \mathbf{B}\,\mathbf{u} && : \text{distributive law} \\
(\alpha\,\mathbf{A})\,\mathbf{u} &= \alpha\,(\mathbf{A}\,\mathbf{u}) && : \text{associative law} \\
\mathbf{0}\,\mathbf{u} &= \mathbf{0} \\
\mathbf{I}\,\mathbf{u} &= \mathbf{u}
\end{aligned} \tag{A.7}$$

Scalar product of tensors

$$\begin{aligned}
\mathbf{A} \cdot \mathbf{B} &= \mathbf{B} \cdot \mathbf{A} && : \text{commutative law} \\
\mathbf{A} \cdot (\mathbf{B} + \mathbf{C}) &= \mathbf{A} \cdot \mathbf{B} + \mathbf{A} \cdot \mathbf{C} && : \text{distributive law} \\
(\alpha\,\mathbf{A}) \cdot \mathbf{B} &= \mathbf{A} \cdot (\alpha\,\mathbf{B}) = \alpha\,(\mathbf{A} \cdot \mathbf{B}) && : \text{associative law}
\end{aligned} \tag{A.8}$$

Tensor product of tensors

$$\begin{aligned}
(\mathbf{A}\,\mathbf{B})\,\mathbf{C} &= \mathbf{A}\,(\mathbf{B}\,\mathbf{C}) && : \text{associative law} \\
\mathbf{A}\,(\mathbf{B} + \mathbf{C}) &= \mathbf{A}\,\mathbf{B} + \mathbf{A}\,\mathbf{C} && : \text{distributive law} \\
(\mathbf{A} + \mathbf{B})\,\mathbf{C} &= \mathbf{A}\,\mathbf{C} + \mathbf{B}\,\mathbf{C} && : \text{distributive law} \\
\alpha\,(\mathbf{A}\,\mathbf{B}) &= (\alpha\,\mathbf{A})\,\mathbf{B} = \mathbf{A}\,(\alpha\,\mathbf{B}) && : \text{associative law} \\
\mathbf{I}\,\mathbf{T} &= \mathbf{T}\,\mathbf{I} = \mathbf{T} \\
\mathbf{0}\,\mathbf{T} &= \mathbf{T}\,\mathbf{0} = \mathbf{0}
\end{aligned} \tag{A.9}$$

Transposed tensor

$$
\begin{aligned}
(\mathbf{A}+\mathbf{B})^T &= \mathbf{A}^T+\mathbf{B}^T \\
(\alpha\,\mathbf{A})^T &= \alpha\,\mathbf{A}^T \\
(\mathbf{A}\,\mathbf{B})^T &= \mathbf{B}^T\,\mathbf{A}^T \\
\mathbf{w}\cdot(\mathbf{A}\mathbf{u}) &= (\mathbf{A}^T\mathbf{w})\cdot\mathbf{u} \\
(\mathbf{A}\mathbf{B})\cdot\mathbf{I} &= \mathbf{B}\cdot\mathbf{A}^T=\mathbf{B}^T\cdot\mathbf{A}
\end{aligned}
\tag{A.10}
$$

Symmetric and skew-symmetric tensor

$$
\begin{aligned}
\operatorname{sym}\mathbf{A} &= \tfrac{1}{2}\,(\mathbf{A}+\mathbf{A}^T) \\
\operatorname{skw}\mathbf{A} &= \tfrac{1}{2}\,(\mathbf{A}-\mathbf{A}^T) \\
\longrightarrow\ \mathbf{A} &= \operatorname{sym}\mathbf{A}+\operatorname{skw}\mathbf{A}
\end{aligned}
\tag{A.11}
$$

Inverse tensor

$$
\begin{aligned}
\mathbf{A}\,\mathbf{A}^{-1} &= \mathbf{A}^{-1}\,\mathbf{A}=\ \mathbf{I} \\
(\mathbf{A}^{-1})^T &= (\mathbf{A}^T)^{-1}=:\mathbf{A}^{T-1} \\
(\mathbf{A}\,\mathbf{B})^{-1} &= \mathbf{B}^{-1}\,\mathbf{A}^{-1}
\end{aligned}
\tag{A.12}
$$

Vector and tensor analysis:

Basic rules

$$
\begin{aligned}
(\mathbf{a}\otimes\mathbf{b})' &= \mathbf{a}'\otimes\mathbf{b}+\mathbf{a}\otimes\mathbf{b}' \\
(\mathbf{A}\,\mathbf{B})' &= \mathbf{A}'\,\mathbf{B}+\mathbf{A}\,\mathbf{B}' \\
(\mathbf{A}^{-1})' &= -\mathbf{A}^{-1}\,\mathbf{A}'\,\mathbf{A}^{-1}
\end{aligned}
\tag{A.13}
$$

The gradient operator

$$
\begin{aligned}
\operatorname{grad}\phi(\mathbf{x}) &:= \frac{\mathrm{d}\phi(\mathbf{x})}{\mathrm{d}\mathbf{x}} =: \mathbf{w}(\mathbf{x}) && \longrightarrow \quad \text{vector field} \\
\operatorname{grad}\mathbf{v}(\mathbf{x}) &:= \frac{\mathrm{d}\mathbf{v}(\mathbf{x})}{\mathrm{d}\mathbf{x}} =: \mathbf{S}(\mathbf{x}) && \longrightarrow \quad \text{tensor field} \\
\operatorname{grad}\mathbf{T}(\mathbf{x}) &:= \frac{\mathrm{d}\mathbf{T}(\mathbf{x})}{\mathrm{d}\mathbf{x}} =: \overset{3}{\mathbf{U}}(\mathbf{x}) && \longrightarrow \quad \text{tensor field of 3-rd order} \\
\operatorname{Grad}\phi(\mathbf{X}) &:= \frac{\mathrm{d}\phi(\mathbf{X})}{\mathrm{d}\mathbf{X}}
\end{aligned}
\tag{A.14}
$$

The divergence operator

$$
\begin{aligned}
\operatorname{div}\mathbf{v}(\mathbf{x}) &:= \operatorname{grad}\mathbf{v}(\mathbf{x})\cdot\mathbf{I} =: \phi(\mathbf{x}) && \longrightarrow \quad \text{result is a scalar field}\\
\operatorname{div}\mathbf{T}(\mathbf{x}) &:= [\operatorname{grad}\mathbf{T}(\mathbf{x})]\,\mathbf{I} =: \mathbf{v}(\mathbf{x}) && \longrightarrow \quad \text{result is a vector field}\\
\operatorname{Div}\mathbf{v}(\mathbf{X}) &:= \operatorname{Grad}\mathbf{v}(\mathbf{X})\cdot\mathbf{I}
\end{aligned}
\tag{A.15}
$$

Rules for the operators grad (·) and div (·)

$$
\begin{aligned}
\operatorname{grad}(\phi\psi) &= \phi\operatorname{grad}\psi + \psi\operatorname{grad}\phi\\
\operatorname{grad}(\phi\mathbf{v}) &= \mathbf{v}\otimes\operatorname{grad}\phi + \phi\operatorname{grad}\mathbf{v}\\
\operatorname{grad}(\phi\mathbf{T}) &= \mathbf{T}\otimes\operatorname{grad}\phi + \phi\operatorname{grad}\mathbf{T}\\
\operatorname{grad}(\mathbf{u}\cdot\mathbf{v}) &= (\operatorname{grad}\mathbf{u})^T\,\mathbf{v} + (\operatorname{grad}\mathbf{v})^T\,\mathbf{u}\\
\operatorname{div}(\mathbf{a}\otimes\mathbf{b}) &= \mathbf{a}\operatorname{div}\mathbf{b} + (\operatorname{grad}\mathbf{a})\,\mathbf{b}\\
\operatorname{div}(\phi\mathbf{v}) &= \mathbf{v}\cdot\operatorname{grad}\phi + \phi\operatorname{div}\mathbf{v}\\
\operatorname{div}(\mathbf{T}\mathbf{v}) &= (\operatorname{div}\mathbf{T}^T)\cdot\mathbf{v} + \mathbf{T}^T\cdot\operatorname{grad}\mathbf{v}\\
\operatorname{div}(\operatorname{grad}\mathbf{v})^T &= \operatorname{grad}\operatorname{div}\mathbf{v}\\
\operatorname{div}(\mathbf{u}\times\mathbf{v}) &= (\operatorname{grad}\mathbf{u}\times\mathbf{v})\cdot\mathbf{I} - (\operatorname{grad}\mathbf{v}\times\mathbf{u})\cdot\mathbf{I}\\
\operatorname{div}(\phi\,\mathbf{T}) &= \mathbf{T}\operatorname{grad}\phi + \phi\operatorname{div}\mathbf{T}\\
\operatorname{div}(\mathbf{T}\,\mathbf{S}) &= (\operatorname{grad}\mathbf{T})\,\mathbf{S} + \mathbf{T}\operatorname{div}\mathbf{S}\\
\operatorname{div}(\mathbf{v}\times\mathbf{T}) &= \mathbf{v}\times\operatorname{div}\mathbf{T} + \operatorname{grad}\mathbf{v}\times\mathbf{T}\\
\operatorname{div}(\mathbf{v}\otimes\mathbf{T}) &= \mathbf{v}\otimes\operatorname{div}\mathbf{T} + (\operatorname{grad}\mathbf{v})\,\mathbf{T}^T
\end{aligned}
\tag{A.16}
$$

Integral theorems 1

$$
\begin{aligned}
\int_{\mathcal{S}} \mathbf{u}\otimes \mathrm{d}\mathbf{a} &= \int_V \operatorname{grad}\mathbf{u}\,\mathrm{d}v\\
\int_{\mathcal{S}} \phi\,\mathrm{d}\mathbf{a} &= \int_V \operatorname{grad}\phi\,\mathrm{d}v\\
\int_{\mathcal{S}} \mathbf{u}\cdot\mathrm{d}\mathbf{a} &= \int_V \operatorname{div}\mathbf{u}\,\mathrm{d}v\\
\int_{\mathcal{S}} \mathbf{T}\,\mathrm{d}\mathbf{a} &= \int_V \operatorname{div}\mathbf{T}\,\mathrm{d}v
\end{aligned}
\tag{A.17}
$$

Integral theorems 2

$$
\begin{aligned}
\int_{\mathcal{S}} \mathbf{u} \times \mathbf{T} \, \mathrm{d}\mathbf{a} &= \int_{V} \operatorname{div}(\mathbf{u} \times \mathbf{T}) \, \mathrm{d}v \\
\int_{\mathcal{S}} \mathbf{u} \otimes \mathbf{T} \, \mathrm{d}\mathbf{a} &= \int_{V} \operatorname{div}(\mathbf{u} \otimes \mathbf{T}) \, \mathrm{d}v
\end{aligned}
\tag{A.18}
$$

Additional rules

$$
\frac{\mathrm{d}}{\mathrm{d}\mathbf{T}} \det\mathbf{T} = \det\mathbf{T} \, \mathbf{T}^{T-1} \tag{A.19}
$$

Appendix B: Derivations

Notation:

$$
\begin{aligned}
(\cdot)^{\boldsymbol{\cdot}} \; = \; \frac{d}{dt}\,(\cdot) \quad &: \quad \text{total time derivative} \\
\frac{\partial}{\partial\, t}\,(\cdot) \quad &: \quad \text{partial time derivative} \\
\mathbf{v} \quad &: \quad \text{velocity}
\end{aligned}
\tag{B.1}
$$

Basic rules:

$$
\begin{aligned}
(\alpha\,\beta)' \quad &= \quad (\alpha)'\,\beta \, + \, \alpha\,(\beta)' \quad : \quad \text{product rule} \\
\left(\frac{\alpha}{\beta}\right)' \quad &= \quad \frac{(\alpha)'\,\beta \, - \, \alpha\,(\beta)'}{\beta^2} \quad : \quad \text{quotient rule}
\end{aligned}
\tag{B.2}
$$

Specific rules:

$$
\frac{\partial}{\partial\, x}(x\,\mathrm{ln}x - x) \quad = \quad \mathrm{ln}x
\tag{B.3}
$$

Linearization of $\det \mathbf{F}_S$**:**

Using a standard linearization procedure, one obtains in a first step

$$
(\det \mathbf{F}_S)_{lin} = \quad \det \mathbf{F}_S \Big|_{\mathbf{F}_{0S}} \; + \; \frac{\partial\,(\det \mathbf{F}_S)}{\partial\, \mathbf{F}_S}\Big|_{\mathbf{F}_{0S}} \cdot (\mathbf{F}_S \; - \; \mathbf{F}_{0S})\,.
\tag{B.4}
$$

Considering

$$
\begin{aligned}
\mathbf{F}_S \quad &= \quad \mathrm{Grad}\,\mathbf{x}_S = \mathrm{Grad}\,\mathbf{u}_S + \mathbf{I}\,, \\
\mathbf{F}_{0S} \quad &= \quad \mathbf{I}\,, \\
\frac{\partial\,(\det \mathbf{F}_S)}{\partial\, \mathbf{F}_S} \quad &= \quad \det\mathbf{F}_S\,\mathbf{F}^{T-1}\,,
\end{aligned}
\tag{B.5}
$$

the linearization of $\det \mathbf{F}_S$ yields then

$$
\begin{aligned}
(\det \mathbf{F}_S)_{lin} \quad &= 1 + \mathbf{I} \cdot \mathrm{Grad}_S\,\mathbf{u}_S \\
&= 1 + \mathrm{Div}\,\mathbf{u}_S\,.
\end{aligned}
\tag{B.6}
$$

Linearization of $(\det \mathbf{F}_S)^{-1}$**:**

Proceeding from

$$
[(\det \mathbf{F}_S)^{-1}]_{lin} = \quad (\det \mathbf{F}_S)^{-1}\Big|_{\mathbf{F}_{0S}} \; + \; \frac{\partial\,(\det \mathbf{F}_S)^{-1}}{\partial\, \mathbf{F}_S}\Big|_{\mathbf{F}_{0S}} \cdot (\mathbf{F}_S \; - \; \mathbf{F}_{0S})\,,
\tag{B.7}
$$

and considering

$$\frac{\partial\,(\det \mathbf{F}_S)^{-1}}{\partial\,\mathbf{F}_S} \;=\; -(\det\mathbf{F}_S)^{-1}\,\mathbf{F}^{-T}\,, \tag{B.8}$$

one obtains, in analogy to (B.6),

$$\begin{aligned}[(\det \mathbf{F}_S)^{-1}]_{lin} &= 1 - \mathbf{I}\cdot \mathrm{Grad}\,\mathbf{u}_S \\ &= 1 - \mathrm{Div}\,\mathbf{u}_S\,.\end{aligned} \tag{B.9}$$

Linearization of n^S:

In order to obtain the linearized volume fraction of the solid, the relations (3.20), (3.28) and (3.30) are once again listed below

$$\begin{aligned}\mathbf{F}_S &= \mathbf{F}_{Sm}\mathbf{F}_{S\theta}\,,\\ n^S &= n^S_{0S}\,(\det\mathbf{F}_{Sm})^{-1}\,,\\ \det\mathbf{F}_{S\theta} &= e^{3\,\alpha^S\,\Delta\theta^S}\,.\end{aligned} \tag{B.10}$$

Proceeding from $(\mathrm{B.10})_1$, it follows that

$$[(\det \mathbf{F}_S)^{-1}]_{lin} \;=\; [(\det \mathbf{F}_{Sm})^{-1}\,(\det \mathbf{F}_{S\theta})^{-1}]_{lin}\,. \tag{B.11}$$

Furthermore, inserting (B.9) and $(\mathrm{B.10})_3$ into (B.11), one obtains

$$[(\det \mathbf{F}_{Sm})^{-1}]_{lin} = (1-\mathrm{div}\,\mathbf{u}_S)\,e^{3\,\alpha^S\,\Delta\theta^S}\,, \tag{B.12}$$

so that the combination of $(\mathrm{B.10})_2$ and (B.12) yields

$$n^S_{lin} = n^S_{0S}\,(1-\mathrm{div}\,\mathbf{u}_S)\,e^{3\,\alpha^S\,\Delta\theta^S}\,. \tag{B.13}$$

The time derivative of $\det\mathbf{F}$:

In a first step, use is made of the well-known volume transport theorem (cf., e. g., Altenbach [1], Becker and Bürger [4] or Haupt [47]) via

$$\mathrm{d}v \;=\; \det\mathbf{F}\,\mathrm{d}V_0\,, \tag{B.14}$$

where $\mathrm{d}V_0$ represents the initial volume element at time t_0 and $\mathrm{d}v$ the corresponding volume element in the actual configuration. Furthermore, taking advantage of (2.28), (2.29), (A.19) and $(\mathrm{B.2})_1$, one obtains for the time derivation of (B.14)

$$\begin{aligned}(\mathrm{d}v)^{\boldsymbol{\cdot}} &= (\det\mathbf{F}\,\mathrm{d}V_0)^{\boldsymbol{\cdot}}\\ &= \frac{\mathrm{d}}{\mathrm{d}\mathbf{F}}\det\mathbf{F}\cdot(\mathbf{F})^{\boldsymbol{\cdot}}\,\mathrm{d}V_0\\ &= \mathrm{div}\mathbf{v}\,\det\mathbf{F}\,\mathrm{d}V_0\\ &= \mathrm{div}\,\mathbf{v}\,\mathrm{d}v\,.\end{aligned} \tag{B.15}$$

Note that

$$(\mathrm{d}V_0)^{\boldsymbol{\cdot}} = 0 \tag{B.16}$$

has been additionally considered in (B.15). On the other hand, according to the product rule $(B.2)_1$ and the condition (B.16), (B.15) can also be given as

$$\begin{aligned}(\mathrm{d}v)^{\boldsymbol{\cdot}} &= (\det\mathbf{F}\,\mathrm{d}V_0)^{\boldsymbol{\cdot}} \\ &= (\det\mathbf{F})^{\boldsymbol{\cdot}}\,\mathrm{d}V_0 \\ &= (\det\mathbf{F})^{\boldsymbol{\cdot}}\,(\det\mathbf{F})^{-1}\,\mathrm{d}v\,.\end{aligned} \tag{B.17}$$

Therein, (B.14) has been incorporated. Comparing (B.15) with (B.17), one finally obtains

$$(\det\mathbf{F})^{\boldsymbol{\cdot}} = \det\mathbf{F}\,\mathrm{div}\,\mathbf{v}\,. \tag{B.18}$$

The time derivative of the gas density:

Proceeding from the ideal gas law from (3.82) via

$$\rho^{GR} = \frac{p^{GR}}{\bar{R}^G\,\theta^G} \tag{B.19}$$

and taking advantage of $(B.2)_2$, it follows that

$$(\rho^{GR})'_S = \frac{1}{\bar{R}^G\,(\theta^G)^2}\,\left[\theta^G\,(p^{GR})'_S - p^{GR}\,(\theta^G)'_S\right]\,. \tag{B.20}$$

For the gradient of the density, one obtains analogously

$$\mathrm{grad}\,\rho^{GR} = \frac{1}{\bar{R}^G\,(\theta^G)^2}\,\left(\theta^G\,\mathrm{grad}\,p^{GR} - p^{GR}\,\mathrm{grad}\,\theta^G\right)\,. \tag{B.21}$$

Furthermore, proceeding from (2.21), it follows

$$(\rho^{GR})'_G = (\rho^{GR})'_S + \mathrm{grad}\,\rho^{GR}\cdot\mathbf{w}_G\,. \tag{B.22}$$

The incorporation of (B.20) and (B.21) in (B.22) yields then

$$\begin{aligned}&(\rho^{GR})'_G = \\ &= \frac{1}{\bar{R}^G\,(\theta^G)^2}\,\left[\theta^G\,(p^{GR})'_S - p^{GR}\,(\theta^G)'_S + \left(\theta^G\,\mathrm{grad}\,p^{GR} - p^{GR}\,\mathrm{grad}\,\theta^G\right)\cdot\mathbf{w}_G\right]\,.\end{aligned} \tag{B.23}$$

The time derivative of the solid entropy $\bar{\eta}^S$:

Using $(B.2)_2$, one obtains

$$\left(\frac{\theta^S}{\theta^G}\right)'_S = \frac{1}{(\theta^G)^2}\,[\theta^G\,(\theta^S)'_S - \theta^S\,(\theta^G)'_S]\,. \tag{B.24}$$

Moreover, it holds that

$$(e^{3\,\alpha^S \Delta\theta^S})'_S = 3\,\alpha^S\,(\theta^S)'_S\,e^{3\,\alpha^S \Delta\theta^S}\,. \tag{B.25}$$

Finally, using (B.24) and (B.25) and taking advantage of $(\text{B.2})_1$, it follows

$$\begin{aligned}
(\bar\eta^S)'_S &= \left(-\frac{3\,\alpha^S\,\theta^S}{\rho^{SR}_{0S}\,\theta^G}\,p^{GR}\,e^{3\,\alpha^S\Delta\theta^S}\right)'_S\\
&= -3\,\frac{\alpha^S}{\rho^{SR}_{0S}}\left(\frac{\theta^S}{\theta^G}p^{GR}\,e^{3\,\alpha^S\Delta\theta^S}\right)'_S\\
&= -3\,\frac{\alpha^S}{\theta^G\rho^{SR}_{0S}}\,e^{3\,\alpha^S\Delta\theta^S}\left[p^{GR}\,(\theta^S)'_S - \frac{\theta^S}{\theta^G}\,p^{GR}\,(\theta^G)'_S + \right.\\
&\quad\left. + \theta^S\,(p^{GR})'_S + 3\,\alpha^S\,\theta^S\,p^{GR}\,(\theta^S)'_S\right].
\end{aligned} \tag{B.26}$$

Reformulation of $\operatorname{div}(n^G\,p^{GR}\,\mathbf{I})$:

Using $(\text{A.7})_6$, $(\text{A.16})_{10}$ and $(\text{B.2})_1$, one obtains

$$\begin{aligned}
\operatorname{div}(n^G\,p^{GR}\,\mathbf{I}) &= \mathbf{I}\,\operatorname{grad}(n^G\,p^{GR}) + n^G\,p^{GR}\,\underbrace{\operatorname{div}\mathbf{I}}_{\mathbf{0}}\\
&= \operatorname{grad}(n^G\,p^{GR})\\
&= p^{GR}\operatorname{grad}n^G + n^G\operatorname{grad}p^{GR}\,.
\end{aligned} \tag{B.27}$$

Reformulation of terms in equation (B.67):

It is to verify that

$$-\,n^G\,\rho^{GR}\,\frac{\partial\,\psi^G}{\partial\,\rho^{GR}}\,(\rho^{GR})'_G - n^G\,p^{GR}\operatorname{div}\overset{\prime}{\mathbf{x}}_G = p^{GR}\operatorname{grad}n^G\cdot\mathbf{w}_G - p^{GR}\,(n^S)'_S\,. \tag{B.28}$$

To this end, first the equations from (3.11), (3.14), (3.75) and $(3.95)_2$, respectively, are once again listed below

$$\begin{aligned}
0 &= (n^G)'_G\,\rho^{GR} + n^G(\rho^{GR})'_G + n^G\rho^{GR}\operatorname{div}\overset{\prime}{\mathbf{x}}_G\,,\\
p^{GR} &= (\rho^{GR})^2\frac{\partial\psi^G}{\partial\rho^{GR}}\,,\\
(n^G)'_G &= (n^G)'_S + \operatorname{grad}n^G\cdot\mathbf{w}_G\,,\\
(n^G)'_S &= -(n^S)'_S\,.
\end{aligned} \tag{B.29}$$

Using $(\text{B.29})_2$, one obtains for the first term in (B.28)

$$-\,n^G\,\rho^{GR}\,\frac{\partial\,\psi^G}{\partial\,\rho^{GR}}\,(\rho^{GR})'_G = -\,n^G\,\frac{p^{GR}}{\rho^{GR}}\,(\rho^{GR})'_G\,. \tag{B.30}$$

Furthermore, considering $(B.29)_1$, $(B.29)_3$ and $(B.29)_4$, the time derivative of the gas density can be alternatively given as

$$\begin{aligned}(\rho^{GR})'_G &= -\frac{\rho^{GR}}{n^G}\left[(n^G)'_G + n^G \operatorname{div} \overset{\prime}{\mathbf{x}}_G\right]\\ &= -\frac{\rho^{GR}}{n^G}\left[-(n^S)'_S + \operatorname{grad} n^G \cdot \mathbf{w}_G + n^G \operatorname{div} \overset{\prime}{\mathbf{x}}_G\right].\end{aligned} \tag{B.31}$$

From inspection of (B.30) and (B.31) it is now obvious that (B.28) is verified.

The non-linear solid stress tensor:

Proceeding from the thermodynamic potential $(3.45)_1$, $\mathbf{T}^S_E$ can be given through the differentiation of the solid stored energy (3.84). To this end, taking advantage of the identities $(A.9)_5$, $(A.10)_5$, $(A.12)_1$ and $(A.19)_1$, the integration of (3.84) with respect to the deformation gradient yields

$$\rho^S_{0S}\frac{\partial \psi^S}{\partial \mathbf{F}_S} = \mu^S \mathbf{F}_S + m^S \Delta\theta^S \mathbf{F}_S^{T-1} + \lambda^S \ln(\det\mathbf{F}_S)\, \mathbf{F}_S^{T-1}. \tag{B.32}$$

Furthermore, incorporating (B.32) in the potential $(3.45)_1$, one obtains the *extra* solid stress as

$$\begin{aligned}\mathbf{T}^S_E &= n^S \rho^{SR}\frac{\partial \psi^S}{\partial \mathbf{F}_S}\mathbf{F}_S^T\\ &= \rho^S_{0S}(\det\mathbf{F}_S)^{-1}\frac{\partial \psi^S}{\partial \mathbf{F}_S}\mathbf{F}_S^T\\ &= (\det\mathbf{F}_S)^{-1}\left(\mu^S(\mathbf{B}_S - \mathbf{I}) + m^S \Delta\theta^S \mathbf{I} + \lambda^S \ln(\det\mathbf{F}_S)\,\mathbf{I}\right),\end{aligned} \tag{B.33}$$

where, additionally, relations (2.6), $(2.25)_1$ and (2.43) have been used. Looking at (B.33), it is obvious that $\mathbf{T}^S_E$ is identical to the *Cauchy* stress tensor from (2.35), i. e.

$$\mathbf{T}^S_E = (\det\mathbf{F}_S)^{-1}\boldsymbol{\tau}^S_E \tag{B.34}$$

with $\boldsymbol{\tau}^S_E$ as the *Kirchhoff* stress tensor via

$$\boldsymbol{\tau}^S_E = 2\,\mu^S \mathbf{K}_S + m^S \Delta\theta^S \mathbf{I} + \lambda^S \ln(\det\mathbf{F}_S)\,\mathbf{I}. \tag{B.35}$$

Therein, the *Karni-Reiner* strain from $(2.26)_2$ has been considered.

The entropy function of the solid constituent:

Non-linear solid:

According to the thermodynamic potential $(3.45)_3$, the *extra* entropy of the solid can be obtained by the differentiation of (3.84) with respect to the solid temperature, i. e.

$$\begin{aligned} \eta^S_E &= -\frac{\partial \psi^S}{\partial \theta^S} \\ &= -\left[\frac{1}{\rho^S_{0S}} m^S \ln(\det \mathbf{F}_S) - C^S_V \ln \frac{\theta^S}{\theta^S_{0S}} \right] . \end{aligned} \tag{B.36}$$

Given (B.36), the entire solid entropy (3.77) can now be written as

$$\eta^S = \frac{\theta^S}{\theta^G} p^{GR} \frac{1}{(\rho^{SR})^2} \frac{\partial \rho^{SR}}{\partial \theta^S} + C^S_V \ln \frac{\theta^S}{\theta^S_{0S}} - \frac{1}{\rho^S_{0S}} m^S \ln(\det \mathbf{F}_S) . \tag{B.37}$$

If isotropic thermal expansions can be presumed for the solid, one obtains, with the aid of (3.32), for the derivative of the solid density in (B.37)

$$\frac{\partial \rho^{SR}}{\partial \theta^S} = -3\alpha^S \rho^{SR}_{0S} e^{-3\alpha^S \Delta\theta^S} \tag{B.38}$$

so that the entire entropy is then of the following form:

$$\eta^S = -\frac{3\alpha^S \theta^S}{\rho^{SR}_{0S} \theta^G} p^{GR} e^{3\alpha^S \Delta\theta^S} + C^S_V \ln \frac{\theta^S}{\theta^S_{0S}} - \frac{1}{\rho^S_{0S}} m^S \ln(\det \mathbf{F}_S) . \tag{B.39}$$

Linear solid:

The linearized entropy can be obtained, by use of (3.87) and $(3.45)_3$, in analogy to (B.36), viz.:

$$\begin{aligned} \eta^S_{E_{lin}} &= -\frac{\partial \psi^S_{lin}}{\partial \theta^S} \\ &= -\left(\frac{1}{\rho^S} m^S \boldsymbol{\varepsilon}_S \cdot \mathbf{I} - C^S_V \ln \frac{\theta^S}{\theta^S_{0S}} \right) . \end{aligned} \tag{B.40}$$

Thus, the entire entropy for a solid skeleton with small strains as well as isotropic thermal expansions is now given, according to (B.39), via

$$\eta^S_{lin} = -\frac{3\alpha^S \theta^S}{\rho^{SR}_{0S} \theta^G} p^{GR} e^{3\alpha^S \Delta\theta^S} + C^S_V \ln \frac{\theta^S}{\theta^S_{0S}} - \frac{1}{\rho^S} m^S \boldsymbol{\varepsilon}_S \cdot \mathbf{I} . \tag{B.41}$$

The free energy of the gas constituent:

On the one hand, the free energy ψ^G can be gained from the thermodynamic potential (3.75) when therein additionally the ideal gas law (3.82) is incorporated. This procedure yields in a first step

$$\frac{\partial \psi^G}{\partial \rho^{GR}} = \bar{R}^G \theta^G \frac{1}{\rho^{GR}} \ . \tag{B.42}$$

Considering $(3.47)_2$, ψ^G can then be determined through the integration of (B.42) and is given by

$$\begin{aligned} \psi^G &= \int \bar{R}^G\,\theta^G\,\frac{1}{\rho^{GR}}\,\mathrm{d}\rho^{GR} \\ &= \bar{R}^G\,\theta^G \ln \rho^{GR} + \bar{f}(\theta^G)\,. \end{aligned} \tag{B.43}$$

Furthermore, one obtains for the differentiation of ψ^G with respect to θ^G

$$\frac{\partial\,\psi^G}{\partial\,\theta^G} = \bar{R}^G \ln \rho^{GR} + \frac{\partial\,\bar{f}}{\partial\,\theta^G}\,. \tag{B.44}$$

On the other hand, ψ^G can also be deduced from (3.80) through the integration via

$$\begin{aligned} \frac{\partial\,\psi^G}{\partial\,\theta^G} &= -\int \frac{1}{\theta^G}\,C_V^G\,\mathrm{d}\theta^G \\ &= -\,C_V^G \ln \theta^G + \bar{g}(\rho^{GR})\,. \end{aligned} \tag{B.45}$$

Thus, comparing (B.44) with (B.45), the introduced functions $\bar{f}$ and $\bar{g}$, respectively, are now unambiguously identified as

$$\begin{aligned} \frac{\partial\,\bar{f}}{\partial\,\theta^G} &= -C_V^G \ln \theta^G\,, \\ \bar{g}(\rho^{GR}) &= \bar{R}^G \ln \rho^{GR}\,. \end{aligned} \tag{B.46}$$

Taking advantage of (B.3), one obtains furthermore

$$\bar{f}(\theta^G) = -C_V^G\,(\theta^G \ln \theta^G - \theta^G)\,. \tag{B.47}$$

Inserting (B.47) into (B.43), the free energy function ψ^G can finally be represented as below

$$\psi^G = \bar{R}^G\,\theta^G \ln \rho^{GR} - C_V^G\,(\theta^G \ln \theta^G - \theta^G)\,. \tag{B.48}$$

Mixture momentum balance equation:

Proceeding from the general momentum balance equation of a constituent $(2.39)_2$, the mixture momentum balance can now be obtained by summing up the momentum balances of φ^S and φ^G via

$$\rho^S\,\overset{\prime\prime}{\mathbf{x}}_S + \rho^G\,\overset{\prime\prime}{\mathbf{x}}_G = \operatorname{div}\mathbf{T}^S + \operatorname{div}\mathbf{T}^G + \rho^S\,\mathbf{b}^S + \rho^G\,\mathbf{b}^G + \hat{\mathbf{p}}^S + \hat{\mathbf{p}}^G\,. \tag{B.49}$$

Therein, using (2.14), (2.21) and (3.94), the gas acceleration can be expressed alternatively as follows

$$\begin{aligned} \overset{\prime\prime}{\mathbf{x}}_G &= (\overset{\prime}{\mathbf{x}}_S + \mathbf{w}_G)'_G \\ &= (\overset{\prime}{\mathbf{x}}_S + \mathbf{w}_G)'_S + \operatorname{grad}(\overset{\prime}{\mathbf{x}}_S + \mathbf{w}_G)\,\mathbf{w}_G \\ &= [(\mathbf{u}_S)'_S + \mathbf{w}_G]'_S + \operatorname{grad}[(\mathbf{u}_S)'_S + \mathbf{w}_G]\,\mathbf{w}_G\,. \end{aligned} \tag{B.50}$$

The incorporation of (2.6), (3.4_1), $(3.77)_1$, $(3.77)_2$ and (B.50) in (B.49) yields then the determining mixture momentum balance as follows

$$\begin{aligned} & n^S \rho^{SR} (\mathbf{u}_S)''_S + n^G \rho^{GR} \Big[(\mathbf{u}_S)''_S + (\mathbf{w}_G)'_S + \operatorname{grad} ((\mathbf{u}_S)'_S + \mathbf{w}_G)\, \mathbf{w}_G \Big] = \\ & \operatorname{div} \left(\boldsymbol{\sigma}^S_E - n^S \frac{\theta^S}{\theta^G} p^{GR} \mathbf{I} + \mathbf{T}^G_E - n^G p^{GR} \mathbf{I} \right) + (n^S \rho^{SR} + n^G \rho^{GR})\, \mathbf{b} . \end{aligned} \tag{B.51}$$

Therein,

$$\mathbf{T} = \mathbf{T}^S + \mathbf{T}^G \tag{B.52}$$

has been considered. This is however a simplification, since, in the case of a dynamic formulation, the total stress tensor of the mixture consists, additionally to the partial stresses, of further parts resulting from diffusion effects, cf., e. g., Ehlers [28].

quasi-static formulation:

Neglecting the accelerations (3.93), the mixture momentum balance yields for quasi-static processes

$$\operatorname{div} \left(\boldsymbol{\sigma}^S_E - n^S \frac{\theta^S}{\theta^G} p^{GR} \mathbf{I} + \mathbf{T}^G_E - n^G p^{GR} \mathbf{I} \right) + (n^S \rho^{SR} + n^G \rho^{GR})\, \mathbf{b} = \mathbf{0} . \tag{B.53}$$

Momentum balance equation of the gas:

In analogy to (B.49), the momentum balance of φ^G can be written first in the general form, viz.:

$$\rho^G \overset{\prime\prime}{\mathbf{x}}_G = \operatorname{div} \mathbf{T}^G + \rho^G \mathbf{b}^G + \hat{\mathbf{p}}^G . \tag{B.54}$$

Furthermore, using (2.6), $(3.77)_2$, (3.77_4) and (B.50), the equation (B.54) assumes then the shape

$$\begin{aligned} & n^G \rho^{GR} \Big[(\mathbf{u}_S)''_S + (\mathbf{w}_G)'_S + \operatorname{grad} ((\mathbf{u}_S)'_S + \mathbf{w}_G)\, \mathbf{w}_G \Big] = \\ & + \operatorname{div} \mathbf{T}^G_E - \operatorname{div} (n^G p^{GR} \mathbf{I}) + \frac{\theta^S}{\theta^G} p^{GR} \operatorname{grad} n^G + \hat{\mathbf{p}}^G_E + n^G \rho^{GR} \mathbf{b}^G , \end{aligned} \tag{B.55}$$

which, taking advantage of (B.27), can also be given in the alternative form

$$\begin{aligned} & n^G \rho^{GR} \Big[(\mathbf{u}_S)''_S + (\mathbf{w}_G)'_S + \operatorname{grad} ((\mathbf{u}_S)'_S + \mathbf{w}_G)\, \mathbf{w}_G \Big] = \operatorname{div} \mathbf{T}^G_E - \\ & - p^{GR} \operatorname{grad} n^G - n^G \operatorname{grad} p^{GR} + \frac{\theta^S}{\theta^G} p^{GR} \operatorname{grad} n^G + \hat{\mathbf{p}}^G_E + n^G \rho^{GR} \mathbf{b}^G . \end{aligned} \tag{B.56}$$

quasi-static formulation:

In analogy to (B.53), the quasi-static formulation of (B.56) is defined via

$$\begin{aligned} &\operatorname{div} \mathbf{T}^G_E - p^{GR} \operatorname{grad} n^G - n^G \operatorname{grad} p^{GR} + \\ &+ \frac{\theta^S}{\theta^G} p^{GR} \operatorname{grad} n^G + \hat{\mathbf{p}}^G_E + n^G \rho^{GR} \mathbf{b}^G = \mathbf{0}\,. \end{aligned} \tag{B.57}$$

Mass balance equation of the gas:

Excluding mass productions, the mass balance of gas can be formulated according to $(2.39)_1$, i.e.,

$$(\rho^G)'_G + \rho^G \operatorname{div} \overset{\prime}{\mathbf{x}}_G = 0\,, \tag{B.58}$$

in which now the kinematical measures can be related to the solid constituent. To this end, in a first step, the expression

$$\rho^G \operatorname{div} \overset{\prime}{\mathbf{x}}_S - \rho^G \operatorname{div} \overset{\prime}{\mathbf{x}}_S = 0$$

is added to (B.58), which, considering (2.14), yields

$$(\rho^G)'_G + \rho^G \operatorname{div} \mathbf{w}_G + \rho^G \operatorname{div} \overset{\prime}{\mathbf{x}}_S = 0\,. \tag{B.59}$$

In a further step, by incorporating $(3.95)_1$ in (B.59), one obtains

$$(n^G)'_S \rho^{GR} + n^G (\rho^{GR})'_S + \operatorname{div} (n^G \rho^{GR} \mathbf{w}_G) + n^G \rho^{GR} \operatorname{div} (\mathbf{u}_S)'_S = 0\,. \tag{B.60}$$

Therein, use was additionally made of (2.6), (3.94_1) and the identity $(A.16)_6$. Inserting (3.11) and (B.20) into (B.60), the determining mass balance equation for φ^G is finally identified as

$$\begin{aligned} &\frac{n^G}{\bar{R}^G \theta^G} (p^{GR})'_S - \frac{n^G}{\bar{R}^G (\theta^G)^2} p^{GR} (\theta^G)'_S + \operatorname{div} (n^G \rho^{GR} \mathbf{w}_G) + \\ &+ n^G \rho^{GR} \operatorname{div} (\mathbf{u}_S)'_S - (n^S)'_S \rho^{GR} = 0\,. \end{aligned} \tag{B.61}$$

Energy balance equation of the gas:

An alternative form of the energy balance was already formulated in (2.46), which now for the gas constituent writes

$$-\rho^G [\,(\psi^G)'_G + (\theta^G)'_G \eta^G + \theta^G (\eta^G)'_G\,] + \mathbf{T}^G \cdot \mathbf{L}_G - \operatorname{div} \mathbf{q}^G + \rho^G r^G + \hat{\varepsilon}^G = 0\,. \tag{B.62}$$

It will be seen in the following that (B.62) can be reformulated when corresponding thermodynamic potentials as well as further relations from preceding sections are introduced.

In a first step, the insertion of (2.6), $(3.45)_9$, (3.55) and $(3.77)_2$ into (B.62) yields

$$
\begin{aligned}
& - n^G \rho^{GR} (\psi^G)'_G + n^G \rho^{GR} \frac{\partial \psi^G}{\partial \theta^G} (\theta^G)'_G - n^G \rho^{GR} \theta^G (\eta^G)'_G - n^G p^{GR} \operatorname{div} \overset{\prime}{\mathbf{x}}_G + \\
& + \mathbf{T}^G_E \cdot \mathbf{D}_G - \operatorname{div} \mathbf{q}^G + n^G \rho^{GR} r^G + \hat{\varepsilon}^G = 0 .
\end{aligned}
\tag{B.63}
$$

Considering $(3.45)_9$ and $(3.47)_2$, the time derivatives in (B.63) are identified as

$$
\begin{aligned}
(\psi^G)'_G &= \frac{\partial \psi^G}{\partial \theta^G} (\theta^G)'_G + \frac{\partial \psi^G}{\partial \rho^{GR}} (\rho^{GR})'_G \quad , \\
(\eta^G)'_G &= \frac{\partial \eta^G}{\partial \theta^G} (\theta^G)'_G + \frac{\partial \eta^G}{\partial \rho^{GR}} (\rho^{GR})'_G \\
&= - \frac{\partial^2 \psi^G}{\partial (\theta^G)^2} (\theta^G)'_G - \frac{\partial^2 \psi^G}{\partial \theta^G \partial \rho^{GR}} (\rho^{GR})'_G .
\end{aligned}
\tag{B.64}
$$

The incorporation of the time derivatives above in (B.63) yields

$$
\begin{aligned}
& - n^G \rho^{GR} \frac{\partial \psi^G}{\partial \theta^G} (\theta^G)'_G - n^G \rho^{GR} \frac{\partial \psi^G}{\partial \rho^{GR}} (\rho^{GR})'_G + n^G \rho^{GR} \frac{\partial \psi^G}{\partial \theta^G} (\theta^G)'_G + \\
& + n^G \rho^{GR} \theta^G \frac{\partial^2 \psi^G}{\partial (\theta^G)^2} (\theta^G)'_G + n^G \rho^{GR} \theta^G \frac{\partial^2 \psi^G}{\partial \theta^G \partial \rho^{GR}} (\rho^{GR})'_G + \\
& + \mathbf{T}^G_E \cdot \mathbf{D}_G - n^G p^{GR} \operatorname{div} \overset{\prime}{\mathbf{x}}_G - \operatorname{div} \mathbf{q}^G + n^G \rho^{GR} r^G + \hat{\varepsilon}^G = 0 .
\end{aligned}
\tag{B.65}
$$

Looking at (B.65), it immediately turns out that, therein, the first and the third term cancel each other out. Moreover, the partial derivatives can be determined from (B.48) and are given via

$$
\begin{aligned}
\frac{\partial^2 \psi^G}{\partial (\theta^G)^2} &= - \frac{1}{\theta^G} C^G_V , \\
\frac{\partial^2 \psi^G}{\partial \theta^G \partial \rho^{GR}} &= \frac{1}{\rho^{GR}} \bar{R}^G .
\end{aligned}
\tag{B.66}
$$

Thus, (B.65) can be put into

$$
\begin{aligned}
& - n^G \rho^{GR} \frac{\partial \psi^G}{\partial \rho^{GR}} (\rho^{GR})'_G - n^G p^{GR} \operatorname{div} \overset{\prime}{\mathbf{x}}_G - n^G \rho^{GR} C^G_V (\theta^G)'_G + \\
& + n^G \theta^G \bar{R}^G (\rho^{GR})'_G + \mathbf{T}^G_E \cdot \mathbf{D}_G - \operatorname{div} \mathbf{q}^G + n^G \rho^{GR} r^G + \hat{\varepsilon}^G = 0 .
\end{aligned}
\tag{B.67}
$$

It is shown in (B.28) that the first and the second term in (B.67) can be summarized as below

$$
- n^G \rho^{GR} \frac{\partial \psi^G}{\partial \rho^{GR}} (\rho^{GR})'_G - n^G p^{GR} \operatorname{div} \overset{\prime}{\mathbf{x}}_G = p^{GR} \operatorname{grad} n^G \cdot \mathbf{w}_G - p^{GR} (n^S)'_S . \tag{B.68}
$$

Furthermore, it can be seen in (B.23) that, using the ideal gas law (3.82), one obtains for the time derivative of the gas density:

$$
\begin{aligned}
&(\rho^{GR})'_G = \\
&= \frac{1}{\bar{R}^G\,(\theta^G)^2}\,\big[(p^{GR})'_S\,\theta^G \,-\, p^{GR}\,(\theta^G)'_S \,+\, (\theta^G\,\mathrm{grad}\,p^{GR} \,-\, p^{GR}\,\mathrm{grad}\,\theta^G)\cdot\mathbf{w}_G\big]\;,
\end{aligned}
\tag{B.69}
$$

The incorporation of (B.68) and (B.69) in (B.67) yields finally the determining energy balance equation of φ^G via

$$
\begin{aligned}
&-\,n^G\,\rho^{GR}\,C_V^G\,(\theta^G)'_S \,-\, n^G\,\rho^{GR}\,C_V^G\,\mathrm{grad}\,\theta^G\cdot\mathbf{w}_G \,+\, n^G\,(p^{GR})'_S - \\
&-\frac{n^G}{\theta^G}\,p^{GR}\,(\theta^G)'_S \,+\, n^G\,\mathrm{grad}\,p^{GR}\cdot\mathbf{w}_G \,-\, \frac{n^G}{\theta^G}\,p^{GR}\,\mathrm{grad}\,\theta^G\cdot\mathbf{w}_G + \\
&+p^{GR}\,\mathrm{grad}\,n^G\cdot\mathbf{w}_G \,-\, p^{GR}\,(n^S)'_S \,+\, \mathbf{T}_E^G\cdot\mathbf{D}_G \,-\, \mathrm{div}\,\mathbf{q}^G + \\
&+n^G\,\rho^{GR}\,r^G \,+\, \hat{\varepsilon}^G \,=\, 0\,.
\end{aligned}
\tag{B.70}
$$

Energy balance equation of the solid constituent:

In analogy to (B.62), the energy balance equation of the linear solid can be given via

$$
-\rho^S\,[\,(\psi^S_{lin})'_S + (\theta^S)'_S\,\eta^S_{lin} + \theta^S\,(\eta^S_{lin})'_S\,] + \mathbf{T}^S\cdot\mathbf{L}_S - \mathrm{div}\,\mathbf{q}^S + \rho^S r^S + \hat{\varepsilon}^S = 0\,. \tag{B.71}
$$

Therein, proceeding from $(3.45)_3$ and (B.41), the entropy can be alternatively written as

$$
\begin{aligned}
\eta^S_{lin} &= \bar{\eta}^S + \eta^S_{E_{lin}} \\
&= \bar{\eta}^S - \frac{\partial\,\psi^S_{lin}}{\partial\,\theta^S}\,,
\end{aligned}
\tag{B.72}
$$

with

$$
\begin{aligned}
\bar{\eta}^S &= -\,3\,\frac{\alpha^S\,\theta^S}{\rho^{SR}_{0S}\,\theta^G}\,p^{GR}\,e^{3\,\alpha^S\,\Delta\theta^S}\,, \\
\bar{\eta}^S_{E_{lin}} &= C_V^S\ln\frac{\theta^S}{\theta^S_{0S}} - \frac{1}{\rho^S}\,m^S\,\boldsymbol{\varepsilon}_S\cdot\mathbf{I}\,.
\end{aligned}
\tag{B.73}
$$

In addition, one obtains for the time derivatives in (B.71)

$$
\begin{aligned}
(\psi^S_{lin})'_S &= \frac{\partial\,\psi^S_{lin}}{\partial\,\theta^S}\,(\theta^S)'_S + \frac{\partial\,\psi^S_{lin}}{\partial\,\boldsymbol{\varepsilon}_S}\cdot(\boldsymbol{\varepsilon}_S)'_S\;, \\
(\eta^S_{lin})'_S &= (\bar{\eta}^S)'_S + \frac{\partial\,\eta^S_{E_{lin}}}{\partial\,\theta^S}\,(\theta^S)'_S + \frac{\partial\,\eta^S_{E_{lin}}}{\partial\,\boldsymbol{\varepsilon}_S}\cdot(\boldsymbol{\varepsilon}_S)'_S \\
&= (\bar{\eta}^S)'_S - \frac{\partial^2\,\psi^S_{lin}}{\partial\,(\theta^S)^2}\,(\theta^S)'_S - \frac{\partial^2\,\psi^S_{lin}}{\partial\,\boldsymbol{\varepsilon}_S\,\partial\,\theta^S}\cdot(\boldsymbol{\varepsilon}_S)'_S\,,
\end{aligned}
\tag{B.74}
$$

where use was made of $(3.45)_3$. Furthermore, taking advantage of the thermodynamic potential (3.52), the solid stress can be given from $(3.77)_1$ via

$$
\begin{aligned}
\mathbf{T}^S &= -\, n^S \, \frac{\theta^S}{\theta^G} \, p^{GR} \, \mathbf{I} \, + \, \boldsymbol{\sigma}^S_E \\
&= -\, n^S \, \frac{\theta^S}{\theta^G} \, p^{GR} \, \mathbf{I} \, + \, n^S \, \rho^{SR} \, \frac{\partial \, \psi^S_{lin}}{\partial \, \boldsymbol{\varepsilon}_S} \, .
\end{aligned} \tag{B.75}
$$

Therein, relation (3.53) was additionally considered. The incorporation of (B.72), (B.74) and (B.75) in (B.71) leads to

$$
\begin{aligned}
&-\, n^S \, \rho^{SR} \, \frac{\partial \, \psi^S_{lin}}{\partial \, \theta^S} \, (\theta^S)'_S \, - \, n^S \, \rho^{SR} \, \frac{\partial \, \psi^S_{lin}}{\partial \, \boldsymbol{\varepsilon}_S} \cdot (\boldsymbol{\varepsilon}_S)'_S \, - \, n^S \, \rho^{SR} \, \bar{\eta}^S \, (\theta^S)'_S \, + \\
&+\, n^S \, \rho^{SR} \, \frac{\partial \, \psi^S_{lin}}{\partial \, \theta^S} \, (\theta^S)'_S \, - \, n^S \, \rho^{SR} \, \theta^S \, (\bar{\eta}^S)'_S \, + \, n^S \, \rho^{SR} \, \theta^S \, \frac{\partial^2 \, \psi^S_{lin}}{\partial \, (\theta^S)^2} \, (\theta^S)'_S \, + \\
&+\, n^S \, \rho^{SR} \, \theta^S \, \frac{\partial^2 \, \psi^S_{lin}}{\partial \, \boldsymbol{\varepsilon}_S \, \partial \, \theta^S} \cdot (\boldsymbol{\varepsilon}_S)'_S \, - \, n^S \, \frac{\theta^S}{\theta^G} \, p^{GR} \, (\boldsymbol{\varepsilon}_S)'_S \cdot \mathbf{I} \, + \, n^S \, \rho^{SR} \, r^S \, + \\
&+\, n^S \, \rho^{SR} \, \frac{\partial \, \psi^S_{lin}}{\partial \, \boldsymbol{\varepsilon}_S} \cdot (\boldsymbol{\varepsilon}_S)'_S \, - \, \operatorname{div} \mathbf{q}^S \, + \, \hat{\varepsilon}^S = 0 \, .
\end{aligned} \tag{B.76}
$$

Note that also relations (2.6) and (3.51) have been used in (B.76). This equation can be reduced, since therein some terms cancel each other out. Thus,

$$
\begin{aligned}
&-\, n^S \, \rho^{SR} \, \bar{\eta}^S \, (\theta^S)'_S \, - \, n^S \, \rho^{SR} \, \theta^S \, (\bar{\eta}^S)'_S \, + \, n^S \, \rho^{SR} \, \theta^S \, \frac{\partial^2 \, \psi^S_{lin}}{\partial \, (\theta^S)^2} \, (\theta^S)'_S \, + \\
&+\, n^S \, \rho^{SR} \, \theta^S \, \frac{\partial^2 \, \psi^S_{lin}}{\partial \, \boldsymbol{\varepsilon}_S \, \partial \, \theta^S} \cdot (\boldsymbol{\varepsilon}_S)'_S \, - \, n^S \, \frac{\theta^S}{\theta^G} \, p^{GR} \, (\boldsymbol{\varepsilon}_S)'_S \cdot \mathbf{I} \, + \, n^S \, \rho^{SR} \, r^S \, - \\
&-\, \operatorname{div} \mathbf{q}^S \, + \, \hat{\varepsilon}^S = 0 \, .
\end{aligned} \tag{B.77}
$$

For the partial derivatives in (B.77), one obtains from (3.87) the following identifications:

$$
\begin{aligned}
\frac{\partial^2 \, \psi^S_{lin}}{\partial \, (\theta^S)^2} &= -\, \frac{1}{\theta^S} \, C^S_V \, , \\
\frac{\partial^2 \, \psi^S_{lin}}{\partial \, \boldsymbol{\varepsilon}_S \, \partial \, \theta^S} &= \frac{1}{\rho^S} \, m^S \, \mathbf{I} \, .
\end{aligned} \tag{B.78}
$$

Moreover, it can be seen in (B.26) that the time derivative of the overbared entropy is defined via

$$
\begin{aligned}
(\bar{\eta}^S)'_S \; = \; -\, 3 \, \frac{\alpha^S}{\theta^G \rho^{SR}_{0S}} \, e^{3\, \alpha^S \Delta \theta^S} \, \Big[& p^{GR} \, (\theta^S)'_S \, - \, \frac{\theta^S}{\theta^G} \, p^{GR} \, (\theta^G)'_S \, + \\
& + \theta^S \, (p^{GR})'_S \, + \, 3 \, \alpha^S \, \theta^S \, p^{GR} \, (\theta^S)'_S \Big] \, .
\end{aligned} \tag{B.79}
$$

Inserting (B.78) and (B.79) into (B.77), the energy balance equation of the solid constituent finally is given by

$$\begin{aligned} & 3\,\alpha^S\, n^S \frac{\theta^S}{\theta^G}\, p^{GR} \left[2\,(\theta^S)'_S - \frac{\theta^S}{\theta^G}\,(\theta^G)'_S + \frac{1}{p^{GR}}\,\theta^S\,(p^{GR})'_S + \right. \\ & \left. + 3\,\alpha^S\,\theta^S\,(\theta^S)'_S \right] - n^S\,\rho^{SR}\,C_V^S\,(\theta^S)'_S + \theta^S\,m^S\,\mathbf{I}\cdot(\boldsymbol{\varepsilon}_S)'_S + \\ & + n^S\,\rho^{SR}\,r^S - n^S\,\frac{\theta^S}{\theta^G}\,p^{GR}\,\mathbf{I}\cdot(\boldsymbol{\varepsilon}_S)'_S - \operatorname{div}\mathbf{q}^S + \hat{\varepsilon}^S = 0\,, \end{aligned} \tag{B.80}$$

where the equation (3.32) has been additionally considered.

Transformations of volume integrals to surface integrals:

For the weak form of the mixture momentum balance equation:

After (B.53) is multiplied by the test function $\delta\mathbf{u}_S$, the divergence term

$$\int\limits_\Omega \operatorname{div}\left(\boldsymbol{\sigma}_E^S - n^S\,\frac{\theta^S}{\theta^G}\,p^{GR}\,\mathbf{I} + \mathbf{T}_E^G - n^G\,p^{GR}\,\mathbf{I}\right)\cdot\delta\mathbf{u}_S\,\mathrm{d}v \tag{B.81}$$

can be reformulated as follows. First, applying the identity $(\text{A.16})_7$ to the expression above, one obtains

$$\begin{aligned} & \int\limits_\Omega \operatorname{div}\left(\boldsymbol{\sigma}_E^S - n^S\,\frac{\theta^S}{\theta^G}\,p^{GR}\,\mathbf{I} + \mathbf{T}_E^G - n^G\,p^{GR}\,\mathbf{I}\right)\cdot\delta\mathbf{u}_S\,\mathrm{d}v = \\ & \int\limits_\Omega \operatorname{div}\left[\left(\boldsymbol{\sigma}_E^S - n^S\,\frac{\theta^S}{\theta^G}\,p^{GR}\,\mathbf{I} + \mathbf{T}_E^G - n^G\,p^{GR}\,\mathbf{I}\right)^T\cdot\delta\mathbf{u}_S\right]\mathrm{d}v - \\ & - \int\limits_\Omega \left(\boldsymbol{\sigma}_E^S - n^S\,\frac{\theta^S}{\theta^G}\,p^{GR}\,\mathbf{I} + \mathbf{T}_E^G - n^G\,p^{GR}\,\mathbf{I}\right)\cdot\operatorname{grad}\delta\mathbf{u}_S\,\mathrm{d}v\,. \end{aligned} \tag{B.82}$$

In a further step, taking advantage of the identities (A.10) and $(\text{A.17})_3$, (B.82) assumes the shape

$$\begin{aligned} & \int\limits_\Omega \operatorname{div}\left(\boldsymbol{\sigma}_E^S - n^S\,\frac{\theta^S}{\theta^G}\,p^{GR}\,\mathbf{I} + \mathbf{T}_E^G - n^G\,p^{GR}\,\mathbf{I}\right)\cdot\delta\mathbf{u}_S\,\mathrm{d}v = \\ & \int\limits_{\Gamma_t} \left(\boldsymbol{\sigma}_E^S - n^S\,\frac{\theta^S}{\theta^G}\,p^{GR}\,\mathbf{I} + \mathbf{T}_E^G - n^G\,p^{GR}\,\mathbf{I}\right)\mathbf{n}\cdot\delta\mathbf{u}_S\,\mathrm{d}a - \\ & - \int\limits_\Omega \left(\boldsymbol{\sigma}_E^S - n^S\,\frac{\theta^S}{\theta^G}\,p^{GR}\,\mathbf{I} + \mathbf{T}_E^G - n^G\,p^{GR}\,\mathbf{I}\right)\cdot\operatorname{grad}\delta\mathbf{u}_S\,\mathrm{d}v\,, \end{aligned} \tag{B.83}$$

where use was additionally made of

$$\mathbf{n}\,\mathrm{d}a = \mathrm{d}\mathbf{a}\,. \tag{B.84}$$

For the weak form of mass balance equation:

The multiplication of (B.61) with the test function δp^{GR} yields *inter alia* the following divergence term

$$\int_\Omega \mathrm{div}\,(n^G\,\rho^{GR}\,\mathbf{w}_G)\,\delta p^{GR}\,\mathrm{d}v\,, \tag{B.85}$$

which, using the identity $(\mathrm{A.16})_6$, is put into the form

$$\begin{aligned}
&\int_\Omega \mathrm{div}\,(n^G\,\rho^{GR}\,\mathbf{w}_G)\,\delta p^{GR}\,\mathrm{d}v \;= \\
&\int_\Omega \mathrm{div}\,(n^G\,\rho^{GR}\,\mathbf{w}_G\,\delta p^{GR})\,\mathrm{d}v \;-\; \int_\Omega n^G\,\rho^{GR}\,\mathbf{w}_G\cdot\mathrm{grad}\,\delta p^{GR}\,\mathrm{d}v\,.
\end{aligned} \tag{B.86}$$

Furthermore, transforming the volume integral into a surface integral according to $(\mathrm{A.17})_3$, (B.86) finally becomes

$$\begin{aligned}
&\int_\Omega \mathrm{div}\,(n^G\,\rho^{GR}\,\mathbf{w}_G)\,\delta p^{GR}\,\mathrm{d}v \;= \\
&\int_{\Gamma_v} \delta p^{GR}\,n^G\,\rho^{GR}\,\mathbf{w}_G\cdot\mathbf{n}\,\mathrm{d}a \;-\; \int_\Omega n^G\,\rho^{GR}\,\mathbf{w}_G\cdot\mathrm{grad}\,\delta p^{GR}\,\mathrm{d}v\,.
\end{aligned} \tag{B.87}$$

For the weak form of energy balances equation:

Using the identity $(\mathrm{A.16})_6$, the respective divergence terms of the energy balances for the solid and the fluid, resulting from the multiplication of the energy balances by the corresponding test functions, can be reformulated as follows

$$\int_\Omega \delta\theta^\alpha\,\mathrm{div}\,\mathbf{q}^\alpha\,\mathrm{d}v \;=\; \int_\Omega \mathrm{div}\,(\delta\theta^\alpha\,\mathbf{q}^\alpha)\,\mathrm{d}v \;-\; \int_\Omega \mathbf{q}^\alpha\cdot\mathrm{grad}\,\delta\theta^\alpha\,\mathrm{d}v\,, \tag{B.88}$$

which, by use of $(\mathrm{A.17})_3$, yields

$$\int_\Omega \delta\theta^\alpha\,\mathrm{div}\,\mathbf{q}^\alpha\,\mathrm{d}v \;=\; \int_{\Gamma_{q^{\theta\alpha}}} \delta\theta^\alpha\,\mathbf{q}^\alpha\cdot\mathbf{n}\,\mathrm{d}a \;-\; \int_\Omega \mathbf{q}^\alpha\cdot\mathrm{grad}\,\delta\theta^\alpha\,\mathrm{d}v\,. \tag{B.89}$$

Bibliography

[1] Altenbach, J. & Altenbach, H.: *Einführung in die Kontinuumsmechanik.* Teubner, Stuttgart 1994.

[2] Axelsson, O. & Barker, V. A.: *Finite Element Solution of Boundary Value Problems.* Academic Press, Orlando 1994.

[3] Baehr, H. D.: *Thermodynamik.* Springer-Verlag, Berlin 1989.

[4] Becker, E. & Bürger, W.: *Kontinuumsmechanik.* Teubner, Stuttgart 1975.

[5] Biot, M. A.: Le problème de la consolidation de matières argileuses sous une charge. *Annales de la Societé Scientifique de Bruxelles* **B 55** (1935), 110–113.

[6] Biot, M. A.: General theory of three-dimensional consolidation. *Journal of Applied Physics* **12** (1941), 155–164.

[7] Blome, P.: *Ein Mehrphasen-Stoffmodell für Böden mit Übergang auf Interface-Gesetze.* Dissertation, Bericht Nr. II-10 aus dem Institut für Mechanik (Bauwesen), Universität Stuttgart 2003.

[8] Bluhm, J.: Modelling of saturated thermo-elastic porous solids with different phase temperatures. In Ehlers, W. & Bluhm, J. (eds.): *Porous Media: Theory, Experiments and Numerical Applications*, Springer-Verlag, Berlin 2002, pp. 87–118.

[9] Bluhm, J.: A model for liquid-saturated compressible porous solids. In Walther, W. (ed.): *Festschrift zum 60. Geburtstag von Prof. Dr.-Ing. Reint de Boer: Beiträge zur Mechanik*, Forschungsberichte aus dem Fachbereich Bauwesen, Heft 66, Universität-GH Essen 1995, pp. 41–50.

[10] Bluhm, J.: *A consistent model for saturated and empty porous media.* Forschungsberichte aus dem Fachbereich Bauwesen, Heft 74, Universität-GH Essen 1997.

[11] de Boer, R.: Highlights in the historical development of porous media theory: toward a consistent macroscopic theory. *Applied Mechanics Review* **49** (1996), 201–262.

[12] de Boer, R.: *Vektor- und Tensorrechnung für Ingenieure.* Springer-Verlag, Berlin 1982.

[13] de Boer, R.: *Theory of Porous Media.* Springer-Verlag, Berlin 2000.

[14] de Boer, R. & Ehlers, W.: The development of the concept of effective stresses. *Acta Mechanica* **83** (1990), 77–92.

[15] de Boer, R. & Ehlers, W.: Uplift, friction and capillarity – three fundamental effects for liquid-saturated porous media. *International Journal of Solids and Structures* **26** (1990), 43–57.

[16] de Boer, R. & Ehlers, W.: *Theorie der Mehrkomponentenkontinua mit Anwendung auf bodenmechanische Probleme*. Forschungsberichte aus dem Fachbereich Bauwesen, Heft 40, Universität-GH-Essen 1986.

[17] Bowen, R. M.: Incompressible porous media models by use of the theory of mixtures. *International Journal of Engineering Sciences* **18** (1980), 1129–1148.

[18] Bowen, R. M.: Compressible porous media models by use of the theory of mixtures. *International Journal of Engineering Sciences* **20** (1982), 697–735.

[19] Bowen, R. M.: Theory of mixtures. In Eringen, A. C. (ed.): *Continuum Physics, Vol. III*, Academic Press, New York 1976, pp. 1–127.

[20] Chen, F.-J.: *Effects of blowing ratio on heat transfer to the throat region of a porous walled nozzle*. Air Force Institute of Technology, Report No. A855792, Ohio 1995.

[21] Coleman, B. D. & Noll, W.: The thermodynamics of elastic materials with heat conduction and viscosity. *Arch. Rational Mech. Anal.* **13** (1963), 167–178.

[22] Danilov, A.: *Numerical treatment of dynamics in porous media*. Master Thesis, Report Nr. II-5, Institute of Applied Mechanics (CE), Universität Stuttgart 2004.

[23] Diebels, S.: *Mikropolare Zweiphasenmodelle: Formulierung auf der Basis der Theorie Poröser Medien*. Habilitation, Bericht Nr. II-4 aus dem Institut für Mechanik (Bauwesen), Universität Stuttgart 2000.

[24] Diebels, S. & Ehlers, W.: Dynamic analysis of a fully saturated porous medium accounting for geometrical and material non-linearities. *International Journal for Numerical Methods in Engineering* **39** (1996), 81–97.

[25] Droste, A.: *Beschreibung und Anwendung eines elastisch-plastischen Materialmodells mit Schädigung für hochporöse Metallschäume*. Dissertation, Bericht Nr. II-9 aus dem Institut für Mechanik (Bauwesen), Universität Stuttgart 2002.

[26] Ehlers, W.: On thermodynamics of elasto-plastic porous media. *Archive of Mechanics* **41** (1989), 73–93.

[27] Ehlers, W.: Grundlegende Konzepte in der Theorie Poröser Medien. *Technische Mechanik* **16** (1996), 63–76.

[28] Ehlers, W.: Foundations of multiphasic and porous materials. In Ehlers, W. & Bluhm, J. (eds.): *Porous Media: Theory, Experiments and Numerical Applications*, Springer-Verlag, Berlin 2002, pp. 3–86.

[29] Ehlers, W.: Continuum and numerical simulation of porous materials in science and technology. In und V. N. Ghionna, G. C. & Giovine, P. (eds.): *Modeling and Mechanics of Granular and Porous Materials*, Birkhäuser, Boston 2002, pp. 244–292.

[30] Ehlers, W.: Shear band localization in fluid-saturated granular elasto-plastic porous media. In Fleck, N. A. & Cocks, A. C. F. (eds.): *IUTAM Symposium on Mechanics of Granular and Porous Materials*, Solid Mechanics and its Applications, Kluwer Academic Publishers, Dordrecht 1997, pp. 377–388.

[31] Ehlers, W.: *Poröse Medien – ein kontinuumsmechanisches Modell auf der Basis der Mischungstheorie.* Habilitation, Forschungsberichte aus dem Fachbereich Bauwesen, Heft 47, Universität-GH-Essen 1989.

[32] Ehlers, W.: *Einführung in die Kontinuumsmechanik für Mehrphasenmaterialien.* Vorlesung Höhere Mechanik II B, Universität Stuttgart 2000.

[33] Ehlers, W.: *Continuum mechanics of single- and multiphasic materials.* COMMAS Courses and Lectures, Universität Stuttgart 2001/02.

[34] Ehlers, W. & Ellsiepen, P.: PANDAS: Ein FE-System zur Simulation von Sonderproblemen der Bodenmechanik. In Wriggers, P.; Meißner, U.; Stein, E. & Wunderlich, W. (eds.): *Finite Elemente in der Baupraxis: Modellierung, Berechnung und Konstruktion*, Ernst & Sohn, Berlin, 1998, pp. 391–400.

[35] Ehlers, W. & Markert, B.: A linear viscoelastic biphasic model for soft tissues based on the Theory of Porous Media. *ASME Journal of Biomechanical Engineering* **123** (2001), 418–424.

[36] Ehlers, W. & Markert, B.: A viscoelastic two-phase model for articular cartilage tissues. In Ehlers, W. (ed.): *IUTAM Symposium on Theoretical and Numerical Methods in Continuum Mechanics of Porous Materials*, Kluwer, Dordrecht 2001, pp. 87–92.

[37] Eipper, G.: *Theorie und Numerik finiter elastischer Deformationen in fluidgesättigten porösen Medien.* Dissertation, Bericht Nr. II-1 aus dem Institut für Mechanik (Bauwesen), Universität Stuttgart 1998.

[38] Ellsiepen, P.: *Zeit- und ortsadaptive Verfahren angewandt auf Mehrphasenprobleme poröser Medien.* Dissertation, Bericht Nr. II-3 aus dem Institut für Mechanik (Bauwesen), Universität Stuttgart 1999.

[39] Fillunger, P.: *Erdbaumechanik?.* Selbstverlag des Verfassers, Wien 1936.

[40] Fitts, D. D.: *Nonequilibrium Thermodynamics: A phenomenological theory of irreversible processes in fluid systems.* McGraw-Hill Book Company, New York 1962.

[41] Fröhlke, K.; Haidn, O. & Serbest, E.: New experimental results on tranpiration cooling for H_2 /O_2 rocket combustion chambers. American Institute of Aeronautics and Astronautics (AIAA), Report No. AIAA 98-3443, 34th Joint Propulsion Conference, Cleaveland OH, July 13-15, 1998.

[42] Greuel, D.; Herbertz, A.; Haidn, O.; Ortelt, M. & Hald, H.: Transpiration cooling applied to c/c liners of cryogenic liquid rocket engines. American Institute of Aeronautics and Astronautics (AIAA), Report No. AIAA 2004-3682, 40th AIAA/ASME/SAE/ASEE/JPC, Fort Lauderdale, Florida, July 11-14, 2004.

[43] Grigull, U.: *Wärmeübertragung*. Springer-Verlag, Berlin 1963.

[44] Hald, H.: *Faserkeramiken für heiße Strukturen von Wiedereintrittsfahrzeugen: Simulation, Test und Vergleich mit experimentellen Flugdaten*. Dissertation, Deutsches Zentrum für Luft- und Raumfahrt, Institut für Bauweisen- und Konstruktionsforschung, Bericht Nr. DLR-FB-2001-17, Stuttgart 2001.

[45] Hald, H. & Haidn, O.: Eine treibende Kraft – Schubkammertechnologie für die Zukunft. *Magazin des Deutschen Zentrums für Luft und Raumfahrt* **108** (2004), 36–41.

[46] Hassanizadeh, S. M. & Gray, W. G.: General conservation equations for multiphase systems: 1. Averaging procedure. *Advances in Water Resources* **2** (1979), 131–144.

[47] Haupt, P.: *Continuum Mechanics and Theory of Materials*. Springer-Verlag, Berlin 2000.

[48] Heinrich, G. & Desoyer, K.: Hydromechanische Grundlagen für die Behandlung von stationären und instationären Grundwasserströmungen. *Ingenieur-Archiv* **23** (1955), 182–185.

[49] Helmig, R.: *Multiphase Flow and Transport Processes in the Subsurface*. Springer-Verlag, Berlin 1997.

[50] Herbertz, A.: *Parametrische Zyklus-Untersuchung eines Nebenstromtriebwerks mit Effusionskülung*. Deutsches Zentrum für Luft- und Raumfahrt, Institut für Raumfahrtantriebe, Bericht Nr. DLR-IB 647-2003/02, Köln 2003.

[51] Kays, W. M. & Crawford, M. E.: *Convective Heat and Mass Transfer*. 3rd edn, McGraw-Hill Inc, 1993.

[52] Larch, S.: *Experimente zur Effusionskühlung in Raketenbrennkammern und ihre Auswirkung auf die Wandtemperatur*. Deutsches Zentrum für Luft- und Raumfahrt, Institut für Raumfahrtantriebe, Bericht Nr. DLR-IB 645-98/30, Lampoldshausen 1998.

[53] Lezuo, M.: *Untersuchungen zum Wärmetransport in H_2 transpirativ gekühlten Brennkammerkomponenten*. Dissertation, Luft- und Raumfahrttechnik, Bericht Nr. 3-8265-4481-1, RWTH-Aachen 1998.

[54] Liu, W. & Chen, Q.: The effect of transpiration cooling with liquid oxygen on the flow field. American Institute of Aeronautics and Astronautics (AIAA), Report No. AIAA 98-3515, 34th Joint Propulsion Conference, Cleaveland OH, July 13-15, 1998.

[55] LUENBERGER, D. V.: *Introduction to Linear and Nonlinear Programming.* Addison-Wesley, Massachusetts 1973.

[56] MAHNKEN, R.: *Theoretische und numerische Aspekte zur Parameteridentifikation und Modellierung bei metallischen Werkstoffen.* Habilitation, Forschungs- und Seminarberichte aus dem Bereich der Mechanik der Universität Hannover, Bericht-Nr. F. 98/2, Universität Hannover 1998.

[57] MAHNKOPF, D.: *Lokalisierung fluidgesättigter poröser Festkörper bei finiten elasto-plastischen Deformationen.* Dissertation, Bericht Nr. II-5 aus dem Institut für Mechanik (Bauwesen), Universität Stuttgart 2000.

[58] MAY, L. & BURKHARDT, W. M.: *Transpiration cooled throat for hydrocarbon rocket engines.* NASA, Report No. KEE6-FR, December 1991.

[59] MUEGGENBURG, H. H.; HIDAHL, J. W.; KESSLER, E. L. & ROUSAR, D. C.: Platelet actively cooled thermal management devices. American Institute of Aeronautics and Astronautics (AIAA), Report No. AIAA 92-3127, 28th Joint Propulsion Conference, Nashville TN, July 6-8, 1992.

[60] MÜLLERSCHÖN, H.: *Spannungs-Verzerrungsverhalten granularer Materialien am Beispiel von Berliner Sand.* Dissertation, Bericht Nr. II-6 aus dem Institut für Mechanik (Bauwesen), Universität Stuttgart 2000.

[61] NASA/SP-8087: Liquid rocket engine fluid-cooled combustion chambers. In *NASA SPACE VEHICLE DESIGN CRITERIA (Chemical)*, NASA Lewis Research Center, Report No. SP-8087, Cleveland OH, United States, April 1972.

[62] NASA/SP-8124: Liquid rocket engine self-cooled combustion chambers. In *NASA SPACE VEHICLE DESIGN CRITERIA (Chemical)*, NASA Lewis Research Center, Report No. SP-8124, Cleveland OH, United States, September 1977.

[63] NICKERSON, G.; BERKER, D.; COATS, D. & DUNN, S.: TDK: Two-dimentional kinetics. In *Nozzle Performance Computer Programm Volume II, Users Manual*, Software and Engineering Associates, Inc. for George C. Marshall Space Flight Center, 1993.

[64] RANNIE, W. D.: *Simplified theory of porous wall cooling.* Jet Propulsion Laboratory California Institute of Technology, Passadena California, Report No. W-33-038-ac-4320, November 1947.

[65] RUBESIN, M. W. & PAPPAS, C. C.: An analysis of the turbulent boundary layer characteristics on a flat plate with distributed light gas injection. National Advisory Committee for Aeronatics (NACA), TN 4149, Washington 1958.

[66] SCHÄFER, R.: *Thermisch-mechanisches Verhalten heisser Strukturen in der Wechselwirkung mit einem umströmenden Fluid.* Dissertation, Deutsches Zentrum für Luft- und Raumfahrt, Institut für Bauweisen- und Konstruktionsforschung, Bericht Nr. DLR-FB-2005-02, Stuttgart 2005.

[67] Schwarz, H. R.: *Methode der Finiten Elemente.* Teubner, Stuttgart 1991.

[68] Schwefel, H. P.: *Evolution and Optimum Seeking.* John Wiley & Sons, Chicester, 1995.

[69] Serbest, E.: *Untersuchungen zur Anwendung der Effusionskühlung bei Raketenbrennkammern.* Dissertation, Luft- und Raumfahrttechnik, Bericht Nr. 3-8322-0219-6, RWTH-Aachen 2002.

[70] Serbest, E.; Haidn, O.; Hald, H.; Korger, G. & Winkelmann, P.: Rocket combustors applying fiber reinforced ceramics. American Institute of Aeronautics and Astronautics (AIAA), Report No. AIAA 99-2911, 35th Joint Propulsion Conference, Los Angeles California, June 20-24, 1999.

[71] Spellucci, P.: *Numerische Verfahren der nichtlinearen Optimierung.* Birkhäuser Verlag, Basel 1993.

[72] Sutton, G. P. & Biblarz, O.: *Rocket Propulsion Elements.* Wiley, New York 2001.

[73] Terzaghi, K.: *Erdbaumechanik auf bodenphysikalischer Grundlage.* Franz Deuticke, Leipzig 1925.

[74] Thielecke, F.: *Parameteridentifizierung von Simulationsmodellen für das viskoplastische Verhalten von Metallen – Theorie, Numerik, Anwendung.* Dissertation, Braunschweiger Schriften zur Mechanik No. 34-1998, Mechanik-Zentrum, TU Braunschweig 1998.

[75] Truesdell, C.: *Rational Thermodynamics.* 2nd Edition. Springer-Verlag, New York 1984.

[76] Truesdell, C.: Thermodynamics of diffusion. In Truesdell, C. (ed.): *Rational Thermodynamics*, Springer-Verlag, New York 1984, 2nd edn., pp. 219–236.

[77] Truesdell, C. & Toupin, R. A.: The classical field theories. In Flügge, S. (ed.): *Handbuch der Physik*, Vol. III/1, Springer-Verlag, Berlin 1960, pp. 226–902.

[78] VDI-Wärmeatlas: *Berechnungsblätter für den Wärmeübergang.* 5., erweiterte Auflage. VDI-Verlag, Düsseldorf 1988.

[79] Volk, W.: *Untersuchung des Lokalisierungsverhaltens mikropolarer poröser Medien mit Hilfe der Cosserat-Theorie.* Dissertation, Bericht Nr. II-2 aus dem Institut für Mechanik (Bauwesen), Universität Stuttgart 1999.

[80] Walton, T. E.: Free-flight investigations of subliming ablators and transpiration cooling at hypersonic velocities. *Journal of Spacecraft and Rockets* **1** (1964), 498–501.

[81] Wheeler, H. L. & Duwez, P.: Heat transfer through sweat cooled porous tubes. *Jet Propulsion* **25** (1955), 519–524.

[82] WHITAKER, S.: *The Method of Volume Averaging (Theory and Application of Transport in Porous Media)*. Kluwer Academic Publishers, Dordrecht 1999.

[83] ZIENKIEWICZ, O. C. & TAYLOR, R. L.: *The Finite Element Method – Basic Formulation and Linear Problems*. McGraw-Hill, London 1989.

Curriculum Vitae

Name:	Saeed Reza Ghadiani
Date of birth:	November 21st, 1973
Place of birth:	Tehran, Iran
Nationality:	German
Education:	1979 - 1988 Elementary and Secondary School, 1st - 9th grade: Tehran (Iran)
	1988 - 1989 Secondary School, 10th grade: Bernhard Adelung Schule, Darmstadt (Germany)
	1989 - 1992 Secondary School, 11th - 13th grade: Gymnasium Bertolt Brecht Schule, Darmstadt (Germany)
	1992 - 1998 Study of Civil Engineering at the University of Applied Sciences, Darmstadt (Germany)
	1998 - 2000 Study of Lightweight Structures and Structural Mechanics at the University of Kassel (Germany)
Professional Occupation:	since 2000 Research Activities on Actively Cooled Space Constructions at the Institute of Structures and Design (Space System Integration), German Aerospace Center (DLR) Stuttgart

Released Report Series

II-1 Gernot Eipper: *Theorie und Numerik finiter elastischer Deformationen in fluidgesättigten porösen Festkörpern*, June 1998.

II-2 Wolfram Volk: *Untersuchung des Lokalisierungsverhaltens mikropolarer poröser Medien mit Hilfe der Cosserat-Theorie*, May 1999.

II-3 Peter Ellsiepen: *Zeit- und ortsadaptive Verfahren angewandt auf Mehrphasenprobleme poröser Medien*, July 1999.

II-4 Stefan Diebels: *Mikropolare Zweiphasenmodelle: Formulierung auf der Basis der Theorie Poröser Medien*, March 2000.

II-5 Dirk Mahnkopf: *Lokalisierung fluidgesättigter poröser Festkörper bei finiten elastoplastischen Deformationen*, March 2000.

II-6 Heiner Müllerschön: *Spannungs-Verformungsverhalten granularer Materialien am Beispiel von Berliner Sand*, August 2000.

II-7 Stefan Diebels (ed.): *Zur Beschreibung komplexen Materialverhaltens: Beiträge anläßlich des 50. Geburtstages von Herrn Prof. Dr.-Ing. Wolfgang Ehlers*, August 2001.

II-8 Jack Widjajakusuma: *Quantitative Prediction of Effective Material Parameters of Heterogeneous Materials*, June 2002.

II-9 Alexander Droste: *Beschreibung und Anwendung eines elastisch-plastischen Materialmodells mit Schädigung für hochporöse Metallschäume*, October 2002.

II-10 Peter Blome: *Ein Mehrphasen-Stoffmodell für Böden mit Übergang auf Interface-Gesetze*, October 2003.

II-11 Martin Ammann: *Parallel Finite Element Simulations of Localization Phenomena in Porous Media*, April 2005.

II-12 Bernd Markert: *Porous Media Viscoelasticity with Application to Polymeric Foams*, July 2005.

II-13 Saeed Reza Ghadiani: *A Multiphasic Continuum Mechanical Model for Design Investigations of an Effusion-Cooled Rocket Thrust Chamber*, May 2005.